Regional Geographies of Extreme Heat

Colin S. Raymond

Submitted in partial fulfillment of the

requirements for the degree of

Doctor of Philosophy

in the Graduate School of Arts and Sciences

Columbia University

2019

Abstract

Regional Geographies of Extreme Heat

Colin S. Raymond

Shaped by countless influences from the atmosphere, biosphere, hydrosphere, and anthroposphere acting across a wide spectrum of spatiotemporal scales, spatial variations in climate are ubiquitous. Meanwhile, the warming signal from anthropogenically elevated greenhouse-gas concentrations is emerging as an overriding determinant for more and more aspects of the climate system, extreme heat among them. In this dissertation, I explore the interaction of these two effects, and the implications of the patterns they create.

A key finding is that rapid increases in extreme heat are already occurring, by some metrics having already doubled in the past 40 years, and further nonlinear increases are expected. Another is the strong dependence of extreme heat-humidity combinations on atmospheric moisture, creating subseasonal and interannual patterns dictated by the principal source of regional warm-season moisture — pre-monsoonal advection in some cases, local evapotranspiration in others. These relationships lead to the demonstrated potential for improvements in predictive power, on the basis of sea-surface temperatures and other canonical modes of large-scale climate variability.

In contrast to this overall confidence in current temporal patterns and long-term projections, I show that extreme heat at small spatial scales is much more poorly characterized in gridded products, and that these biases are especially acute along coastlines. While summer daytime temperature differences between the shoreline of the Northeast U.S. and locations 60 km inland are often 5°C or more, I find that recent high-resolution downscaled Earth-system models typically represent no more than 25% of this difference. Across the globe, ERA-Interim reanalysis

similarly underestimates extreme humid heat by >3°C, a highly significant margin given the large sensitivity of health and economic impacts to marginal changes in the most extreme conditions. I find that these biases propagate into projections, and their importance is also amplified by the large populations living in the affected areas.

Rapid mean warming is pushing the climate system to more and more frequently include extreme heat-humidity combinations beyond that which the human species has likely ever experienced. Such conditions, which had not been previously reported in weather-station data, are described in detail and some of the associated characteristics examined. Several channels of analysis highlight that these events are driven primarily by rising sea-surface temperatures in shallow subtropical gulfs, and the subsequent impingement of marine air on the coastline. Given the severity of potential impacts on infrastructure and agriculture, and the size of the populations exposed, this result underscores that major research and adaptation efforts are needed to avoid calamitous outcomes from the emergence of extreme heat-humidity combinations too severe to tolerate in the absence of artificial cooling.

This dissertation discusses strategies for advancing knowledge of extreme heat's natural variations and its behavior under climate change, in order to design metrics, models, methodologies, and presentation types such that essential findings are translated into tangible action in the most effective way possible. Sustained and integrated efforts are necessary to transition to a climate-system management style encompassing more foresight than the effectively unplanned experiment which has been pursued so far, and which has already exacerbated extreme heat events so much.

Table of Contents

List of Figures

Acknowledgments

A doctoral dissertation is the capstone of years of dedication — sustained by the intrinsically motivating search for knowledge, the extrinsically motivating need to pass certain courses and exams, but above all by the support and encouragement of advisors, colleagues, family, and friends. I certainly would not have traveled this far down the climate-science path without them. I am grateful to have had nudges in the right direction, at crucial moments, from those who could more easily see the long-term picture. Such people include my parents, for all the countless ways they've contributed to my growth; my fiancée, Ariel Goerl, for her tireless support and her understanding of the necessary late nights; my committee members Mingfang Ting and Jason Smerdon, for judiciously providing advice that always rang true; Deepti Singh and Justin Mankin, for helping me develop the skills and confidence to be a better scientist; and my advisor, Radley Horton, for friendly sagacity in all things academic and for inspiring me with his example of just how dynamic and multifaceted a climate scientist can be.

For my mentors – formal and informal, professional and personal, fleeting and long-lasting

Introduction

Many lines of evidence converge on the conclusion that the heat extremes of the coming decades and centuries will be ever more severe than those of the past. These include robust observed increases of heat extremes in recent decades (Russo et al., 2017; Meehl et al., 2009) and a wide variety of modeling studies (Sillmann et al., 2013; Kharin et al., 2013). In the global sum, heat extremes are closely correlated with global mean temperature (Argüeso et al., 2016), and paleoclimatic evidence for the latter suggests that current temperatures are already higher than any observed in the Holocene (Marsicek et al., 2018).

As global mean temperatures continue to increase, heat extremes and their impacts rise at an even faster rate, a consequence of extreme-value statistics whose ultimate expression is modulated by a web of feedbacks involving atmospheric dynamics, ecological responses, anthropogenic land-use decisions, and economic and social behaviors (Lhotka et al., 2018; Mora et al., 2017; Coumou et al., 2014; Argüeso et al., 2014). This complexity means that, beneath the façade of a strong and easily predictable net response of extreme heat to global-mean warming, there remains much to discover about the changing behavior of heat extremes of particular kinds, in particular locations, and under particular conditions. The impacts of extreme heat on agriculture, health, productivity, and the environment, combined with the growing wealth and interconnectedness of the global population, mean that adapting successfully to the future requires a detailed understanding of the hazards presented by extreme heat, where they will be located, and when they can be expected.

This dissertation focuses on advancing the state of knowledge for extreme heat at regional and subregional scales, and especially the overlap of extreme temperatures with extreme humidity. In examining essential scientific questions, the dissertation builds thematically from the areas

closest to existing literature — in Chapter 1, I add to the body of work on extreme-temperature projections by conducting an observational validation along coastlines — to progress to the frontier area of extreme-humid-heat intensity and spatiotemporal characteristics in Chapter 2, and then it goes further (in Chapter 3) to consider the warming rate and impacts of the globally-most-severe humid heat. Consequently, the chapters are arranged to first highlight contributions in more-established fields, and then to follow an argumentative arc which leads toward research in the most cutting-edge and still-uncertain areas concerning extreme humid heat. The conclusions that I draw throughout the dissertation are applicable both to historical climate variability and to future-21st-century climates defined by the overriding influence of anthropogenic warming.

Regional Geographic Effects on Extreme Heat

From the tropics to the high mid-latitudes, extreme heat nearly always requires a persistent anticyclonic circulation that suppresses convection and precipitation, and which increases temperatures through a combination of insolation, warm-air advection, and adiabatic warming (Perkins, 2015). Underneath this basic picture, however, differences between and within regions affect the expression of extreme heat on multiple scales. Such differences include predominantly geographic factors such as terrain, water bodies, land use and land cover, and preceding land-surface conditions, as well as predominantly atmospheric factors such as monsoons and blocked anticyclones (Alvarez-Castro et al., 2018; Vogel et al., 2017; Loikith and Broccoli, 2012; Diffenbaugh, 2009). For example, foehn winds often lead to short-term temperature spikes, while coastlines generate sea breezes which moderate extreme heat on a diurnal basis (Takane and Kusaka, 2011; Arritt, 1993); similarly, built environments tend to increase ambient temperatures, while vegetation and irrigation cool them via a Bowen-ratio effect (Zhao et al., 2018; Mueller et

al., 2016). Each of these phenomena is better understood on a theoretical level than an empirical one, and is more readily evaluated in models than in observations. As a result, empirical estimates of the net effects of regional factors, and their associated feedbacks, on modulating extreme heat are in their infancy. Descriptions of the mechanisms by which they do so, such as identification and quantification of particular dynamical or thermodynamic interactions, are similarly weakly developed.

An especially important type of regional feedback is land-atmosphere interactions, which are known to significantly increase extreme temperatures when soil moisture is low (Donat et al., 2017; Herold et al., 2016; Perkins, 2015) and to decrease extreme temperatures when evapotranspiration is high (Mueller et al., 2016). Such effects are felt across all timescales, from diurnal temperature variations to millennial averages (Christidis et al., 2013), and in fact in some places have thus far outweighed the effects of increasing greenhouse-gas concentrations (Alter et al., 2018). Much ongoing work is aimed at further quantifying the contingent nature of these and other feedbacks, made difficult in many cases by their specific regional or local characteristics, or by their evolution in response to rapidly changing conditions (such as deforestation or the melting of Arctic sea ice).

Sea-surface-temperature [SST] patterns provide a major predictive element for extreme heat through both their facilitation of particular large-scale circulation patterns and through their more local land-sea contrast effects, both of which are highly region-specific (Perkins, 2015; Hoerling et al., 2014; Feudale and Shukla, 2011; Kenyon and Hegerl, 2008). As an example of the hemispheric-scale teleconnections that they foster, SSTs in the central Pacific are linked with eastern-U.S. heat waves through Rossby wave trains (McKinnon et al., 2016), while SSTs in the western Pacific are linked with California heat waves through a similar mechanism (Lee and

Grotjahn, 2019). In both cases, the effects are highly dependent both on the geographic locations of the SST anomalies and those of the extreme heat under consideration. At a smaller spatial scale, SSTs significantly reduce temperatures along the shoreline in many regions, including California (Lebassi et al., 2009). However, the limited number and non-comprehensive scope of current studies of SST-extreme heat relationships leaves in question both the importance of various multi-scale mechanisms, and the sensitivity of the relationships to conditions both within and beyond the observed historical climate range.

Extreme-Heat Impacts

Across the globe, health effects of extreme heat are large and robust (Gasparrini et al., 2015). At the highest temperatures, the sensitivity of negative health outcomes (including mortality) to marginal temperature increases becomes exponential (Petkova et al., 2014; Anderson and Bell, 2009). Consequently, significant differences in health effects occur in response to minor variations in ambient conditions across neighborhoods (Schinasi et al., 2018; Hass et al., 2016; Rosenthal et al., 2014), as well as between urban and rural areas (Wouters et al., 2017). The impacts of a severe event, especially one of unprecedented magnitude for a region, can rank among the most damaging natural disasters of any kind. The 2003 European and 2010 Russian heat wave each have been implicated in more than 5,000 (and up to 75,000) deaths (Barriopedro et al., 2011; Robine et al., 2008). Recent studies have been able to attribute double-digit-percentage increases in observed extreme-heat mortality in certain events to 20th-century global-mean warming (Mitchell et al., 2016). At the same time, there is substantial evidence of the human body's physiological adaptation capabilities with respect to extreme heat: for example, less mortality occurs later in the summer and in hotter regions (Anderson and Bell, 2011), and on balance

populations have become more resilient to given levels of extreme heat over time (Bobb et al., 2014). The ways in which these forces interact have not been fully ascertained for either historical or future conditions.

Urban heat islands [UHIs] result from heat generation and trapping within cities, and from the partitioning of this heat into sensible rather than latent forms (Argüeso et al., 2014; Kanda, 2007). Typical UHI magnitude is 1-4°C (McCarthy et al., 2010), and interaction effects between heat waves and UHI in the mid-latitudes increase urban temperatures by an additional 0.5-2.0°C compared to non-heat-wave UHI (Zhao et al., 2018; Oleson et al., 2015). Furthermore, urban extreme heat is a growing challenge, with annual maximum temperatures increasing about 0.3°C per decade in megacities compared to 0.2°C globally (Papalexiou et al., 2018; Mishra et al., 2015). The combination of growing wealth and continuing urbanization, mapped onto existing UHIs, will cause air-conditioning waste heat to drive very rapid increases in future cooling demand (Argüeso et al., 2015; Davis and Gertler, 2015; Kolokotroni et al. 2012). This will amount to a key emerging source of greenhouse-gas emissions, a budgetary strain (particularly on the developing world), and a deterioration in livability for low-income households (Quinn et al., 2014). Consequently, the primary avenue for mitigating the health impacts of an ever-hotter climate comprises behavioral and technological changes that risk exacerbating wealth-based effects of climate change (Dell et al., 2012).

Labor studies have shown that temperatures above approximately 30°C cause exponential decreases in productivity, particularly in sectors involving significant amounts of outdoor exposure, such as agriculture, mining, and construction (Hsiang et al., 2014; Zivin and Neidell, 2014). Predominantly intellectual work is also affected, with cognition negatively affected among soldiers in one case study (Radakovic et al., 2007). The combined effect of decreases in labor

productivity and decreases in agricultural yields could reduce economic output in tropical and subtropical developing countries by generally 25%, and up to 75%, by 2100 under an unmitigated climate-change scenario (Burke et al., 2015). Even developed countries in the historical period have seen non-negligible gross-domestic-product losses as a result of extreme heat (Zander et al., 2015).

Extreme heat is also correlated with other natural and quasi-natural hazards such as severe air-pollution episodes and increased probability of power failures (Schnell and Prather, 2017; Chapman et al. 2013), and extreme heat can affect key infrastructure like water supply and power grids; natural resources like forests; and societies writ large through economic instability and migration (Bartos and Chester, 2015; AghaKouchak et al., 2014; Mueller et al., 2014; Chapman et al., 2013). Increasing extreme heat is expected to substantially reduce overall agricultural yields in the 21st century, though with large variations by crop type, as well as negatively affect livestock health (Morignat et al., 2014). Combined with increasing food demand, these relationships are expected to severely stress global food networks in the coming decades if major adaptation steps are not taken (Porter et al., 2014; Battisti and Naylor, 2009). On a global level, the physical-science aspects of these extreme-heat corollaries are now fairly well understood, whereas the regional details and the social and political aspects remain opaque, particularly when multiple interacting elements of the climate system are at work.

Extreme Humid Heat

Commonly measured by wet-bulb temperature, wet-bulb globe temperature, or heat-stress metrics (Davis et al., 2016), extreme humid heat is the co-occurrence of high levels of both temperature and moisture. Humidity levels are a key factor in human health and comfort,

particularly during extreme events (Davis et al., 2016; Pal and Eltahir, 2016; Sherwood and Huber, 2010), and consequently also affect broad societal- and economic-relevant metrics like labor productivity, energy demand, and migration (Davis and Gertler, 2015; Mueller et al., 2014; Dunne et al., 2013). Extreme humid heat can cause major societal impacts across the low- and mid-latitude regions of the world (Gasparrini et al., 2015), and has been implicated in recent severe mortality

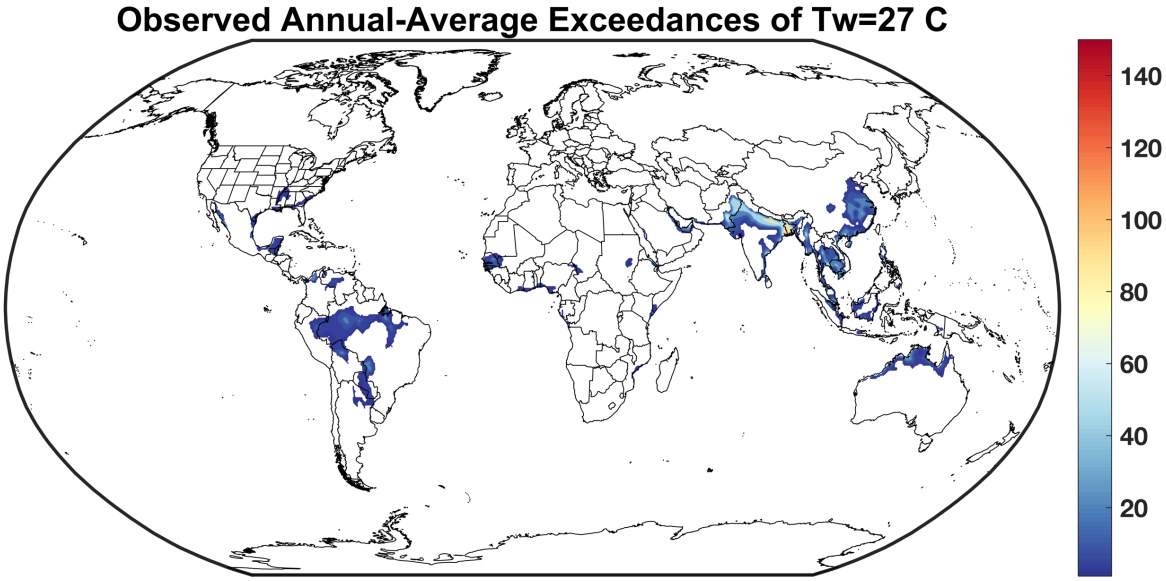

Figure 0.1: Global number of annual-average exceedances of a wet-bulb temperature of 27°C in 6-hourly ERA-Interim data, averaged over 1979-2017. Values are typically largest in coastal areas of the subtropics, as well as in South Asia. From Raymond, Matthews, Horton, (2019), in review.

events such as the 2015 South Asian heat wave (Wehner et al., 2016). The largest impacts occur where large and socioeconomically vulnerable populations reside (Mora et al., 2017; Coffel et al., 2017; Horton et al., 2016; Rosenthal et al., 2014; Dunne et al., 2013; Miller et al., 2008). Approximately 35% of the global population (2.7 billion people) experience a daily maximum wet-bulb temperature of 27°C or warmer — 'strong' heat stress that occurs less than once per year in most of the United States, and that is closely tied to significantly elevated mortality (Matthews,

2018) — at least annually, and 7 million people in South Asia and the Persian Gulf shoreline suffer these conditions more than 100 times per year (Figure 0.1).

Extreme humid heat has seen little study on the level of specific regions, individual events, or the complex interactions with social, cultural, and economic factors that ultimately determine its impacts. The existing literature can be categorized into global-scale overviews, often theoretical and/or model-based (Matthews, 2018; Knutson and Ploshay, 2016; Fischer and Knutti, 2013); case studies, often targeted at developing statistics for specific regions (Im et al., 2017; Pal and Eltahir,

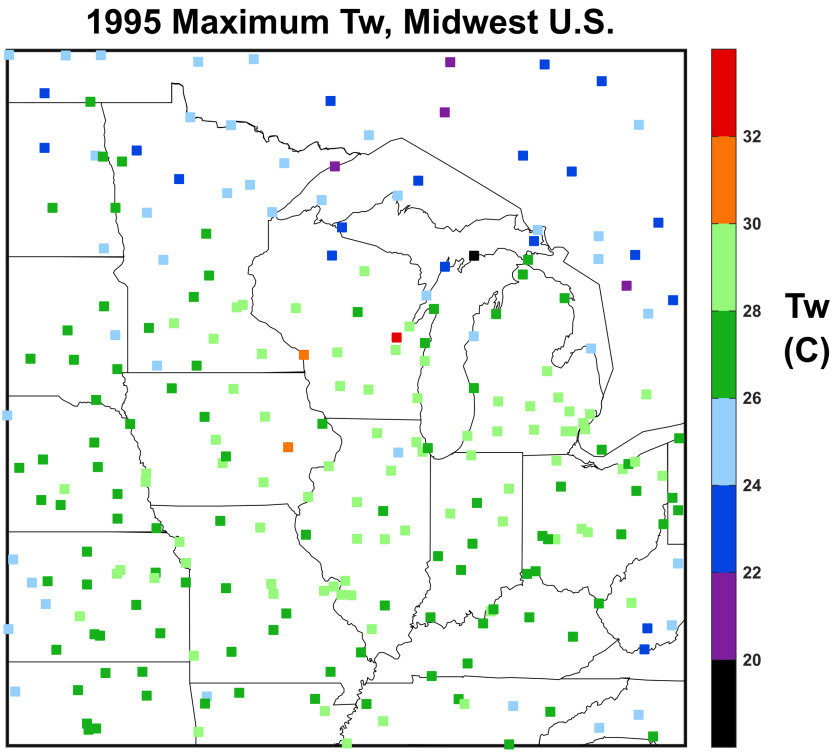

Figure 0.2: Maximum wet-bulb temperature observed during the 1995 Midwest-U.S. heat wave, calculated at hourly temporal resolution from weather stations in the NCEI Integrated Surface Database. Intra-regional variations in maximum wet-bulb temperature, resulting from unobserved local fluctuations in moisture, are on the order of 2-3°C.

2016); and epidemiological or occupational-health analyses, often designed for a small area or specific purpose (Kjellstrom et al., 2016; Parsons, 2006; Sawka et al., 2003). The global-scale overviews have established that due to simultaneous increases in dry-bulb temperature and specific

humidity, extreme humid heat will increase rapidly and with greater spatial consistency than will either of its constituent variables (Russo et al., 2017; Fischer and Knutti, 2013).

The existence of large spatiotemporal variations in both observational studies (Hass et al., 2016; Kunkel et al., 1996) and in models (Pal and Eltahir, 2016) underscores the difficulty in identifying and constraining the decisive subregional factors. The well-documented 1995 Midwest-U.S. heat wave, for instance, contained variations in peak wet-bulb temperature on the order of 5°C over scales of less than 100 km, despite the flat terrain and relatively uniform land cover (Figure 0.2), emphasizing the importance of typically unobserved local perturbations to the background meteorological conditions. Case studies in the literature have discovered several important attributes of extreme humid heat in South Asia and the Middle East: its close association with high sea-surface temperatures (Schär, 2016), and its approach (in brief instances) of the human physiological survivability limit (Im et al., 2017; Pal and Eltahir, 2016), as discussed in more detail in Chapter 3. Trends over the historical period in these globally hottest regions have not previously been examined due to questions about the reliability of local weather-station data and the relative shortness of their period of record.

Overview of Chapters

In Chapter 1, I quantify the reduction of extreme heat in coastal areas of the eastern United States, evaluate the performance of two ensembles of downscaled Earth System Models in representing this reduction, and consider the implications for existing projections of coastal extreme heat.

In Chapter 2, I add moisture to the analysis and consider how patterns of extreme humid heat differ from those of extreme dry-bulb heat. I investigate the physical mechanisms that shape

extreme heat-humidity combinations, with a particular focus on explaining geographic and seasonal variability.

In Chapter 3, I examine recent values and trends of extreme humid heat, discovering observations that are closer to the human physiological survivability limit than previously reported, and present evidence for the systematic and significant underestimation of these very highest values by standard gridded products.

Lastly, I conclude with a summary of the principal themes, a contextualization of the results, and a description of important future topics of study for which this dissertation has laid the groundwork.

Chapter 1: Small-scale patterns of extreme heat in coastal environments

Raymond, C., and Mankin, J. S. Coastal moderation of extreme heat in the eastern United States. In second-stage review at *Geophys. Res. Lett.*

Introduction

Extreme heat varies substantially on spatiotemporal scales finer than those regularly represented by global or even regional climate models. Variations in land-cover type, differences between thermal characteristics of land and water, and anthropogenic waste heat can all cause certain locations to experience especially marked complexity in their spatial patterns of extreme heat (Hass et al., 2016; Loikith and Broccoli, 2012). These mechanisms — acting at spatial scales of ~100 km or smaller, and temporal scales of ~1 day or shorter — have in many cases been studied only sparingly, even though they often play a crucial role in heat extremes (Lebassi et al., 2009; Diffenbaugh, 2009; Hall et al., 2008; Seneviratne et al., 2006; Diffenbaugh et al., 2005).

Such fine-scale interactions prevail in coastal areas, which frequently experience warm-season daytime cooling relative to nearby inland areas. If the coastal-inland temperature difference is large enough and conditions are otherwise favorable, this cooling can be directly related to a well-defined sea breeze, but it has been observed in the absence of a sea breeze as well (Meir et al., 2013; Lebassi-Habtezion et al., 2011). As a result, hot summer days in the eastern U.S. are typically cooler near the coast, with major implications for population exposure to extreme heat. Previous studies have noted the importance of 'coastal cooling' for ameliorating heat and pollution (Clemesha et al., 2018; Melecio-Vazquez et al., 2018; Meir et al., 2013), and have found large regional heterogeneity in projected future changes in coastal cooling (Zhao et al., 2011).

However, comprehensive studies of the characteristics of this coastal cooling are lacking. This may be because suitable datasets are not readily available: the cooling exists on too small of a scale to be easily captured by climate models, and it is also difficult to assess using weather stations, due to a patchy observational network. Much recent work on temperature extremes in the U.S. has used Earth System Models [ESMs] or reanalysis datasets that are too spatially coarse to resolve coast-to-inland temperature gradients and the coastal-cooling phenomenon (Papalexiou et al., 2018; Ashfaq et al., 2016; Wuebbles et al., 2015; Thibeault and Seth, 2014); the studies that do use high-resolution gridded products typically take a broader view in their analysis (Zobel et al., 2018; Gao et al., 2012). In a world where heat extremes are rapidly increasing (Horton et al., 2016), and where complex interacting atmospheric and marine processes make regional generalizations and comparisons difficult (Lebassi et al., 2009), comprehensively understanding and quantifying coastal moderation of extreme heat on a region-specific basis is crucial in order to better evaluate how strong projected increases in extreme heat and its impacts will be manifested (Zobel et al., 2017; Ning et al., 2015; Thibeault & Seth, 2014; Gao et al., 2012). Accurate assessment of the spatial footprint of future heat extremes is essential to local- and regional-scale efforts to manage heat exposure and its risks, as this knowledge enables financial, educational, medical, and other resources to be allocated precisely according to need.

In this chapter, I illustrate how current heat extremes are moderated by marine influences along the coastlines of the eastern U.S., and demonstrate that even high-resolution gridded products are unable to represent these effects, causing them to suffer substantial biases for societally relevant metrics such as population exposure to extreme heat. In turn, this situation results in considerable overestimation of extreme heat for coastal and near-coastal areas in future projections. I then analyze regional patterns of coastal cooling over the recent historical record to

position my consideration of how projections of future heat extremes may be biased due to the model challenges I describe. This chapter considers temperature exclusively, in line with the bulk of the heat-health literature (Mitchell et al., 2016; Gasparrini et al., 2015); subsequent chapters add in humidity, which in combination with temperature is more highly correlated with health outcomes (Davis et al., 2016).

Region	Coastal Gridpts	Regional Hot Days	Mean Intensity (C)	Mean Distance (km)
Northern New England	95	561	4.52 (1.81-7.36)	38.7
New Jersey and Delmarva	49	529	2.69 (0.49-5.35)	30.2
Carolinas and Georgia	116	540	2.24 (0.31-4.44)	32.0
Florida Peninsula, Atl Coast	105	462	2.07 (0.34-4.04)	29.7
Florida Peninsula, Gulf Coast	59	484	1.88 (0.35-3.91)	28.5
Central Gulf Coast	182	458	2.42 (0.52-4.61)	34.9
Texas	104	404	3.69 (1.29-6.55)	40.5

Table 1.1: (Columns 1 and 2) The number of coastal grid points and regional hot days resulting from the PRISM analysis. The total number of points comprising each regional distribution is thus the product of these two columns. (Columns 3 and 4) Summary of the means of the coastal-cooling intensity and distance calculations discussed in the text. Intensity ranges span the 5th-95th percentiles of the distribution, making the cooling significant based on a two-tailed t-test. From Raymond and Mankin (2019), in review.

LOCA		
Model	**Native Lat Res**	**Native Lon Res**
CanESM2	2.79	2.81
CCSM4	0.94	1.25
CESM1(CAM5)	0.94	1.25
CMCC-CM	0.75	0.75
CNRM-CM5	1.40	1.41
CSIRO-Mk3.6.0	1.87	1.88
EC-EARTH	1.12	1.12
GFDL-ESM2M	2.02	2.50
GISS-E2-H	2.00	2.50
HadGEM2-ES	1.25	1.88
IPSL-CM5A-MR	1.27	2.50
MIROC5	1.40	1.41
MRI-CGCM3	1.12	1.13
NorESM1-M	1.89	2.50
Zobel et al. 2017		
Model	**Native Lat Res**	**Native Lon Res**
WCNB (CCSM4)	0.94	1.25
WCB (CCSM4)	0.94	1.25
WGNN (GFDL-ESM2G)	2.02	2.00
WGN (GFDL-ESM2G)	2.02	2.00
WH (HadGEM2-ES)	1.25	1.88

Table 1.2: Models comprising the LOCA and Zobel ensembles. For the Zobel models, abbreviations match those of the authors, with ‘NB’ (‘B’) suffixes referring to non-bias-corrected (bias-corrected) products and 'NN' ('N') suffixes referring to non-nudged (nudged) products. From Raymond and Mankin (2019), in review.

Data and Methods

Here, I primarily use historical daily-maximum temperature data for 1981-2015 from the 4-km-resolution Parameter Regression on Independent Slopes Model [PRISM] (Daly et al., 2008). PRISM takes weather-station data as input and processes it using terrain- and coast-aware statistical approaches to produce a best-estimate gridded product (Daly et al., 2003). In the eastern U.S., PRISM employs a coastal-advection model that assumes a grid point's coastal influence is a simple function of distance from the coast, with bays and inlets treated as transition zones and terrain effects assumed negligible. Previous case studies have demonstrated that 4-km-resolution

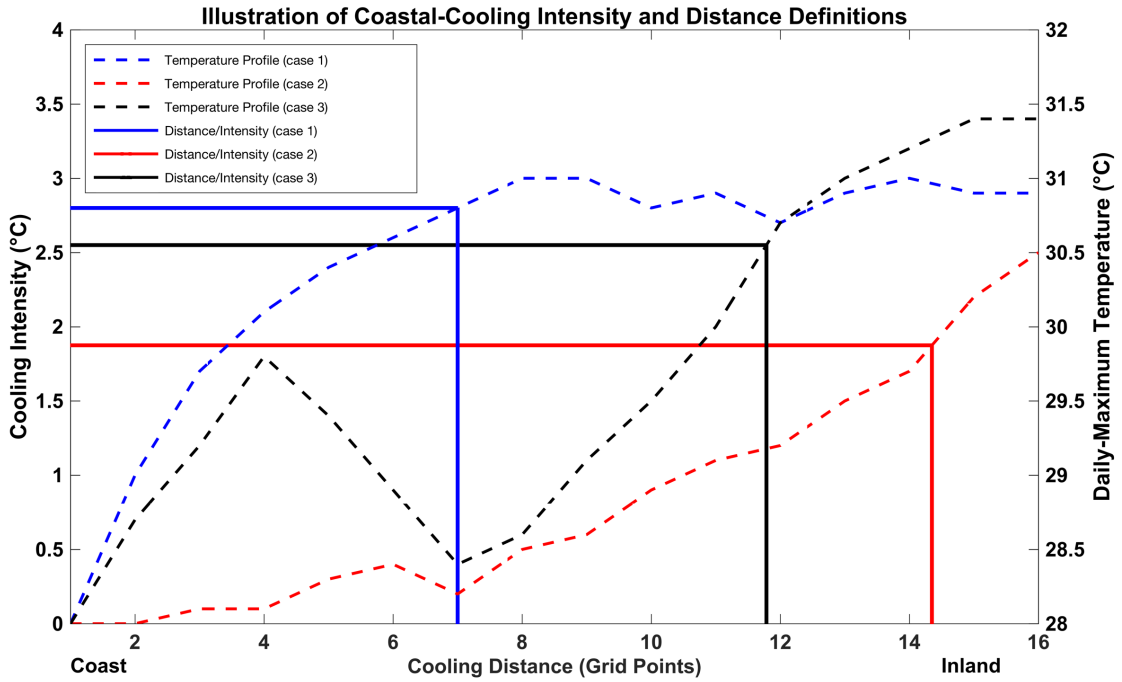

Figure 1.1: Schematic illustration of the definitions of coastal-cooling intensity and distance. Blue, red, and black colors represent three hypothetical coast-to-inland regional-average profiles of daily-maximum temperature, with horizontal (vertical) bars indicating the calculated coastal-cooling intensity (distance). The blue profile shows a case where the cooling extends to where the profile flattens; red, a deep infiltration of coastal cooling; black, a near-coastal fluctuation of small enough scale that we assume coastal cooling is responsible for the continued increase in temperature beyond. From Raymond and Mankin (2019), in review.

gridded data matches well against weather stations (Lebassi-Habtezion et al., 2011; Novak and Colle, 2006), a validation that I also perform using stations from the Global Surface Hourly and Global Historical Climatology Network-Daily datasets (Menne et al., 2012). Regional-scale analyses are conducted for the seven eastern-U.S. regions listed in Table 1.1.

Model data, both historical simulations and future projections, come from two ensembles of daily-resolution downscaled ESMs (Table 1.2). From the Localized Constructed Analogs [LOCA] project (Pierce et al., 2015; Pierce et al., 2014), I use a statistically-downscaled (~6-km-resolution) 14-ESM ensemble of historical runs (1981-2005) and future projections for the high-emissions RCP8.5 scenario (2075-2099) (Meinshausen et al., 2011). From a dataset produced by Zobel et al. [2017, 2018], I use an ensemble of five ESM model variants dynamically downscaled with the Weather Research and Forecasting model to ~10-km resolution [hereafter referred to as Zobel]. These data are for 1995-2004 (historical) and 2085-2094 (future, RCP8.5). The two ensembles are some of the only high-resolution multi-decadal simulations spanning the entire eastern U.S., a spatial comprehensiveness that enables estimation of the degree to which downscaled products overstate coastal extreme heat in both current and future climates. A critical element in coastal extreme heat is sea-surface temperatures (Diffenbaugh et al., 2007), which in both ensembles are not downscaled and are therefore of coarser resolution than the land data. Biases in coastal extreme heat that I find consequently motivate efforts to improve the representation of coastal waters in models and reanalysis products.

Within each of the seven regions, grid points are aggregated based on their distance from the model-defined coastline. To ensure the accuracy of comparisons among the various resolutions of gridded products, I focus the analysis on sections of coastline lacking bays or estuaries larger than 50 km in width, and where coastal weather stations face the open ocean, as indicated by the

heavy black line in Figure 1.2. This approach avoids the problem of different representations of bays and estuaries among ESMs, and the complexity of weather conditions that is often associated with these features (Novak and Colle, 2006). Terrain concerns also motivate the restriction of the study area to the eastern U.S., where terrain variations are small within 100 km of the coast.

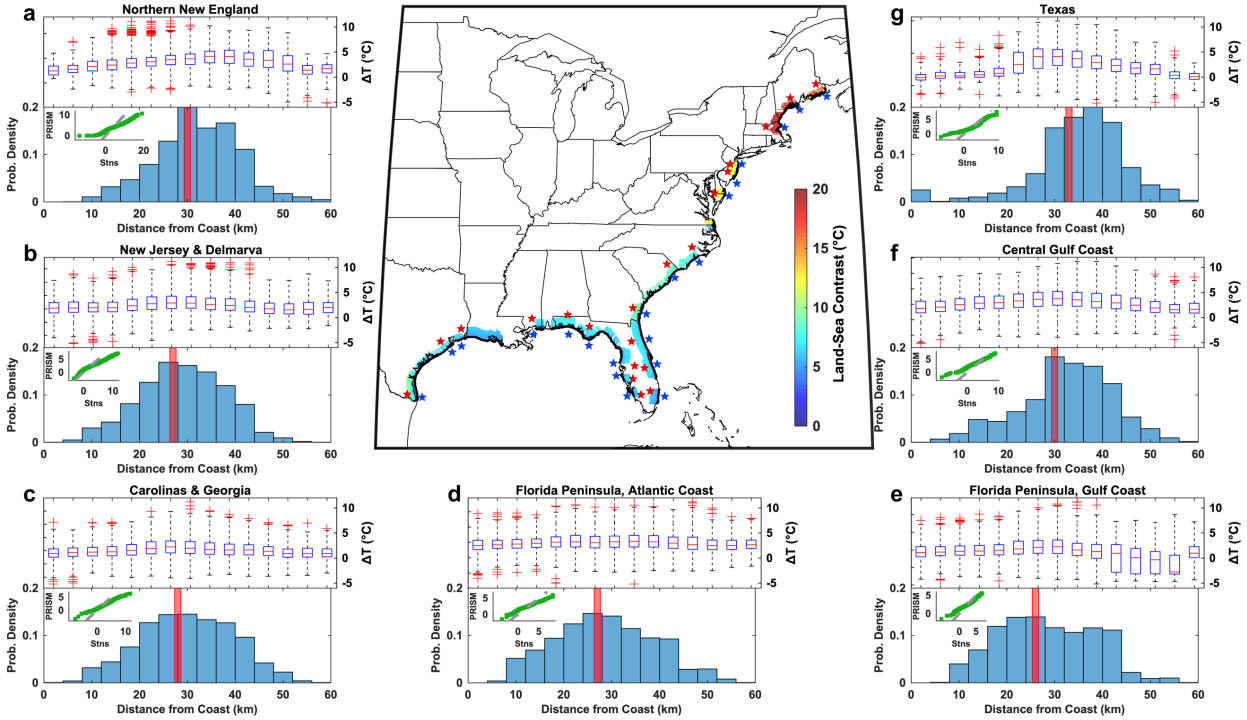

Figure 1.2: (Central map) Land-sea contrast on extreme-heat days in each region (shading). Stars indicate locations of inland (red) and coastal (blue) stations used as verification for each region, with coastal stations offset for visibility. A strong latitudinal correlation is apparent. (a-g) Top panels illustrate the range of coastal-cooling intensities associated with each characteristic coastal-cooling distance bin, while bottom panels illustrate the probability distribution of each coastal-cooling distance, with red lines indicating the mean of the distance distribution. Insets are quantile-quantile plots comparing the coastal-cooling intensity as calculated from the plotted stations (abscissa) with that calculated from the nearest grid points in the PRISM dataset (ordinate), validating the use of PRISM in the analysis. The broad similarity of the coastal-cooling distance distributions among regions stands in contrast to the marked variations in coastal-cooling intensity. From Raymond and Mankin (2019), in review.

For each section of coastline I define an 'inland' area located 60 km away from the coast, perpendicular to the local coastline direction. This 60-km distance is far enough inland to be beyond the typical reach of daytime coastal effects, such as sea breezes, coastal clouds, or

precipitation (Hu and Xue, 2016; Finkele, 1998), and small enough that differences due to synoptic-scale weather conditions are minimized. Due to their complexity and small scale, I focus on the combined long-term-average temperature impacts of these coastal-cooling effects rather than attempting to disentangle the contributions of specific processes on specific days. Daily

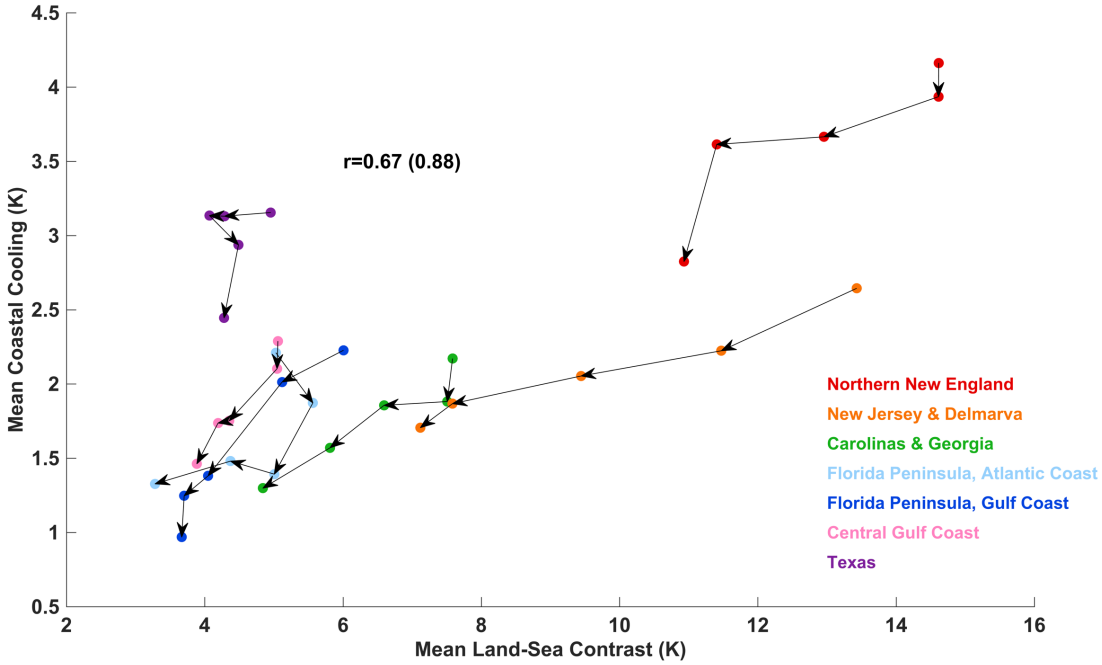

Figure 1.3: Correlation between mean land-sea contrast on regional hot days (ordinate) and mean corresponding coastal cooling (abscissa). Colors represent regions, for which the seasonal evolution of monthly averages from May to September is indicated by the arrows. As noted in the text, the correlation across all regions and months is 0.67, or 0.88 excluding Texas. This strong correlation indicates that land-sea contrast is a good proxy for coastal-cooling intensity, in both a regional and a seasonal sense. From Raymond and Mankin (2019), in review.

maximum temperature at 60 km inland is assumed to represent a counterfactual case for the coast — that is, what temperatures would have been there if not for cooling effects — and the extreme rarity of sea breezes reaching that far inland supports the assertion that few if any inland hot days are affected by coastal cooling. Areas with rolling topography or significant variations in land cover may have consistent local temperature variation that is unaccounted for here, although such variation would be smoothed out and diluted in the regional average. Similarly, urban heat islands

are not explicitly addressed, but their relatively small fraction of total land area limits the impact of this simplification.

I define 'hot days' as the top decile of PRISM daily maximum temperature in May-September, based on a daily grid point climatology temporally smoothed with a Gaussian

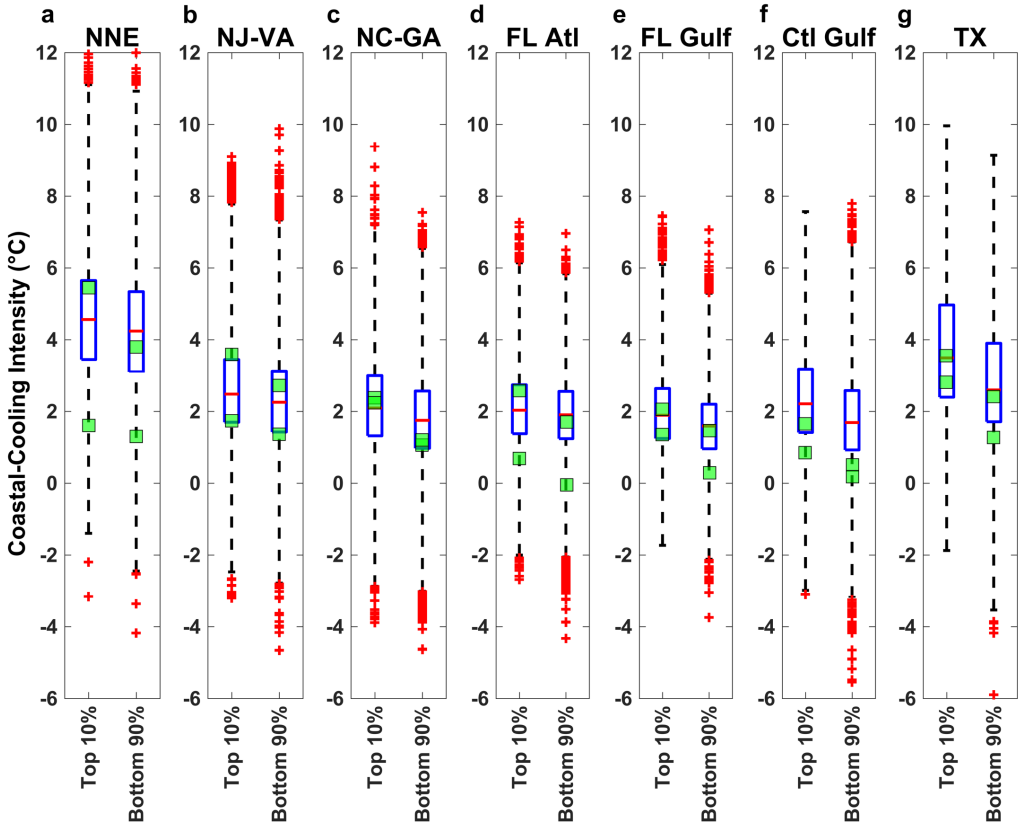

Figure 1.4: For each of the seven eastern-U.S. coastal regions, the complete distribution of differences between inland and coastal regional-average daily-maximum temperature in PRISM on regional hot days (left, top 10%) and all other days (right, bottom 90%). Green squares indicate the mean of differences between the two inland-coastal station pairs for each region, whose locations are shown in Figure 1.2. This figure shows in more detail the inter-regional differences in mean coastal-cooling intensity, as well as the even larger spread when considering individual days. The agreement between the PRISM mean and the station-sample mean gives confidence that the center of the distribution, at least, is well-represented by PRISM. From Raymond and Mankin (2019), in review.

filter, a common method for avoiding spurious day-to-day variations (Freychet et al., 2018). Statistics are averaged across months to gain statistical power, and because subseasonal differences within each region, though significant, are not so large as to obscure the fundamental picture with

respect to spatial patterns or future changes (Figure 1.3). A set of hot days is computed for each of the seven regions, defining 'regional hot days' as those for which at least 50% of regional inland grid points are individually experiencing a hot day, following the methodology of Smith et al. [2013]. The number of regional hot days varies slightly by region as a function of the spatial correlation among its constituent grid points. Averaging over many grid points and hot days (Table 1.1) allows me to draw robust statistical conclusions about coastal ventilation of extreme heat.

For each regional hot day, I define ‘coastal cooling’ as proportional to the difference in daily maximum temperature between a 3-grid-point average along the coast and a 3-grid-point average 60 km inland. The coast-to-inland temperature profile over this 60-km distance can be non-monotonic (Figure 1.1), making it helpful to choose a percentage of the coast-to-inland temperature difference that characterizes the distance over which the coastal cooling is primarily expressed. To obtain a (conservative) estimate for average coastal cooling, I define the ‘coastal-cooling intensity’ as equal to 75% of the magnitude of the coast-to-inland temperature difference (Figure 1.1). ‘Coastal-cooling distance’ is then the distance from the coast where this intensity is met. Choosing a percentage higher (lower) than 75% results in a larger (smaller) value of coastal-cooling intensity, but a sensitivity analysis confirms that it does not affect the comparison among the regions. A large coastal-cooling distance implies deep ventilation of coastal air inland, while a small coastal-cooling distance implies that coastal cooling is confined closer to the coast.

Coastal populations are estimated from the 1-km-resolution Gridded Population of the World dataset (CIESIN, 2016); my resulting estimate of a total of 50 million people residing within 60 km of the Atlantic Ocean and Gulf of Mexico coasts aligns well with a previously reported value of 54 million (Wilson and Fischetti, 2010). In computing future population exposure, I focus on changes in climate by assuming that populations are fixed in size and spatial distribution.

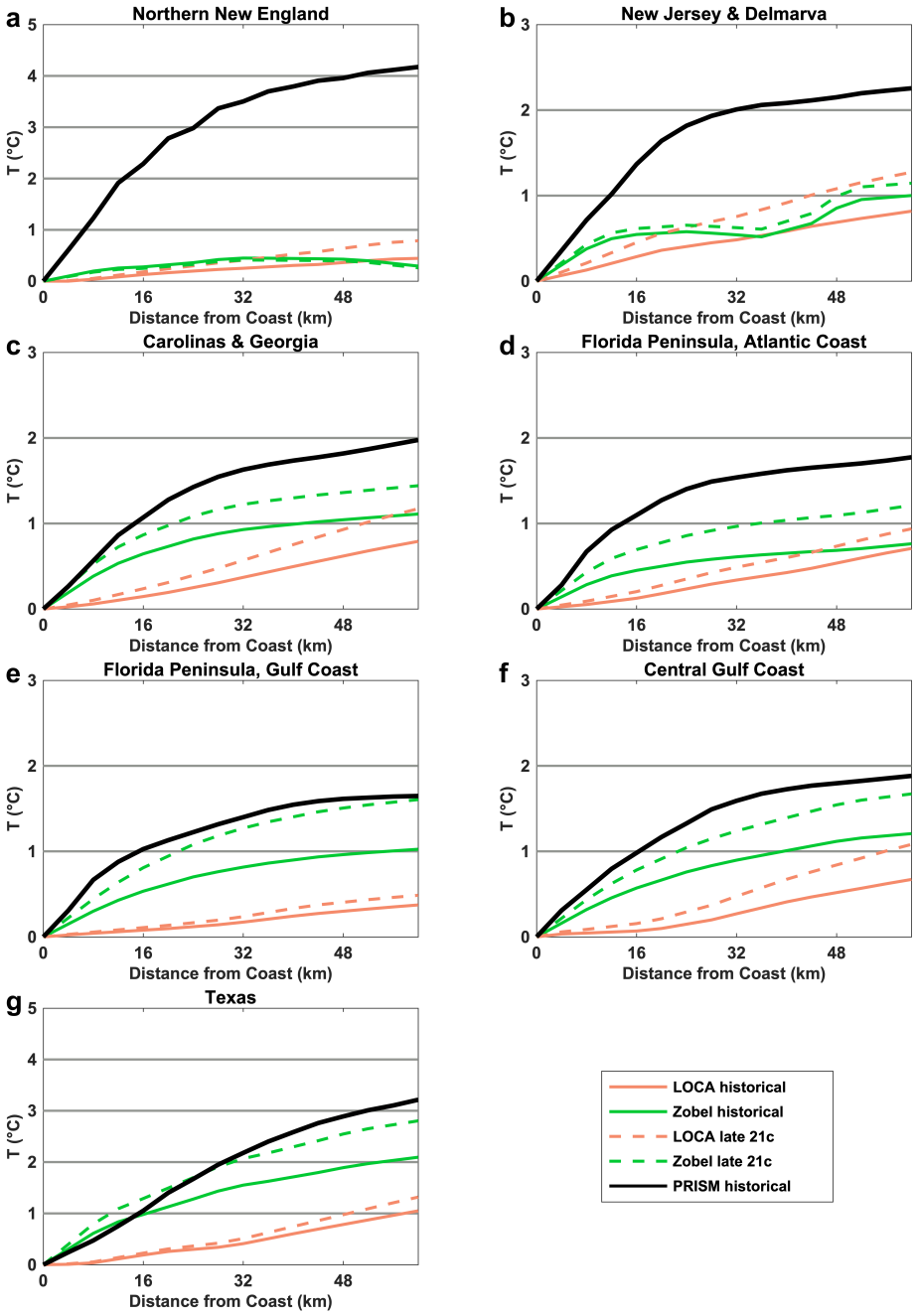

Figure 1.5: Mean maximum temperatures within the 60-km coastal swath on regional hot days, expressed relative to the coastal temperature. For the historical period, 4-km PRISM (black) contrasts with the downscaled products (solid lines): 6-km LOCA and 10-km Zobel. Future projections are dashed. Color-coded numbers indicate the mean coastal-cooling intensity, as defined in Methods. Models underestimate true coastal cooling by a margin which is especially large in the northern regions, but is in most cases at least 50%. Models also are consistent with each other, to within ~1°C, and suggest a modest increase in coastal cooling over the 21st century. From Raymond, Mankin, (2019), in review.

Results and Discussion

Comparing against station data, PRISM captures much of the statistical distribution of observed coastal cooling on hot days but underestimates both positive and negative extremes, as seen in the regional quantile-quantile plots (Figure 1.2). PRISM biases are greatest for coastal cooling greater than 10°C and for coastal warming, deviations which I trace to poor representation of days with fast-changing synoptic conditions and large coast-inland temperature differences. This knowledge allows me to rely on PRISM to draw conclusions that are applicable to the large majority of extreme-heat days: those with coastal-cooling values of approximately 0-7°C.

PRISM daily-maximum temperatures are typically suppressed by several degrees Celsius at the coast relative to nearby inland areas, with the majority of this coastal-cooling intensity occurring within about 30-40 km of the coast (Figure 1.2). The cooling effect can extend past 50 km inland, though such occurrences are rare. The intensity of the cooling at different distances is highly variable across days, denoted by the spread in the box plots shown in Figure 1.2, and across regions, from around 2°C for the Southeast U.S., including Florida, to near 3.5°C (4°C) for Texas (Northern New England) (Figure 1.4). Figure 1.4 also demonstrates that evaluating coastal cooling using pairs of weather stations (one at the coast and one situated 50-60 km inland) validates the PRISM analysis, by illustrating the center of the weather-station distribution agrees well with the PRISM mean.

While the generally positive summer land-sea temperature contrast present in all regions (Figure 1.2, map) is a known driver of sea breezes (Sequera et al., 2015; Lebassi-Habtezion et al., 2011), the data do not suggest that coastal cooling is always due to a localized and well-defined sea breeze. The consistency of coastal cooling across all warm-season days and regions (Figure 1.4) instead supports the notion that the magnitude of regional land-sea temperature contrasts plays

the dominant role in determining cooling intensity, irrespective of whether such contrasts generate a sea breeze. I find that latitudinal differences in mean cooling intensity are strongly correlated with regional land-sea temperature contrasts accounting for seasonal changes ($r=0.67$), corroborating this hypothesis (Figure 1.2; Figure 1.3). The correlation rises to 0.88 when the outlier region of Texas is excluded, indicating that land-sea contrasts explain coastal-cooling intensity well for the other six regions.

These observations are consistent with different physical processes being responsible for the strong coastal cooling in New England and Texas, regions located at opposite ends of the eastern-U.S. coastline. The former has large land-sea contrasts that pull marine air landward at the surface (Dvorak et al., 2013; Miller and Keim, 2003); as the land-sea contrast decreases over the course of the summer, so does the associated cooling effect (Figure 1.3). In Texas, the land-sea-contrast relationship is insignificant, but the region is distinguished by the strong low-level onshore flow it experiences due to its position underneath the westernmost portion of the North Atlantic Subtropical High, a seasonal feature that advects marine air inland through broad sections of eastern Texas during the summer months (Hu and Xue, 2016; Li et al., 2015; Liang et al., 2006). This type of persistent large-scale circulation has the capability to modulate sea breezes, with results including greater inland infiltration of marine air under onshore-flow conditions (Misra et al., 2011; Gilliam et al., 2004; Miller and Keim, 2003; Arritt, 1993).

Although coastal cooling is widespread in space and time, and is a significant suppressor of extreme heat dozens of km inland, it is poorly represented in gridded products. The LOCA and Zobel downscaled model ensembles ubiquitously and severely underestimate historical coastal cooling: their typical mean cooling is 0.5-2°C, at least a factor of two (and up to a factor of 10) smaller than the observed gradients in station-vetted PRISM (Figure 1.5). These factors are much

larger than the ratios between their spatial resolutions (6-km and 10-km) and that of PRISM (4-km); additionally, model coastal-cooling biases vary substantially between regions, and the Zobel product generally exhibits less bias despite its coarser spatial resolution (Figure 1.5).

Together, these lines of evidence suggest that neither statistical nor dynamical downscaling, in itself, sufficiently corrects for a parent model's inability to represent the fine-scale coastal processes governing the coast-to-inland gradient. Previous work has shown similarly large and pervasive model biases in other U.S. coastal areas (Wang & Kotamarthi, 2014; Lebassi et al., 2009), with performance also often varying considerably by model and by region. The reason for the challenge being particularly acute for LOCA may relate to its methodology, which depends on finding analogues among land-based stations and is therefore less likely to capture marine influences (Pierce et al., 2014). Close to the coast, the dynamically-downscaled Zobel ensemble performs somewhat better, reproducing the majority of the coastal-cooling effect for the Gulf Coast regions (Figure 1.5e-g), but missing the large cooling magnitudes in other regions (Figure 1.5a-d). Zobel is particularly skillful for the Texas coast-to-inland temperature gradient, perhaps a function of WRF representing coastal atmospheric processes absent from coarser models.

Therefore, an essential question that this chapter raises is the extent to which coastal model biases result from problems related to parameterization of sub-grid-scale processes — via inheritance from the driving models or in the downscaling procedure, the latter being the single largest source of uncertainty for high-resolution temperature projections (Xie et al., 2015; Li et al., 2012). The modest inter-model spread in coastal cooling that I find provides an example of a case where selecting models on the basis of process representation, the strategy put forth by Maraun et al. [2017], would only partially address the underlying uncertainty. The overall similarity of biases

across two methodologically distinct downscaled products points to the continuing challenge of generating high-quality future projections for extreme heat along coastlines.

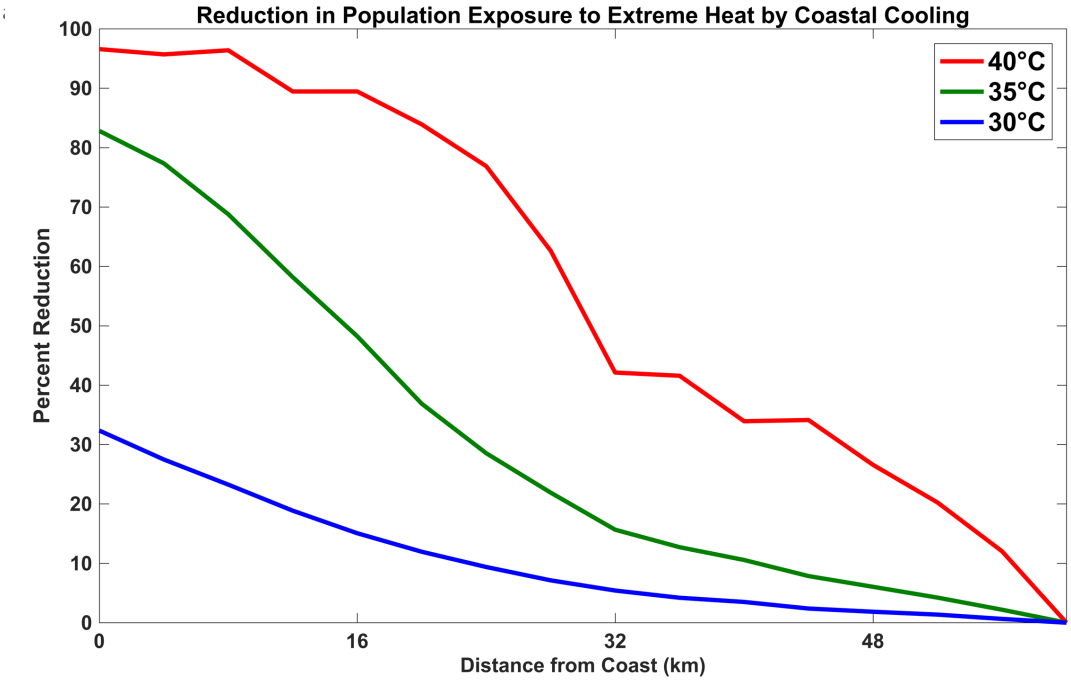

Figure 1.6: Percentage reduction of historical population-weighted exposure to extreme heat, as defined by daily-maximum temperatures exceeding the thresholds shown, from the counterfactual case where the entire coastal swath is the same temperature as 60 km inland. Data are from PRISM. Result shows the dramatic reductions in extreme heat for the highest temperatures, and the exponentially-decaying reductions moving inland from the coast. From Raymond and Mankin (2019), in review.

To better understand the implications of coastal cooling (and its model representation) for heat-impacts assessments, I consider the effect on human exposure to extreme heat. I find that, compared to the counterfactual case where temperatures in the coastal swath are identical to those 60 km inland, observed coastal cooling reduces eastern-U.S. population-weighted exposure to daily-maximum temperatures above 35°C by more than half for locations within 20 km of the coast (Figure 1.6). The greatest reductions occur closest to the coast and for the highest temperatures – for example, 40°C is exceedingly rare along the immediate coast, while such

temperatures are much less exceptional in nearby inland locations. These effects infiltrate far enough inland to affect tens of millions of people. Over the entire 60-km coastal swath and across all regions considered, observed annual exposure to 35°C is about 200 million person-days, or 4 days per person, reduced from 7 days per person in the counterfactual case. These estimates provide an update to previous results obtained at coarser resolution and with an earlier generation of models (Jones et al., 2015), and broaden the conjectures of case studies that the positive health effects of coastal proximity are diffuse and persistent (Burkart et al., 2016). They are also much larger than the numbers obtained from historical downscaled simulations (Figure 1.5), suggesting a major shortcoming of current climate projections along coasts.

The 1-4°C reductions that these numbers reflect are critical from a human-health perspective, as health effects and mortality rise rapidly and often non-linearly for daily-maximum temperatures above 35°C (Wu et al., 2014; Gosling et al., 2007). Applying temperature-mortality relationships from Schwartz et al. [2015] for eastern-U.S. urban areas yields the estimate that observed coastal cooling reduces mortality by ~20%, amounting to around 300 fewer deaths per year for the historical total annual exposure of 200 million person-days. This calculation omits additional economic savings (such as reduced need for air conditioning), which are also multiplied by occurring in densely populated areas. Focusing on temperature, as in this chapter, means that coastal cooling — whether or not associated with a sea breeze — has a simple unidirectional effect on risk; the concomitant increase in humidity means that coastal cooling's effects are more complex and regionally dependent when assessing heat-stress metrics (Diffenbaugh et al., 2007), considered in Chapters 2 and 3.

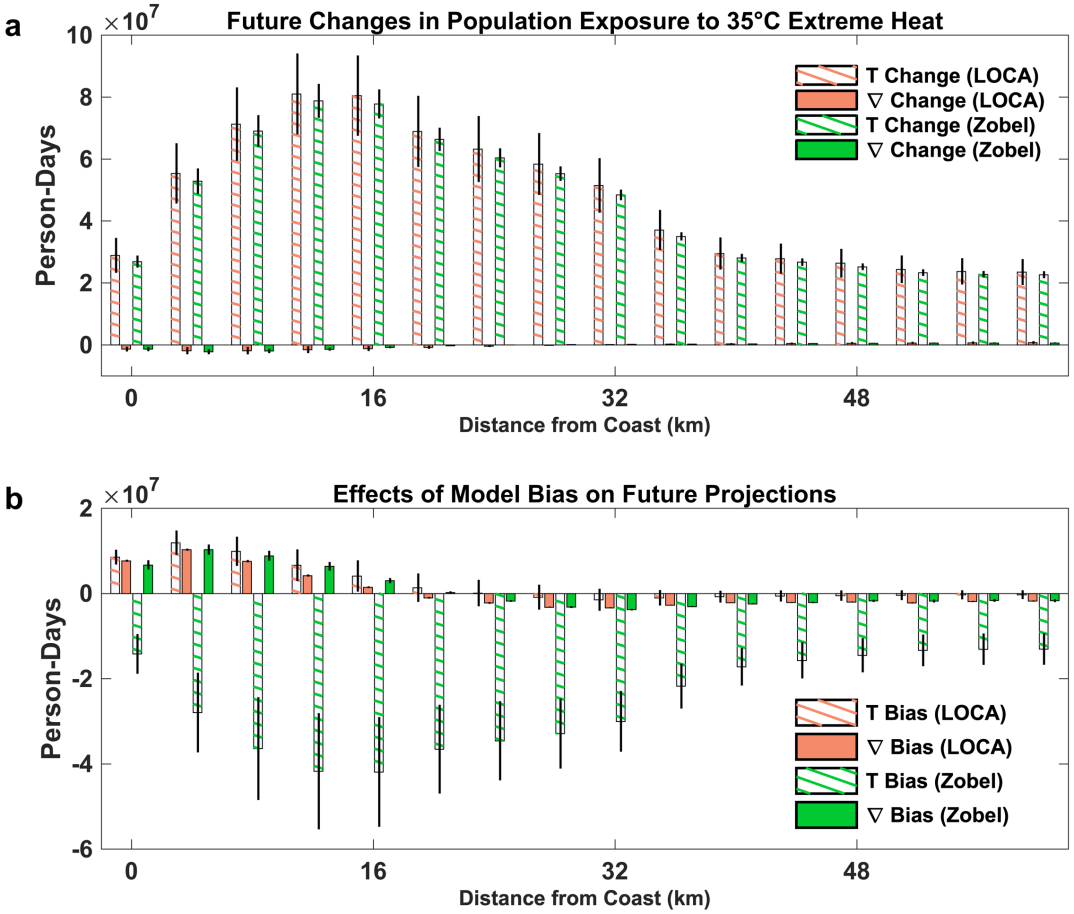

Figure 1.7: (a) Contributions of changes in mean temperature (hatched) and in coast-to-inland-temperature-gradient steepness (solid shading) to future population exposure to extreme heat in the LOCA (orange) and Zobel (green) ensembles. Changes are calculated using bias-corrected values so as to allow for meaningful comparability. Error bars indicate a cross-model uncertainty of +/- one standard deviation from the mean. (b) As in (a) but for contributions from model biases affecting the population-exposure projections. The sum of (a) and (b) returns the non-bias-corrected projections of the two ensembles. Future changes in population exposure to extreme heat are large, well-agreed-upon between the two ensembles, and dominated by changes in mean temperature. Non-bias-corrected projections incorporate major biases, which vary considerably among regions and by type (mean versus gradient). From Raymond and Mankin (2019), in review.

Future changes in population exposure to extreme heat by the end of the 21st century are large and are dominated by mean-summer-temperature increases of 3-6°C (Figure 1.7) (Vose et al., 2017; Lynch et al., 2016). For example, projections indicate an approximately 5-fold increase for extreme heat above the 35°C threshold. Decomposing the change in population exposure into

a component due to mean warming across the 60-km coastal swath and one due to spatially variable warming within that swath, I find that the effects of mean warming predominate, with a slight offsetting effect from a relative strengthening in coastal cooling (magnitude about 0.5°C) in both the LOCA and Zobel ensembles (Figure 1.7a). This modestly increased coastal cooling projected by the models is consistent with my finding of strong correlations between coastal cooling and land-sea temperature gradients (Figure 1.3), and with the expected circulation response to increases in warm-season land-sea temperature gradients (Dong et al., 2009; Joshi et al., 2008). Due to the models' underestimation of coastal-cooling magnitude, the 0.5°C strengthening may be a dampened projection relative to the true response.

Being based on PRISM temperatures adjusted by model changes, these values represent a best estimate of future population exposure near the coast. Without referencing PRISM, the LOCA and Zobel curves would look much different due to their significant biases, as illustrated in Figure 1.7b. An insufficiently steep coast-to-inland temperature gradient in both ensembles leads to positive gradient biases within 16 km of the coast and negative ones further inland. Mean biases vary from moderately positive to strongly negative. These problems have serious implications for accurate assessments and projections of extreme heat, as the exponential tails, which are most important for impacts calculations, are drastically underestimated. Members within each ensemble generally agree well with each other, particularly with regard to the causes of future increases in population exposure. Intermodel agreement about the sign and relative magnitude of these future changes, despite considerable differences over the historical period, is likely due to downscaling's preservation of the forced response to global-mean warming (Hall, 2014).

Characterizing the magnitude and location of extreme-heat impacts is crucial from a policy perspective on multiple levels. First, climate impacts (and adaptations) are experienced (and

adopted) locally, so identifying local risks of extreme heat is essential to effective risk management (Kunreuther et al., 2013). Second, understanding how impacts can vary considerably over small length scales is valuable in evaluating adaptation strategies and allocating resources, particularly for municipalities that include both coastal and inland areas. Finally, to best inform decision-making, it is imperative to articulate the full range of climate impacts consistent with the same level of global-mean warming, even if these impacts are complicated or heterogeneous (Mankin et al., 2017).

In this context, it is evident that future work must better integrate high-resolution observed and/or modeled coastal water temperatures into coastal air-temperature projections, in order to at least reduce the large biases of existing projections. While such modeling frameworks have recently begun to be regularly applied at short temporal scales and small spatial scales (Pullen et al., 2017), they have not yet been generally included in standard long-term gridded products of the type which are employed in climatological assessments. Meteorologically, sea breezes in particular remain poorly understood, so much so that they are not explicitly represented in most models or reanalyses. Efforts to develop parameterizations that account for synoptic-scale forcings, terrain, and urbanization effects are therefore critical to improve representations of extreme heat in coastal areas.

The results of this chapter make evident that future extreme heat will vary widely over distances that are too small for state-of-the-art global models to properly simulate, even when downscaled. This gives the coastal-cooling effect a continuing importance in mitigating population exposure to extreme heat in a world that is rapidly warming (Jones et al., 2018). Local fine-scale processes must therefore be considered carefully in order to ensure an accurate assessment of the present and future risks posed by extreme heat along the coastline of the eastern United States.

In Chapter 2, I continue examining fine-scale processes modulating extreme heat, but include moisture so as to approximate heat stress, a variable of particular relevance to comfort, health, and energy demand. Although of demonstrable utility for impacts, the bivariate nature of heat stress makes it more complex to analyze than temperature alone, meaning the literature is in a more-embryonic state, and consequently my contributions in Chapters 2 and 3 are of a more geographically broad and conceptually fundamental nature.

Chapter 2: Extreme humid heat and its regional patterns

Raymond, C., Singh, D., and Horton, R. M. (2017). Spatiotemporal patterns and synoptics of extreme wet-bulb temperature in the contiguous United States. *J. Geophys. Res. Atmos., 122*. doi:10.1002/2017jd027140.

Raymond, C., Matthews, T. K., and Horton, R. M. The emergence of heat and humidity too severe for human tolerance. In second-stage review at *Sci. Adv.*

Introduction

Extreme heat is one of the most dangerous natural hazards across regions and societal indicators (Raymond et al., in press), and in terms of mortality has resulted in tens of thousands of fatalities in the worst events so far this century (Robine et al., 2008). Extreme heat-humidity combinations are especially potent, in that they interfere with our well-developed capacity for thermoregulation (Davis et al., 2016; Hanna and Tait, 2015). As a result, they have additive impacts that extend beyond direct health outcomes to include reduced individual performance across a range of activities, as well as large-scale economic losses (Matthews et al., 2017; Mora et al., 2017; Kjellstrom et al., 2016). These humid-heat effects have prompted decades of study in medical, military, athletic, and occupational contexts (Parsons, 2006; Sawka et al., 2003). Unlike the extreme dry-bulb heat considered in Chapter 1, consideration of extreme humid heat by climate scientists has emerged as a distinct subfield only in the last decade or so (Schär, 2016; Sherwood and Huber, 2010). Recent work has revealed important patterns of climatological occurrence, but has relied primarily on reanalysis datasets and correlational explanations (Im et al., 2017; Pal and Eltahir, 2016).

Wet-bulb temperature [Tw] is the temperature to which an air parcel would cool if as much water as possible were evaporated into it. The metric therefore provides a good estimate of the cooling efficiency of sweat, and this direct physiological relevance makes it useful for assessments of heat stress. Tw is a nonlinear function of both dry-bulb temperature and specific humidity (Stull,

2011). A more complex quantity, wet-bulb globe temperature, is also used in public-health research but rarely in climate science, due to uncertainties in estimates of its necessary components and its strong correlations with Tw (Willett and Sherwood, 2012).

Across metrics, morbidity and mortality increase sharply with increasing heat and humidity (Willett and Sherwood, 2012; Kalkstein and Davis, 1989), as do economic impacts (Dunne et al., 2013). These impacts would be large even in a stationary climate (Davis et al., 2016; Burke et al., 2015; Wu et al., 2014); adding to their importance is the fact that — in most observational records and all future projections — combined heat-humidity increases are more robust and widespread than increases in temperature or moisture alone (Mora et al., 2017; Grotjahn et al., 2016; Knutson and Ploshay, 2016; Fischer and Knutti, 2013; Anderson et al., 2010). However, regional variations in these increases are affected by local climate (Matthews, 2018), and the question of how Tw extremes will change on a regional basis remains largely unanswered due to uncertainty in relative changes of dry-bulb temperature vis-à-vis specific humidity, which result from complex multiscale interactions involving the atmosphere, ocean, and land surface.

Small-scale variability of Tw, whether spatial or temporal, is especially hard to constrain due to the limited availability of reliable subdaily near-surface humidity data. A few studies have noted seasonal fluctuations in either extreme heat or extreme moisture, such as in the western U.S. (Lee and Grotjahn, 2016; Adams and Comrie, 1997). There have been some previous efforts to separate out the influence of atmospheric temperature and moisture (Pielke et al., 2004), but no such previous analysis has been conducted across multiple regions, nor aimed at characterizing spatiotemporal variations in extreme Tw. My approach in this chapter is to improve estimates of Tw's spatial and temporal (seasonal) heterogeneity, and then leverage these to better identify

where the generally increasing contribution of latent heat to Tw extremes (Matthews, 2018) will likely cause them to rise at a relatively faster or slower rate.

Tw extremes have been hypothesized to relate to unusually warm sea-surface temperatures, but this has not been evaluated except in a few case studies (Im et al., 2018; Pal and Eltahir, 2016). This state of affairs leaves open large areas for investigation relating to Tw predictability on meteorological timescales as well as refinements for decadal- and centennial-scale projections. Systematic surveys often reveal parts of a picture that are obscured when only several regions of interest are focused on, as is the case in the still-emerging field of extreme humid heat. It is for this reason that the scope is the entire United States for some of my analyses here, and the entire world for others, rather than only the hottest most-humid area within each. As in Chapter 1, after establishing the largest-scale picture, I explore regional geographic and meteorological features of interest.

In this chapter, I present the first characterization of the patterns and synoptics of Tw extremes, highlighting differences between regions. I illustrate and discuss basic spatiotemporal patterns of Tw extremes, and develop new methodology to consider the interplay between temperature and specific humidity that underlie them. I then identify associated sea-surface-temperature, atmospheric-circulation, and energy-flux anomalies at hemispheric and regional scales. This chapter surveys Tw extremes broadly, with conclusions primarily applicable to the historical instrumental record; Chapter 3 builds on this one in focusing on the very highest values and their trends and projected changes.

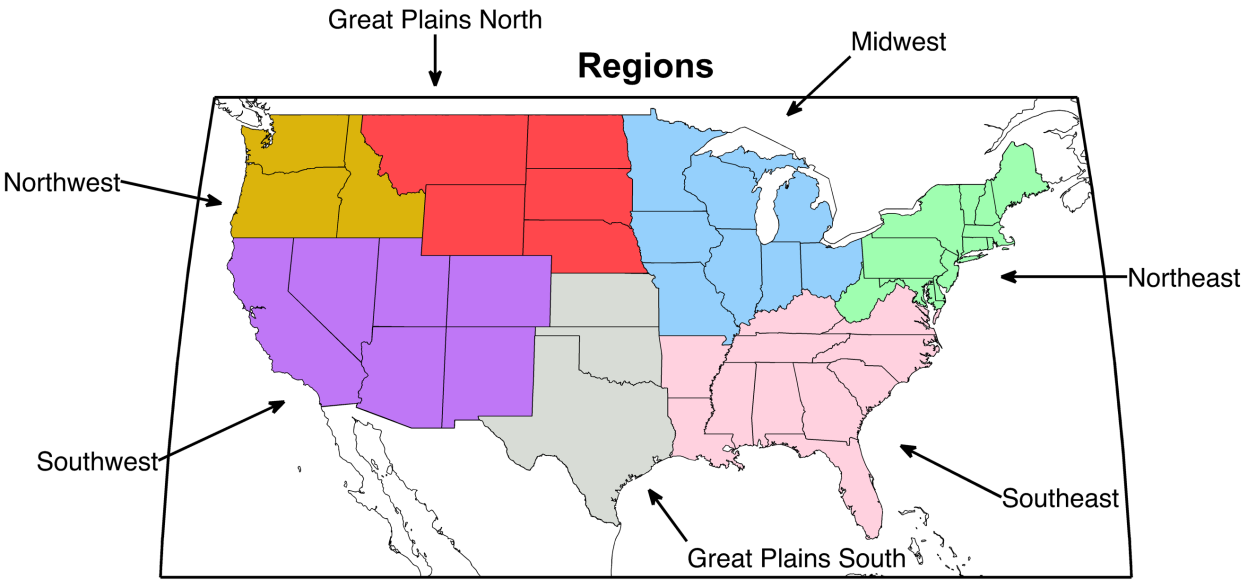

Figure 2.1: The seven regions used in the U.S. portion of this chapter. These are identical to those in the Fourth National Climate Assessment. From Raymond, Singh, Horton, 2017

Data and Methods

Initially, I focus on the United States, where high-quality reanalysis and weather-station data are available. I select stations from the National Climatic Data Center's Integrated Station Database (Smith et al., 2011) that have available hourly data for all years in 1981-2015. For these 520 stations, I standardize irregularly timed observations using linear interpolation such that there is one observation each hour at the top of the hour, and conduct additional interpolation to fill data gaps of up to 4 consecutive hours. I then apply the following two criteria to eliminate station-year combinations: (a) having a data gap of >=4 hours or (b) having >=3% of temperature or relative-humidity data missing. A station is eliminated completely if >33% of its years have been disallowed. I enact additional quality control by algorithmically and visually identifying outliers, and comparing these with other values at the same station and nearby. The final dataset comprises the 175 stations that passed all tests.

Additional atmospheric variables for the U.S. come from the North American Regional Reanalysis [NARR] dataset at 3-hourly, 32-km resolution (Mesinger et al., 2006). I use sea-surface temperature [SST] data from the daily, 0.25°x0.25° NOAA Optimum Interpolation SST dataset (Reynolds et al., 2002). Energy fluxes are computed for daily averages of seven standard NARR variables (upward shortwave, downward shortwave, upward longwave, and downward longwave radiation, and ground, sensible, and latent heat), as well as of temperature [T] and specific-humidity [q] advection, using T and q at 2 m above ground level and wind speed at 10 m. Values of T and q advection in units of W/m^2 are converted to energy fluxes (in units of K/sec and (g/kg)/sec respectively) via:

$$V \cdot \nabla T_{[\frac{W}{m^2}]} = V \cdot \nabla T_{[\frac{K}{sec}]} * c_p * \rho_{column} \quad \textbf{(Equation 2.1)}$$

$$V \cdot \nabla q_{[\frac{W}{m^2}]} = V \cdot \nabla q_{[\frac{\frac{g}{kg}}{sec}]} * L * \rho_{column} \quad \textbf{(Equation 2.2)}$$

where c_p is the specific heat capacity of air at 300 K in J kg^{-1} K^{-1}, ρ_{column} is the mean atmospheric column density in kg/m^2, and L is the latent heat of vaporization of water in J/g. These conversions are my own, though they build on comparisons between horizontally and vertically oriented energy fluxes that have been made previously (Miralles et al., 2014; Trenberth et al., 2011; Nakamura and Oort, 1988).

I compute Tw at weather stations using the formula of Stull [2011]:

Equation 2.3: $\text{Tw} = T \tan^{-1}[0.151977(RH + 8.313659)^{0.5}] + \tan^{-1}(T + RH) - \tan^{-1}(RH - 1.676331) + 0.00391838(RH)^{1.5} \tan^{-1}(0.023101RH) - 4.686035$

where Tw and T are in °C and relative humidity [RH] is in %.

Daily maxima are then computed at individual stations and averaged across seven regions (Figure 2.1) based on those used in the National Climate Assessment (Melillo et al., 2014): Northwest,

Southwest, Great Plains North, Great Plains South, Midwest, Southeast, and Northeast. I compute daily regional maxima by averaging values across all *n* stations within each region, with *n* ranging

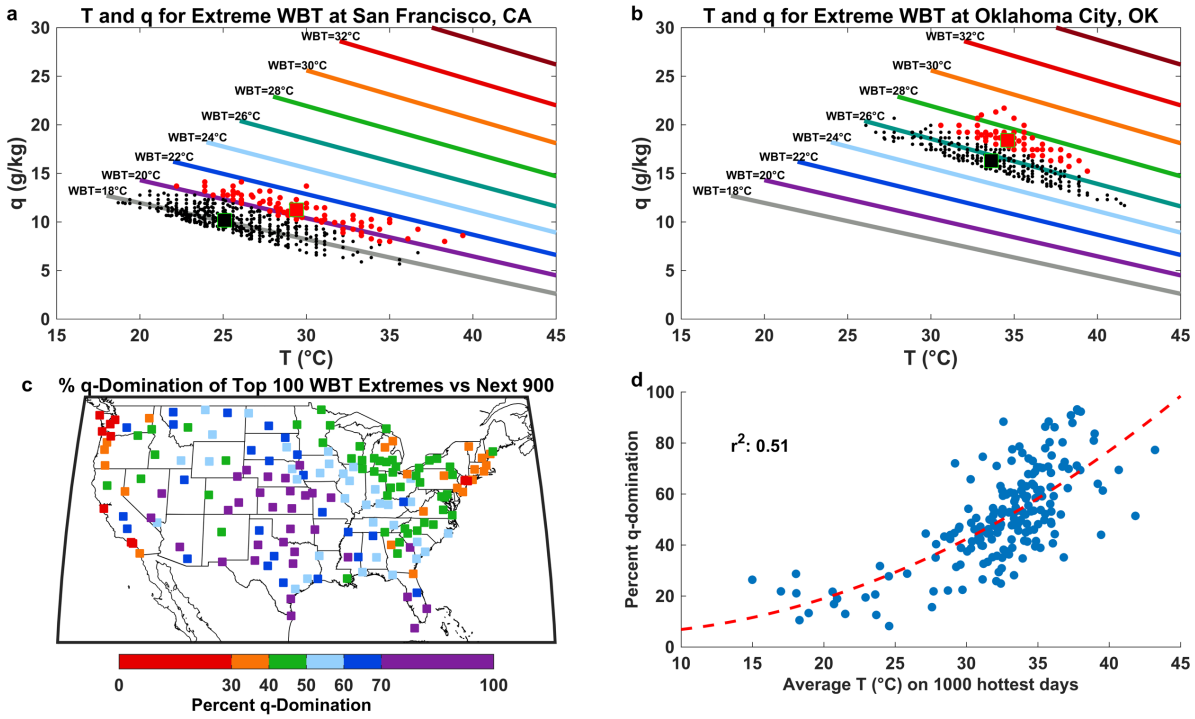

Figure 2.2: (a,b) An illustration of the definition of (a) T-dominated (a) and (b) q-dominated Tw extremes, where red (black) dots represent Tw extremes #1-100 (#101-1000), plotted in T-q space for San Francisco, CA and Oklahoma City, OK. The large squares within the clouds of dots (outlined in light green) are the mean of each set, and the superimposed colored lines are constant values of Tw. The more vertical the vector from the black square to the red square, the more q-dominated are a station's Tw extremes. Due to finite instrument precision, some values may be identical to others and therefore plot directly on top of them. (c) The percent q-dominance for each of the 175 stations, computed using the angle of the vector between the large black dot and the large red dot for each station (as in (a) and (b)), which is converted to a q-dominance percentage where 0° → 0% and 90° → 100%. (d) The percent q-dominance for each station, as in (c), plotted against the mean daily maximum temperature on its 1000 hottest days in the 1981-2015 period. The importance of local climatology for extreme-Tw characteristics is evident. From Raymond, Singh, Horton, 2017.

from 14 (Northwest) to 39 (Southeast). To determine the most extreme days as ranked by temperature, specific humidity, and wet-bulb temperature, I compute (for each variable, at each station) the 100 highest daily maxima of that variable in the warm season (May-October [MJJASO]) for the period 1981-2015. Extreme days are also independently calculated for each

grid cell in the NARR dataset, to provide more-complete spatial coverage and to test whether it can successfully represent the patterns found in the station observations. MJJASO is chosen as the period in which nearly all Tw extremes occur in the contiguous U.S., and 100 as representing approximately the top 1.5% of all days in MJJASO, or an average of about 3 days per year. I consider consecutive extreme days independently, following McKinnon et al. [2016] who find that the final difference in circulation composites is small between heat waves and individual hot days.

To disentangle temperature and moisture effects on extreme Tw, I develop a new decomposition methodology. I calculate the temperature and specific-humidity values corresponding to the exact hour of the daily-maximum Tw for the 100 and 1000 days with the highest Tw at each station. The medians of the top 100 days and next 900 days are then compared. The relative differences between the two sets of days in terms of temperature and specific humidity consequently determine "dominance": an increase in Tw from the 'next 900' to the 'top 100' that is driven entirely by an increase in specific humidity is termed 100% q-dominated; one that is driven equally by temperature and by specific humidity, 50% q-dominated, or alternatively 50% T-dominated; and one that is driven entirely by an increase in temperature, 100% T-dominated. This definition is illustrated in Figure 2.2.

To identify the circulation and surface conditions associated with regional Tw extremes, I create composites for these days of 500-hPa geopotential height [z500] and SST anomalies across the Northern Hemisphere, and of 850-hPa temperature, specific humidity, and wind anomalies across the contiguous U.S. The statistical significance of SST-anomaly composites is assessed via a bootstrapping procedure: for each region, I compute the distribution of months in which the 100 Tw extremes occur. Such a distribution consists of x_1 Junes, x_2 Julys, x_3 Augusts, and x_4 Septembers, for $n_{region}=x_1+x_2+x_3+x_4$ total unique months. I then create 1000 surrogates, each of

which is produced by randomly selecting with replacement n_{region} month-year combinations according to the particular seasonal distribution. Significance is assessed by comparing the 97.5th and 2.5th percentile of SST in each gridcell (across all surrogates) to the value in the observed composite. The usage of monthly (rather than daily) SST averages is justified by the high temporal autocorrelation of SSTs, which makes the difference between daily and monthly averages small in most areas. Not weighting the SSTs by the number of Tw extremes in each month limits the effect of months with many Tw extremes. This is because my interest is more qualitative (i.e. which SST patterns are associated with any Tw extreme in a region) than quantitative (i.e. which SST patterns are associated with the most Tw extremes in a region), as the latter might bias the results toward a handful of occasions with conducive atmospheric-circulation patterns or other unusual circumstances.

At the global scale, I use quality-controlled station observations from HadISD, version 2.0.1.2017f (Dunn et al., 2016; Dunn et al., 2012), and high-resolution reanalysis data from the ERA-Interim reanalysis product (Dee et al., 2011). HadISD is produced by the United Kingdom Met Office Hadley Centre and is the result of additional data-availability and quality-control procedures applied to the Integrated Surface Database. These include tests for both dry-bulb temperature and dewpoint temperature, the two variables required for computing Tw. I develop additional checks to remove stations where Tw extremes occur in conjunction with a dewpoint depression of <1°C; where more than half of Tw readings are missing in the surrounding 5 days; or where the associated dewpoint temperatures are more than 10°C different from the elevation-adjusted values at the closest grid cell and timestep in ERA-Interim. Although spatially extensive, the primary limitation of HadISD is a lack of data in the tropics, meaning that these conclusions

are most reliable in the subtropics and mid-latitudes, and especially at times and places where multiple nearby stations are in agreement.

At individual stations in HadISD, temporal resolutions vary from 1-hourly to 6-hourly. I compute daily maxima of 2-m Tw irrespective of these variations; thus, the reported maxima are a lower bound on the true values. In the global analyses, to better account for elevation effects, I use the much more complex Davies-Jones [2008] formulae instead of that of Stull [2011]. The former result in slightly lower (higher) calculated Tw values at low elevations and high Tw (moderate elevations and moderate Tw), with the Davies-Jones global-average Tw being approximately 0.25°C higher. The Davies-Jones method requires station surface pressure, which is calculated from its elevation using a standard atmosphere and an assumed sea-level pressure of 1010 mb; a sensitivity analysis reveals the error due to this assumption to be on the order of 0.1°C.

Global-scale SST correlations are evaluated as a Pearson correlation at each grid cell between the annual maximum SST and annual mean near-surface air temperature (<T>) over 1979-2017. I select only the last 39 years of SST data for consistency with ERA-Interim. Statistically significant correlations (at the 0.05 level) are found for ~47% of all grid cells worldwide. For these timeseries I employ linear regression, fitting intercept (a0) and slope (a1) coefficients to model annual maximum SST as a linear function of <T>:

Equation 2.4

$$SST = a_0 + a_1\langle T \rangle$$

Rearranging Eq. 2.4 leads to an equation that defines the required warming for an annual maximum monthly-mean SST of at least 35°C:

Equation 2.5

$$\langle T \rangle = \frac{(35 - a_0)}{a_1}$$

Interannual correlations are computed as a Pearson correlation between the detrended SST timeseries and the detrended count of exceedances of a particular Tw threshold.

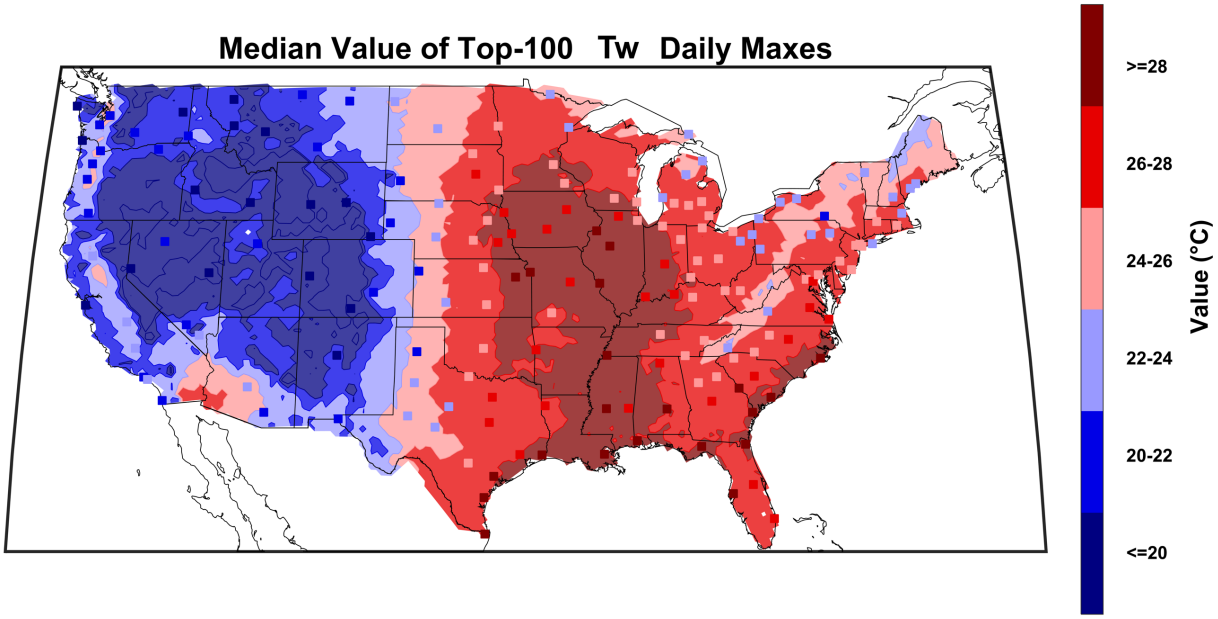

Figure 2.3: The median value of the 100 extreme-Tw days for each station (squares) and NARR grid cell (shading). The highest Tw values are found in the eastern U.S., particularly those parts that experience moisture advection from the Gulf of Mexico or Atlantic Ocean. From Raymond, Singh, Horton, 2017.

Regional and Seasonal Patterns

Within the U.S., the highest values of Tw are found in the Southeast and Mississippi Valley, extending up to the lower Midwest (Figure 2.3), a geographic pattern also seen in earlier heat-wave and summer-mean studies of joint temperature-humidity extremes (Smith et al., 2013; Kalkstein and Valimont, 1986). The northward extent of these extremes around 90°W is associated with the climatological southerly flow of warm and moist air from the Gulf of Mexico (Li et al., 2012). Extreme-Tw values are also in excess of 25°C in the upper Midwest and coastal Northeast. These results quantitatively match previous work that found annual-maximum Tw of 25-28°C across much of the tropics and subtropics (Sherwood and Huber, 2010). Extreme Tw is significantly lower in the drier western half of the U.S., with the highest values there approximately

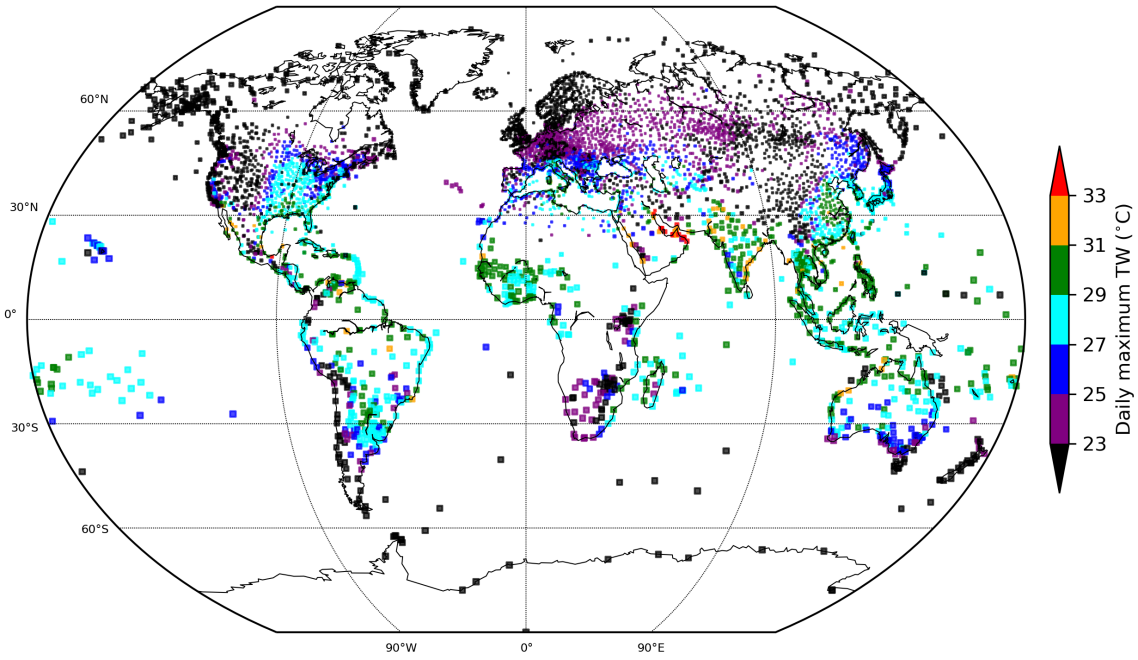

Figure 2.4: The 99.9th percentile of observed daily-maximum Tw for 1979-2017, for HadISD stations with at least 90% data availability over this period. Marker size is inversely proportional to station density. The highest values are consistently found in the coastal subtropics and northern South Asia, where multiple stations are in agreement. From Raymond, Matthews, Horton, 2019, in review.

equaling the lowest ones in the east (Figure 2.3). These patterns are also captured qualitatively by the NARR dataset.

Global Tw extremes are highest around the Persian Gulf (Figure 2.4), with somewhat lesser values found along subtropical coastlines in South Asia, the Middle East, and North America. These latter locations have the commonalities of a semi-enclosed gulf or bay of shallow depth that limits ocean circulation, and proximity to sources of continental dry-bulb heat. That subtropical coastlines are hotspots for heat stress has been noted previously (Byers et al., 2018; Diffenbaugh et al., 2007); the present analysis makes clear the broad geographic scope of this observation, but also the varied intra-regional values (Figure 2.4). Tropical-forest and maritime areas generally experience Tw no higher than 31-32°C, perhaps a consequence of a high evapotranspirative

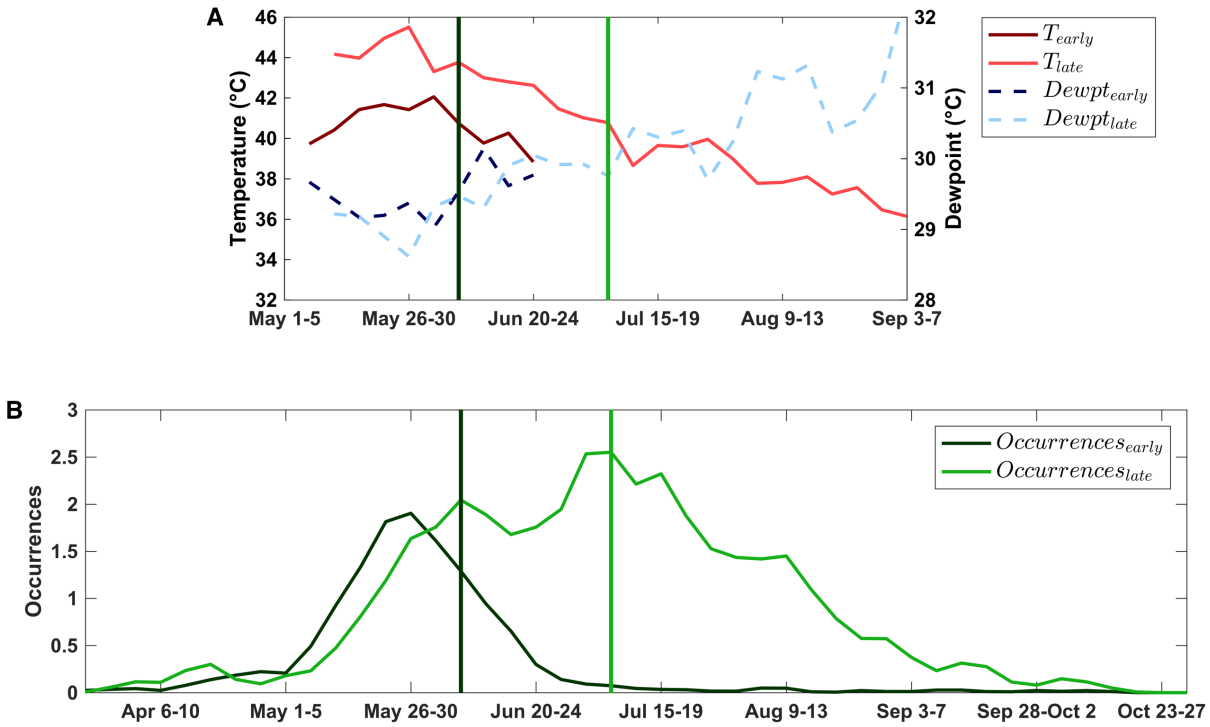

Figure 2.5: (A) Average dry-bulb temperature and dewpoint temperature associated with all Tw exceedances of 31°C in South Asia, by pentad, grouped into those occurring in early-monsoon areas (<Jun 15 average onset date, e.g. Sri Lanka, southern and eastern India, and Bangladesh) and late-monsoon areas (>=Jun 15 average onset date, e.g. Pakistan and northern and western India). Dark green (light green) vertical bars represent the station-weighted-average climatological monsoon onset date for the early (late) monsoon areas. (B) Average annual number of Tw exceedances of 31°C per station in the two areas, by pentad. Tw extremes in South Asia are most frequent in the lead-up to the monsoon, and the arrival of the monsoon changes the character of Tw extremes from more moisture-prominent to more dry-bulb-temperature-prominent. From Raymond, Matthews, Horton, 2019, in review.

potential and cloud cover, along with the greater instability of the tropical atmosphere (Sobel et al., 2001).

South Asia stands as the main exception to the preeminence of coastlines in Figure 2.4. Both there and in the Southwest U.S., observations reveal that the efficient inland transport of humid air by the summer monsoon acts to modulate the timing of Tw extremes (Figure 2.5). Splitting South Asia into ‘early monsoon’ and ‘late monsoon’ subregions demonstrates that the number of Tw extremes is largest just prior to the local climatological monsoon onset date.

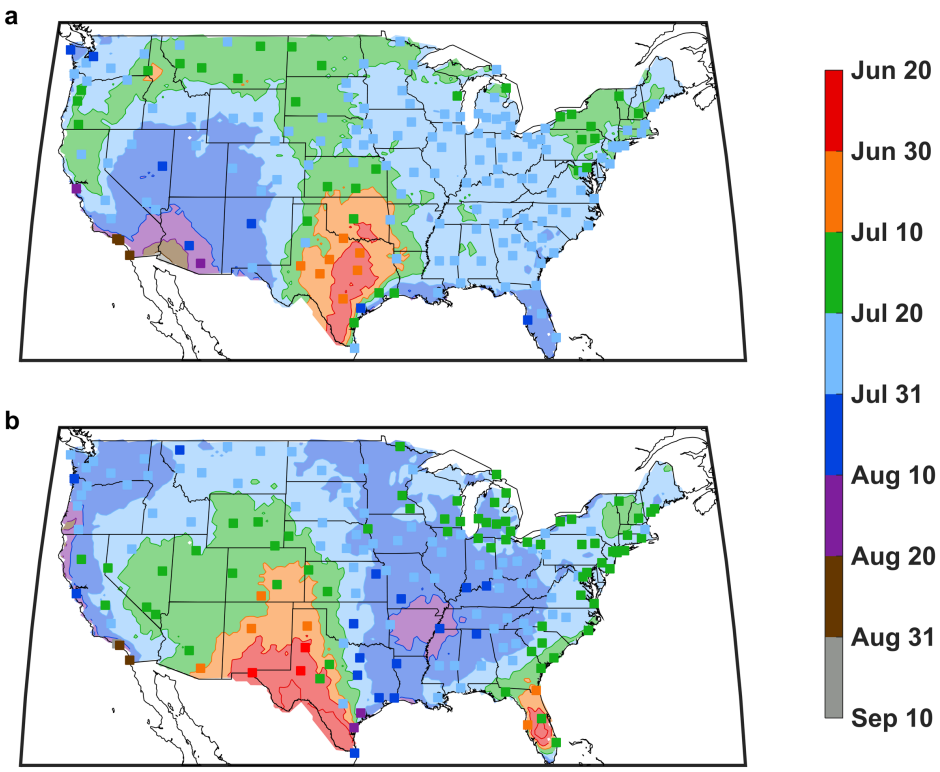

Figure 2.6: The median calendar date of the 100 extreme-Tw days (a) and the 100 extreme-T days (b) for each station (squares) and NARR grid cell (shading). Timing differences are significant, and are largest in regions where they can be directly attributed to subseasonal climatological shifts in winds and consequently moisture advection. From Raymond, Singh, Horton, 2017.

Although equivalent extreme values of Tw are possible before, during, and after the monsoon rains in any given year, they are of a different character, becoming progressively moister and having lower dry-bulb temperatures as summer progresses. Similarly, I find that Southwest Tw extremes typically occur after the onset date of the local monsoon (Figure 2.6), a consequence of low soil moisture, high insolation, and a dry atmosphere in early summer that limit latent-heat contributions (Higgins and Shi, 2000). This systematic association underscores the important role of moisture, and of weather systems on synoptic to subseasonal timescales, in controlling extreme Tw (Im et al., 2017; Raymond et al., 2017).

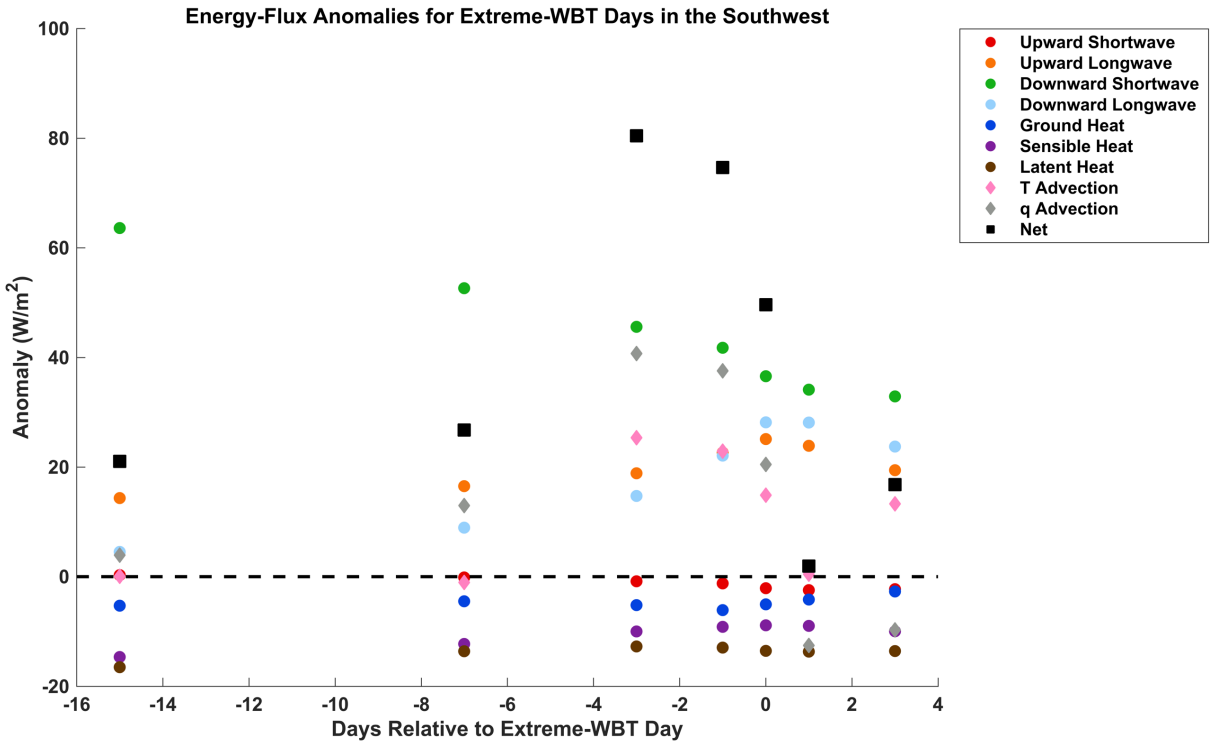

Figure 2.7: Surface energy-flux anomalies calculated from NARR data for Southwest extreme-Tw days, averaged spatially over the Southwest and temporally over the periods (from left): 20-10 days before the extreme; 9-5 days before; 4-2 days before; 1 day before; the extreme day; 1 day after; and 2-4 days after. The conversion of temperature and specific-humidity advection to fluxes in W/m^2 is described in Methods. Result underscores the close relationship between moisture advection and extreme Tw in arid, monsoonal climates. From Raymond, Singh, Horton, 2017.

Driving Mechanisms

I extend the analysis in Figure 2.7, using energy-flux anomalies for Southwest extreme-Tw days. A clear temporal evolution is observed, with the net anomalous positive flux from both temperature and specific-humidity advection peaking around ~40 W/m^2 in the period 2-4 days prior. This net flux is largely driven by an increase in anomalous positive moisture advection, and secondarily by temperature advection. Consequently, moisture advection in the interior Southwest, which I postulate to be a signature of moisture pulses connected with the North American Monsoon (Maddox et al., 1995), is of critical importance for controlling extreme Tw. This constitutes a physical cause for the distinction between extreme-T and extreme-Tw days there (Figure 2.8b).

To illustrate the spatially varying roles of temperature and specific humidity in driving Tw extremes more generally, I compare the percent overlap between 1) days with Tw extremes and days with q extremes (Figure 2.8a) and 2) days with Tw extremes and days with T extremes (Figure 2.8b). Whereas Tw and specific-humidity extremes are frequently simultaneously observed, Tw and temperature extremes generally co-occur less than 30% of the time, with the implication that Tw extremes are primarily driven by conditions that lead to extreme specific humidity. The asynchronous nature of temperature and Tw extremes is most pronounced in the semi-arid southern Great Plains and Southwest, and most muted in the eastern third of the country; these regional patterns are also made evident by the offset of positive temperature anomalies with the epicenter of Tw extremes in the former regions, versus the collocation in the latter regions (Figure 2.9). Greater T-Tw overlap is observed near water bodies such as the Pacific Ocean, Atlantic Ocean, and Great Lakes, and further north at a given longitude. Additional evidence of q-dominance is shown in Figure 2.2c, in which I find specific-humidity excursions to be more important than teemperature excursions in most regions of the U.S, with the degree of this dominance being determined largely by the climatological aridity of a given region. The overall larger role of specific humidity in determining extreme Tw is also underscored by the significantly higher extreme-Tw values in the eastern U.S. (Figure 2.3).

Patterns of future increases in extreme Tw are dependent on regional increases of temperature versus specific humidity, and, at an event level, on the regional sensitivity of extreme Tw to temperature and specific-humidity variation. The weaker-vertical-circulation theory (Held and Soden, 2006), the q-dominance of the hottest regions of the U.S. (Figure 2.2), and the greater nonlinearity of Tw with respect to specific humidity than to temperature (Stull, 2011] all suggest that moisture will play an ever-greater role in determining Tw at the higher temperatures expected

in the future, a prediction analogous to that made by Jones et al. [2010] for extreme precipitation. Thus, my results indicate that q-dominance will most likely increase and spread poleward in the coming decades.

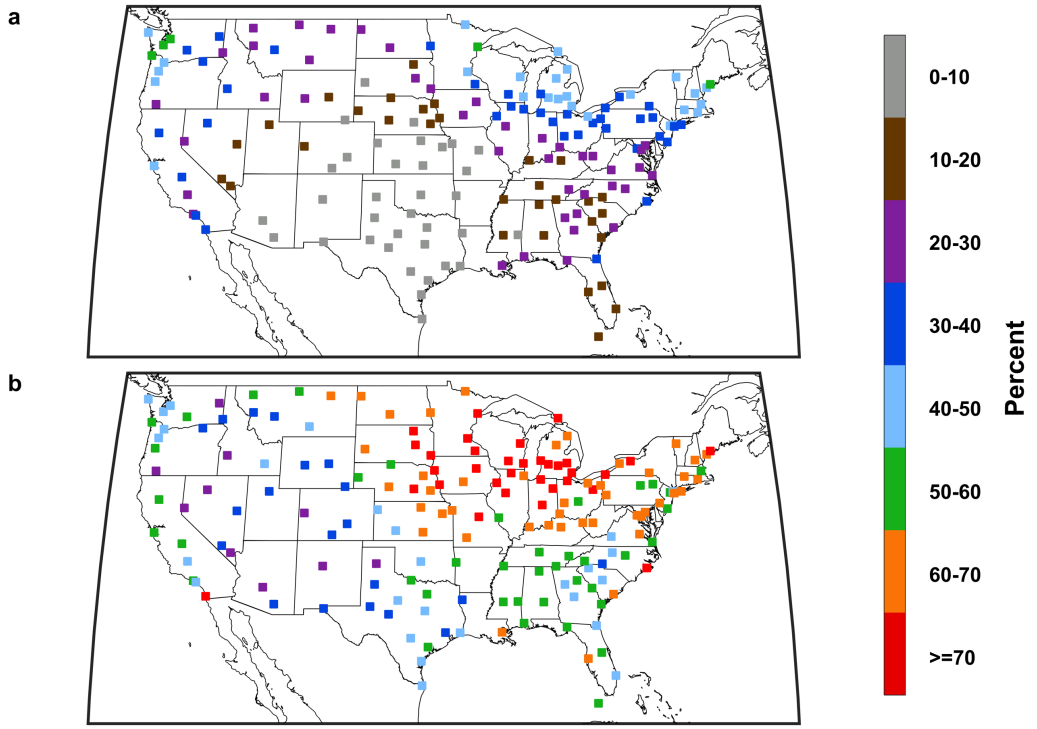

Figure 2.8: (a) The percent overlap between the 100 extreme-Tw days and the 100 extreme-T days at each station. (b) The same metric for Tw/q overlap. The much larger Tw/q overlap is evidence of the importance of moisture for extreme Tw, and the relatively minor role of T. From Raymond, Singh, Horton, 2017.

Variability and Predictability

Extreme humid heat is correlated significantly with remote SST anomalies, whose spatial patterns differ considerably according to the region under consideration. For most U.S. regions, these remote SST anomalies are of larger magnitude than anomalies closer to shore (Figure 2.10), suggesting that the strong relationships with local SSTs found by Pal and Eltahir [2016] for the Persian Gulf may be specific to that setting. SST anomalies for eastern-U.S. Tw extremes (Figure 2.10e-g) closely match in position and magnitude the "Pacific Extreme Pattern" for temperature extremes described in McKinnon et al. [2016] for dry-bulb heat, as well as in other previous studies

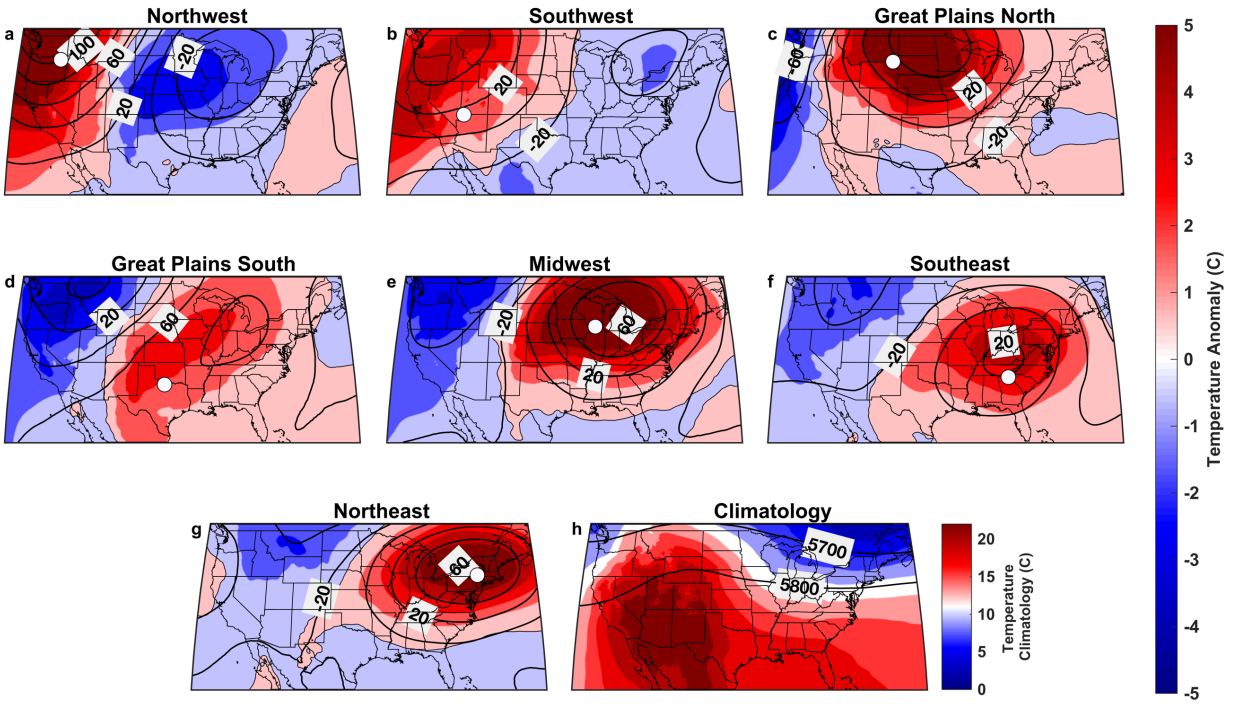

Figure 2.9: (a-g) Daily anomalies of 850-hPa temperature (shading; units of °C) and 500-hPa geopotential height (contours; units of m) from the NARR dataset for the 100 extreme-Tw days in each region. (h) Climatological 850-hPa temperature and 500-hPa geopotential height for JJA. The collocation of T anomalies over the eastern-U.S. regions experiencing extreme Tw is further evidence of the close correlation between temperature, specific humidity, and Tw there, whereas the offset for western regions illustrates the more-complex dynamics that lead to extreme Tw. From Raymond, Singh, Horton, 2017.

(Perkins, 2015; Teng et al., 2013; Loikith and Broccoli, 2012), consistent with the large degree of overlap between dry-bulb and wet-bulb heat in those regions (Figure 2.8). They also resemble the negative phase of the Pacific Decadal Oscillation [PDO], whereas the SST patterns accompanying Northwest and Southwest extreme heat resemble the PDO's positive phase (Mantua and Hare, 2002). These two observations together suggest possible decadal modulation of extreme heat that is region-specific, as has been shown for drought (McCabe et al., 2004). In contrast, extreme-Tw days in the Great Plains are associated with shorter-period SST signatures in the north-central Pacific (Figure 2.10c-d); for the southern Great Plains, there is also a statistically significant connection with the El Niño-Southern Oscillation, resembling a La Niña-like phase (Figure 2.10d).

SST anomalies for the Northwest and Southwest (Northeast and Southeast) bear similarity in period and phasing to z500 anomalies in the Pacific (Atlantic) Ocean, a possible indicator of a 'reinforcing' role for SST with respect to extreme Tw, as has been shown for extreme temperature (Hartmann, 2015; Wang and Schubert, 2014; Feudale and Shukla, 2011). The existence of a clear correlation in the Northwest and Southwest (Figure 2.10a-b) is a novel result, and one that provides motivation for future work to improve forecasts of extreme Tw there on seasonal to interannual timescales.

A sharp peak in the number of global Tw extremes occurs during the strong El Niño events of 1998 and 2016. Detrending reveals that this El Niño-Southern Oscillation [ENSO] correlation is strongest for Tw values that are warm, but not exceptionally so (~27-28°C). While this relationship may derive in part from the effect of ENSO on hydrological extremes at the global scale or on SSTs in particular basins (Lyon, 2004; Sobel et al., 2002), I determine that interannual variability in Tw extremes in the tropics best correlates to mean Tw, with a correlation coefficient near 0.9 (Figure 2.11), indicating that both forcings and modes of internal variability resulting in mean temperature shifts can be expected to substantially modulate tropical Tw extremes. In the subtropics these correlations are somewhat weaker, and are shifted more toward tropical (especially West Pacific) and regional (especially subtropical Atlantic) SST patterns.

More causally oriented than correlations, predictability refers to the existence of antecedent conditions and a pathway, along which it is highly confident that the climate state will evolve, leading directly to the event which is desired to be predicted. Predictability is therefore neither a dynamical calculation nor a statistical relationship, but something of a hybrid indicating the potential for skillful forecasts on subseasonal-to-interannual timescales, if the task is given to a well-constructed model. To expand upon the correlations shown in Figures 2.10 and 2.11, I

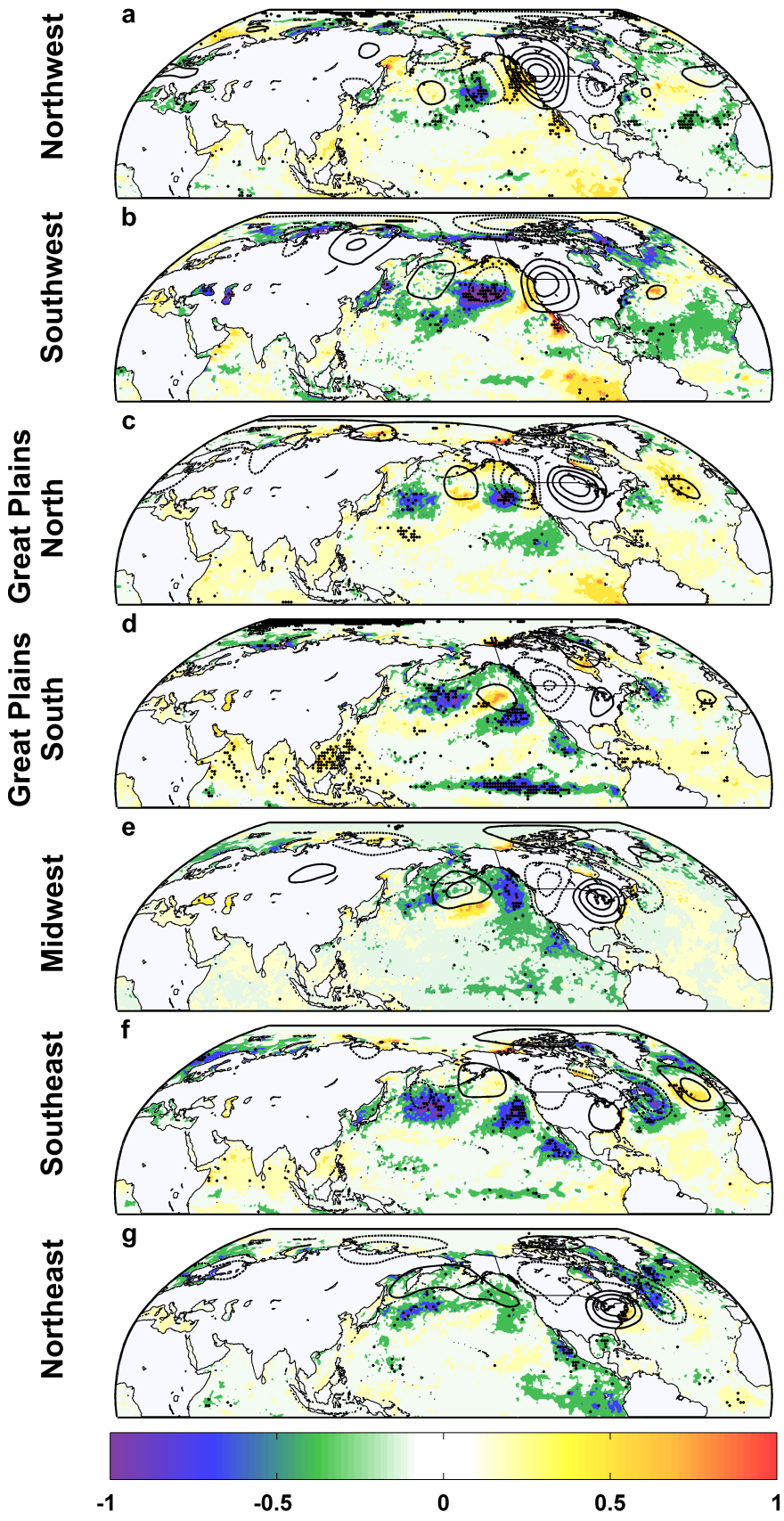

Figure 2.10: Composites of daily z500 anomalies (contours, at 20-m intervals, with negative dashed and zero omitted) and SST anomalies (shading, stippled at 95% significance) on the 100 extreme-Tw days in each region. Colorbar represents SST anomalies in °C. While some regions have positive nearby SST anomalies associated with extreme Tw, the dominant result is the significant, regionally-varying, mid-latitude Pacific SST pattern. From Raymond, Singh, Horton, 2017.

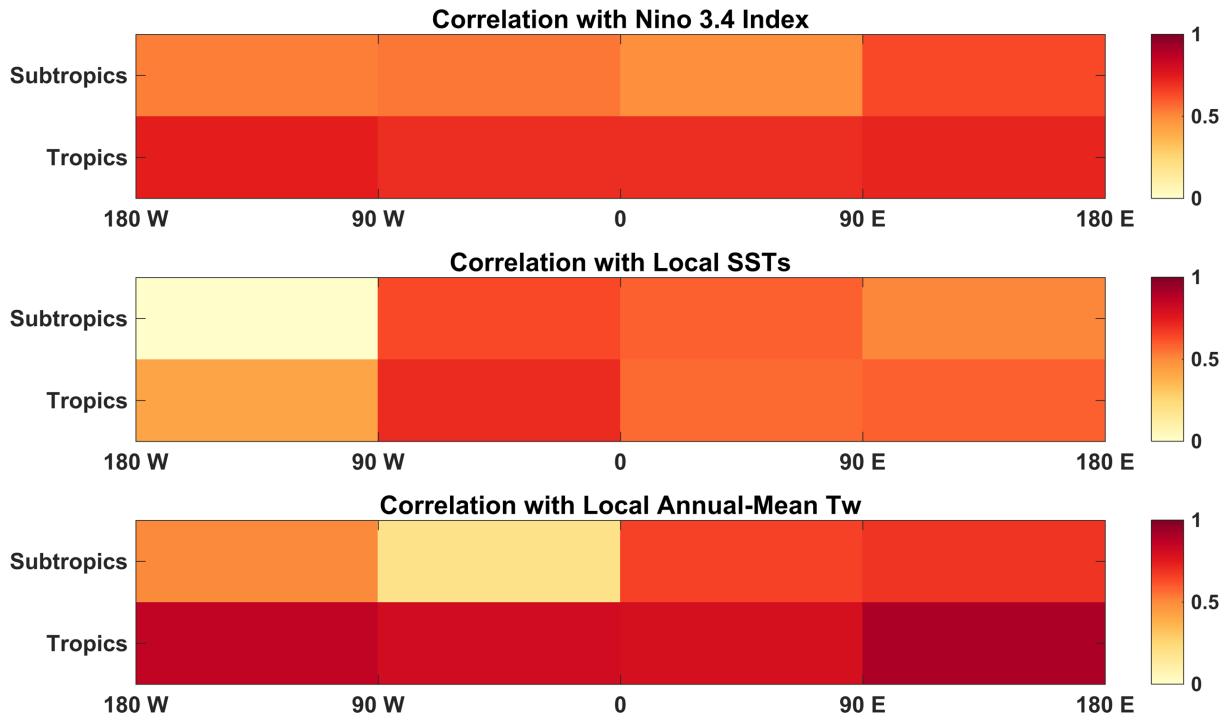

Figure 2.11: Detrended correlation between regional annual station-days exceeding Tw>=27°C and (top) DJF Nino 3.4 index; (middle) local JJA sea-surface temperatures; and (bottom) local annual-mean Tw from HadISD. Tropics (subtropics) are defined as 0°-15° (15°-35°) in each hemisphere. On an annual timescale, tropical extreme Tw is predictable largely from the mean, whereas the predictors of subtropical extreme Tw are not as strong and vary more by longitude. From Raymond, Matthews, Horton, 2019, in review.

investigate the predictability of Tw extremes using a Rossby wave-activity analysis, following the methodology of Teng and Branstator [2017]. In a time series of anomalies of 200-hPa geopotential height [z200] and 200-hPa meridional wind [v200] for Midwest Tw extremes (Figure 2.12), the developing ridge over the Midwest is apparent and statistically significant by 10 days prior to the extreme (Figure 2.12b) in both z200 and v200. The v200 anomalies indicate origination of the wavetrain in the mid-latitudes of the northern Pacific and subsequent propagation across North America, a path very similar to that found by Teng and Branstator [2017]. As the latter paper mentions, 'internal midlatitude dynamics' nonetheless play a major role in ridges over North America, limiting the lead time of predictability from these wavetrains before their power fades to

the level of ‘climatology’ or ‘persistence’ forecasts. This analysis is designed to give more confidence about the origin of the disturbances which ultimately lead to extreme Midwest wet-bulb temperatures than it is to trace back along a multiplicity of pathways, although such an experiment could be conducted. The salient conclusion of Figure 2.12 is that the waves can be identified propagating thousands of km across the mid-latitudes, as suggested by Figure 2.10, rather than emanating from another ultimate source such as the tropical Pacific, which would indicate a different set of generative processes.

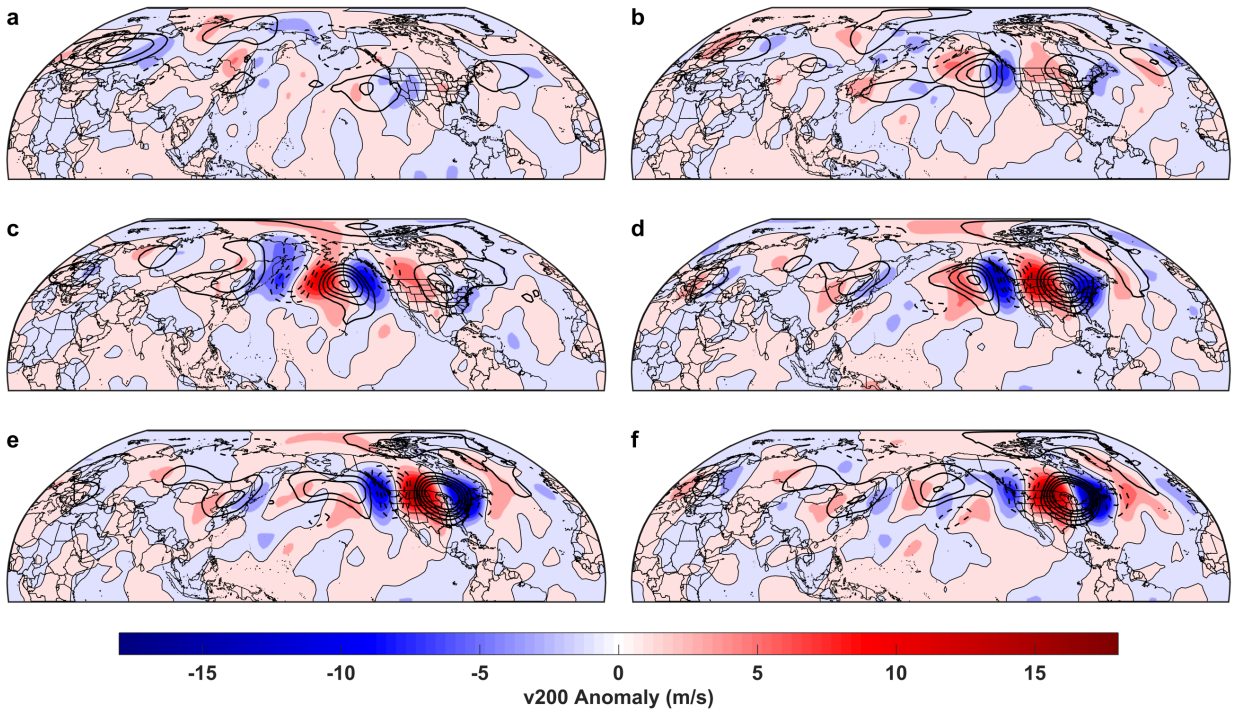

Figure 2.12: Composites of daily anomalies of 200-hPa geopotential height (contours, at 20-m intervals, with negative dashed and zero omitted) and 200-hPa meridional wind (shading) in the period leading up to the 100 extreme-Tw days in the Midwest: a) 20 days prior; b) 10 days prior; c) 5 days prior; d) 2 days prior; e) 1 day prior; f) the extreme-Tw day. Preceding days with an intervening Tw extreme are excluded. Upper-level wave activity associated with extreme Tw, in the same north-central Pacific regions as the strongest SST relationships, suggests the potential for predictability at least 5-10 days in advance. From Raymond, Singh, Horton, 2017.

Discussion

This chapter uses the highest-quality available data to produce the first comprehensive characterization of the climatology and meteorology of Tw extremes. Regionally coherent spatiotemporal patterns of extreme-Tw magnitude, timing, and T/q composition are apparent, many of which are closely linked to the local geography and climatology of each region. A discovery of particular note is the tight relationship between warm-season monsoons and subtropical humid-heat extremes. The importance of specific humidity is evident in both regional and seasonal patterns, and verified for the Southwest U.S. via an energy-flux calculation. Antecedent wavetrains, together with co-occurring SST anomalies, both exhibit significant correlations even in locations far from the subsequent Tw extremes, suggesting the potential for region-specific predictability as well as underscoring the limited role of local conditions.

The results of this chapter reveal the breadth of potential future impactful research on Tw extremes, as well as its nascent current status. Major outstanding questions include the variability in the relative importances of temperature and moisture in a given location; the natural and anthropogenic factors that influence this variability, including its responses under climate change; and the quantification of the additive impacts of moisture during extreme-heat events for particular sectors and demographic or health-based groups. High-resolution modeling, concentrating on the factors hypothesized to be dominant in the most-affected areas, and closely validated against weather-station observations, has an important role to play in realizing these advances.

In Chapter 3, I continue with the study of observed Tw extremes, but focus more narrowly on the patterns and processes associated with the very highest values. This purview leads back to regional coastal analyses that echo Chapter 1, as well as to more-direct insights into how and why Tw extremes will change in the near-to-medium-term future.

Chapter 3: Refining projections of humid heat beyond the physiological survivability limit

Raymond, C., Matthews, T. K., and Horton, R. M. The emergence of heat and humidity too severe for human tolerance. In second-stage review at *Sci. Adv.*

Introduction

Humid-heat extremes have already proven a major constituent of climate-related risk; additionally, large increases in humid-heat extremes are a robust feature of future climate projections (Coffel et al., 2018; Knutson and Ploshay, 2016; Fischer and Knutti, 2013). Chapter 2 considered general characteristics of Tw extremes, gleaned from the top dozens to hundreds of values at each location. In this chapter, I focus on the absolute highest Tw values that have been observed in the instrumental record — conducting some analyses analogous to those in Chapter 2, but focusing more intently on comparisons between point observations and reanalyses to produce a broad global perspective and new constraints on existing projections of peak Tw over the coming decades. In its sections focusing on coastal effects, this chapter also hearkens back to Chapter 1, though with contrasting regional climatologies and with humidity explicitly included in the analysis.

While some impacts of heat-humidity exposure can be avoided through acclimation and behavioral adaptation (Lowe et al., 2011), physiological studies suggest there exists a hard upper limit for survivability, even under idealized conditions of perfect health, total inactivity, full shade, absence of clothing, and unlimited drinking water (Sherwood and Huber, 2010; Parsons, 2006). The reasoning derives from laboratory experiments (Bynum et al., 1978; Craig and Dvorak, 1966) as well as a simple energy-balance calculation: the normal internal human body temperature of 36.8 ± 0.5°C requires skin temperatures of around 35°C to maintain a gradient directing heat outward from the core (Hanna and Tait, 2015; Sherwood and Huber, 2010). Once the air (dry-

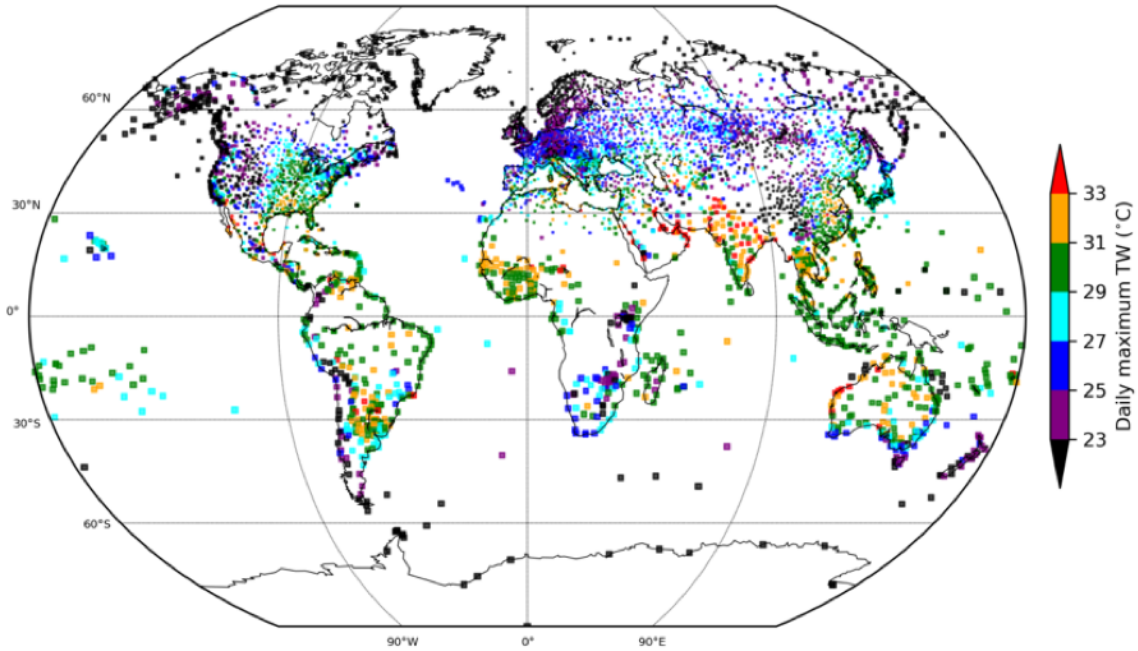

Figure 3.1: All-time maximum of observed daily-maximum Tw for 1979-2017, for global HadISD stations with at least 90% data availability over this period. Marker size is inversely proportional to station density. Various subtropical regions contain multiple stations that have observed Tw>=33°C, and there is geographical consistency as to where these hotspot regions are located. From Raymond, Matthews, Horton, (2019), in review.

bulb) temperature rises above this threshold, metabolic heat can only be shed via sweat-based latent cooling, and at Tw exceeding 35°C, this cooling mechanism loses its effectiveness altogether. Because the ideal physiological and behavioral assumptions are almost never met, severe mortality and morbidity impacts typically occur at much lower values — for example, regions affected by the deadly 2003 European and 2010 Russian heat waves experienced Tw no greater than 28°C (Figure 3.1).

In the literature to date, there have been no observational reports of Tw exceeding 35°C, and few reports exceeding 33°C (Im et al., 2017; Schär, 2016; Pal and Eltahir, 2016). Matthews [2018] observed that the recently produced hourly, ~30-km-resolution ERA5 reanalysis records a maximum Tw value of 35.4°C, but this result does not seem to have received much attention, perhaps partly due to the lack of documented supporting evidence from weather stations or other

available gridded products. The awareness of a physiological limit has prompted several modeling studies to ask how soon it may be crossed, with results suggesting that, under the business-as-usual RCP8.5 emissions scenario, Tw could regularly exceed 35°C in parts of South Asia and the Middle East by the third quarter of the 21st century (Coffel et al., 2018; Im et al., 2017; Pal and Eltahir, 2016). These studies use a mixture of reanalysis products and global-climate-model runs for the historical period, which then serve as a basis for projections using coupled regional climate models. However, due to a paucity of reliable station data in the globally hottest areas, these studies have not explicitly included station data in their evaluations, and the resolutions of the data they employ are no smaller than 25 km in space or 3 hours in time. This lack of truly high-resolution representation of extreme humid heat leaves open the possibility that the very highest values have not been sufficiently represented, as, across multiple climate variables, the magnitude of an extreme tends to correlate with its brevity (Cheng and AghaKouchak, 2014; Andreadis et al., 2005).

Previous studies on extreme dry-bulb temperatures inform knowledge of extreme wet-bulb temperatures, but the comparison is limited. As Chapter 1 showed, it is often the case in arid climates that the overlap of extreme (e.g. >90th-percentile) temperatures and extreme moisture is close to zero. Regional terrain and land-surface conditions control the ultimate sensitivity of extreme temperature and moisture to large-scale meteorological forcings (Vogel et al., 2017; Seneviratne et al., 2006), and the relationships with these variables, each complex in its own right, must be accurately represented to capture changes in extreme humid heat. Unlike for dry-bulb temperatures, where extensive and reliable field-campaign and weather-station data exist, instrumental humidity records are largely absent in areas where Tw nears 35°C, for reasons technical, historical, and political.

In this chapter, I establish baseline values and geographic patterns of the globally highest Tw, and use these recent Tw and SST trends as observationally-based guidance for future Tw projections. This approach offers an independent line of evidence to previous research that used coupled or regional models without explicitly including historical station data. It also builds on Chapters 1 and 2, illustrating how the regional-geographic approaches of Chapter 1 and the bivariate findings of Chapter 2 can be combined to inspire novel questions and produce novel insights about the highly societally relevant issue of Tw extremes at the very leading edge of intensity and impacts.

Data and Methods

This chapter uses station observations from HadISD (Dunn et al., 2016; Dunn et al., 2012) and reanalysis data from ERA-Interim (Dee et al., 2011), as described in Chapter 2. All wet-bulb temperatures are computed with the Davies-Jones [2008] formulae.

Interannual trends are calculated using an ordinary least squares regression, with significance evaluated using a t-test on the slope coefficient. This assessment of extreme Tw frequency considers threshold exceedances in 2°C increments from 35°C to 27°C, so as to strike a balance between values that are sufficiently distinct from one another while being high enough to remain relevant from an impacts perspective. I fit a generalized extreme value [GEV] distribution to the time series of annual maximum Tw from selected grid cells in ERA-Interim, a reanalysis dataset that optimally blends observations with a numerical hindcast and thus provides an estimate of the atmospheric state less sensitive to observation error and microclimatic variability (Dee et al., 2011). While well-suited to identifying and extrapolating global trends, it is inevitable in such an approach that decadal temperature trends and other large-scale variability may affect

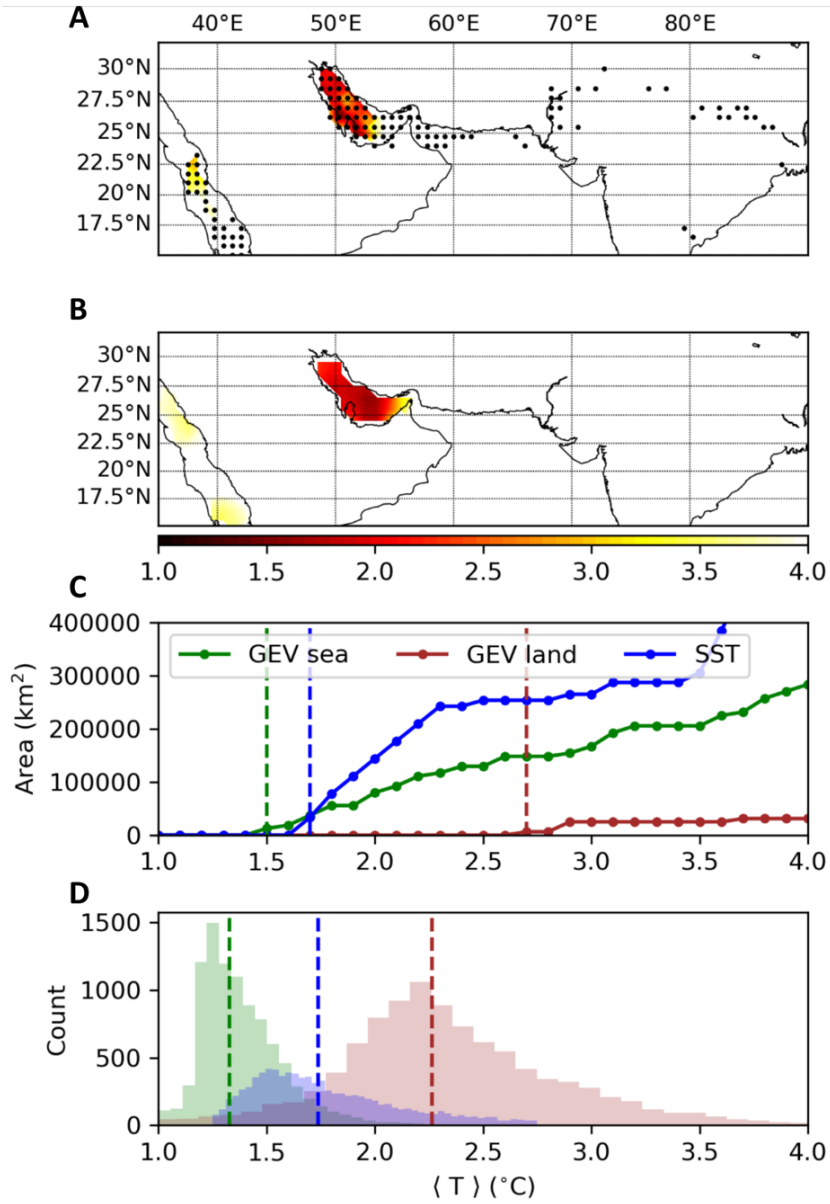

Figure 3.2: Projections of extreme humid heat exceeding the physiological survivability limit. A) Shading shows the amount of global warming (since pre-industrial) until Tw=35°C is projected to become at least a 1-in-30-year event according to a non-stationary GEV model. Black dots indicate ERA-Interim grid cells with a maximum Tw (1979-2017) in the hottest 0.1% of grid cells worldwide. B) As in (A), but communicating the amount of global warming until the mean annual maximum of monthly-mean SST is projected to be at least 35°C, according to a linear regression model. C) Total area with Tw or SST of at least 35°C as a function of mean annual temperature change from the pre-industrial period (<T>). Vertical lines highlight the lowest <T> for non-zero areas of each respective variable (the "*temperature of emergence*"). D) Bootstrap estimates of the temperature of emergence. Tw and SST values are closely linked in the Persian Gulf, although peak Tw values are slightly higher, making for an earlier time of emergence of 35°C in marine air than in the underlying water. From Raymond, Matthews, Horton, (2019), in review.

the results modestly.

The cumulative distribution function [CDF] of the GEV is given by:

Equation 3.1

$$F(x) = e^{-[1+\frac{\kappa(x-\zeta)}{\beta}]^{-\frac{1}{\kappa}}}$$

The Tw quantile for an *n*-year return period can then be evaluated by inverting Eq. 3.1:

Equation 3.2

$$F^{-1}(p) = \zeta + \frac{\beta}{\kappa}\{[-\ln(p)]^{-\kappa} - 1\}$$

where the location, scale, and shape parameters are denoted ζ, β, and κ, respectively. Note that, in this analysis, I use *n*=30 (and hence *p*=0.967), to match standard 30-year climatologies. I estimate these parameters using the method of maximum likelihood, only fitting distributions to series from grid cells whose maximum value over 1979-2017 was in the highest 0.1% worldwide (top 119 grid cells), corresponding to a Tw threshold of 30.6°C.

I incorporate the effect of global warming on the return period by parameterizing ζ as a function of the annual global-mean air-temperature anomaly <T>:

Equation 3.3

$$\zeta(\langle T \rangle) = \alpha_2 + \alpha_3 \langle T \rangle$$

where a2 and a3 and are the intercept and slope coefficients of a linear regression.

The extent of improvement in this non-stationary model for each grid cell is evaluated using a likelihood ratio test, with test statistic lambda:

Equation 3.4

$$\Lambda = 2[L(H_A) - L(H_0)]$$

where L is the log-likelihood of the non-stationary (subscript *A*) and stationary (subscript 0)

models. Under the null hypothesis (that the non-stationary model is not superior), lambda has a chi-squared distribution with one degree of freedom. Of the 119 grid cells fitted with a GEV distribution, for ~83% parameterizing zeta as a function of <T> results in a statistically significant improvement at the p=0.05 level.

I use the non-stationary model to infer the amount of global warming required for annual maximum Tw = 35°C to be at most a 1-in-30-year event. This is calculated by substituting Eq. 3.3 into Eq. 3.2 and solving for <T>:

Equation 3.5

$$\langle T \rangle = \frac{\left(-\frac{\beta}{\kappa}\{[-\ln(p)]^{-\kappa}-1\}+35-\alpha_2\right)}{\alpha_3}$$

Applying Eq. 3.5 to each of the 99 grid cells with non-stationary models therefore enables spatially-explicit assessments of the amount of global warming required until Tw = 35°C should be expected, on average, once per 30-year climate-normal period.

The spatially-resolved estimates of <T> from Eq. 2.5 and Eq. 3.5 provide the means for identifying the "*temperature of emergence",* which I define as the lowest value of <T> returned by Eq. 2.5 or Eq. 3.5. These <T> values are marked with vertical dotted lines in Figure 3.2c. Uncertainty in the temperature of emergence is assessed with a 10,000-member bootstrap simulation. I randomly select (with replacement) 30 years of Tw and SST data, and fit parameters (slope and intercept for Eq. 2.5; slope, intercept, shape, and scale for Eq. 3.5) for each subset. These 10,000 estimates of the temperature of emergence are then sorted to identify the 5th, 50th, and 95th percentiles, the most likely estimate, and the 90% confidence intervals.

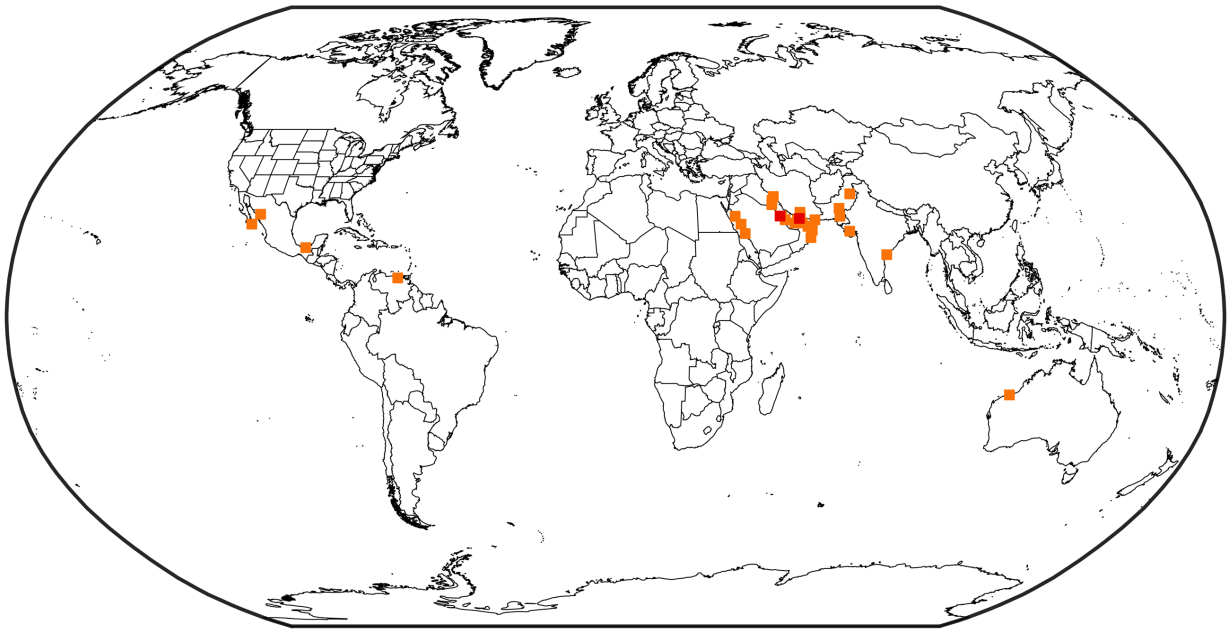

Figure 3.3: HadISD stations that have reached the Tw=33°C (orange) and Tw=35°C (red) thresholds multiple times in the observational record. These very highest Tw values highlight the Red Sea and Persian Gulf coastlines, and the inland valleys of northern South Asia, as the primary global hotspots.

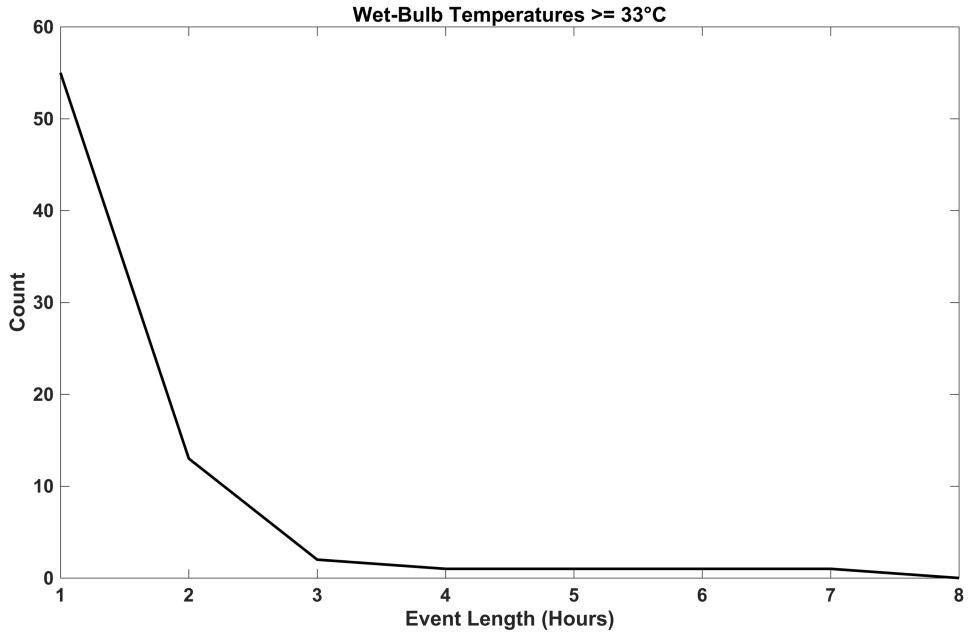

Figure 3.4: Event lengths for all instances in HadISD of Tw>=33°C, considering only the n=12 stations with >=3 occurrences of 33°C and with regular hourly data during those times. When Tw reaches 33°C, it almost never does so for more than 2 hours, underscoring the difficulty of capturing such excursions in gridded products. From Raymond, Matthews, Horton, (2019), in review.

Values and Trends

This survey of the climate record from quality-controlled station data reveals many global Tw exceedances of 31°C and 33°C, and that two stations in the dataset have already recorded multiple daily-maximum Tw values above 35°C (Figure 3.3). The two stations are Dhahran/Dammam (Saudi Arabia, population 1.1 million) and Ras Al Khaimah (UAE, population 0.3 million), both located on the southern Persian Gulf, which attains extraordinarily high SSTs that favor the occurrence of extreme humid heat (Wehner et al., 2016; Pal and Eltahir, 2016). Ras Al Khaimah in fact reached a peak Tw of 36.7°C on July 4, 2009, in association with a dry-bulb temperature of 40°C, a dewpoint temperature of 36°C, and nearby SSTs of 34°C according to reanalysis (a value that could well have been even higher along the immediate coast).

These exceptional >35°C conditions, beyond prolonged human physiological tolerance, have mostly occurred only for 1-2 hours' duration (Figure 3.4). Regionally coherent observational evidence supports the validity of these values: of the stations in the Persian Gulf area with at least 90% data availability, all have an all-time maximum Tw above 31°C (Figure 3.2). Every station around the western and southern coasts of the Persian Gulf, and the southern coast of the Gulf of Oman, has recorded Tw values above 33°C, while such values are not observed even a short distance inland, despite small topographic variations (Figure 3.5).

In the ERA-Interim reanalysis, the highest values are similarly confined to the Persian Gulf and its immediate fringes (Figure 3.6). Over land, reanalysis global maximum Tw has come very close to, but not yet reached, the 35°C threshold (Figure 3.7e). The spatiotemporal averaging inherent in reanalysis products causes ERA-Interim to be unable to represent the short durations and small areas of critical heat stress, resulting in large negative biases for extreme Tw (Figure 3.8). Around the southern Persian Gulf, these biases are consistently near -3 to -4°C (Figure 3.9).

However, biases are sensitive to the processes that generate Tw in each region, with significant inter-regional variability. It may be that ERA-Interim's relatively good performance in the Persian Gulf relates to its ability to represent the fairly uniform marine air masses that exist there, above the ~33-34°C summertime SSTs; nearby land experiences extreme-Tw conditions only when these marine air masses are advected onshore (Pal and Eltahir, 2016; Schär, 2016), facilitated by the near-100% occurrence of afternoon sea breezes in the summer in the southern Persian Gulf (Eager et al., 2008).

This observation underscores the crucial importance of a self-consistent metric and appropriate regional context when considering extreme heat generally. Chapter 1 demonstrated the robust linkage between coastal proximity and dry-bulb temperatures in the humid subtropical and mid-latitude setting of the eastern U.S., and even within that relatively limited area significant inter-regional differences are present. Certain similarities exist with the Persian Gulf, such as climatological large-scale downwelling, but it is the differences that predominate: the downwelling is much stronger, the SSTs much higher, and the continental-marine contrast much sharper in the Persian Gulf region (and this is true across Arabia and South Asia). As Figure 3.1 indicates, the better North American comparison is with northwestern Mexico, with high SSTs and a strong monsoonal circulation causing extreme heat stress along coastlines that would otherwise be much drier, with lower Tw. Furthermore, because during the warm season marine air has a lower temperature but higher specific humidity than continental air, coastal influences are more minimal when evaluated in terms of wet-bulb temperature than dry-bulb temperature. Thus, in addition to the definitional differences, the ubiquitous humidity in the eastern U.S. can be considered a major distinguishing factor between the results of Chapter 1 and those described here.

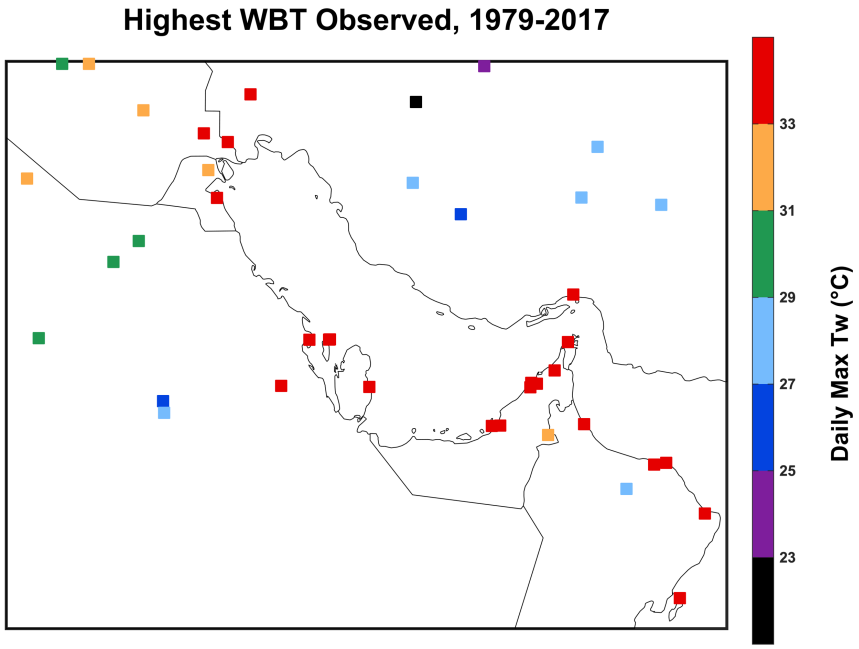

Figure 3.5: All-time maximum of observed daily-maximum Tw for 1979-2017, for Persian-Gulf-area HadISD stations with at least 90% data availability over this period. The highest values of Tw are concentrated along or very close to coastlines. From Raymond, Matthews, Horton, (2019), in review.

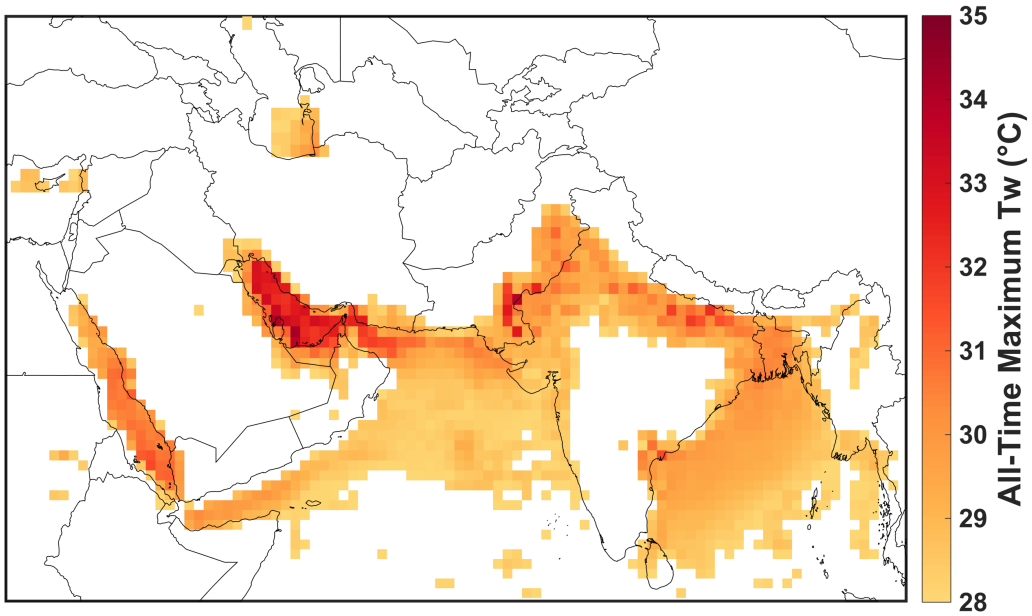

Figure 3.6: All-time maximum of observed daily-maximum Tw for 1979-2017, as represented by ERA-Interim. Spatial patterns agree well with station data, but values are typically negatively biased by several °C. From Raymond, Matthews, Horton, (2019), in review.

Across the globe, I find that temperature and humidity variations occur within a well-defined bivariate space (Figure 3.10). Rarely are Tw extremes observed with relative humidities above 80% or below 40%, emphasizing (as in Chapter 2) the necessary contributions of both dry-bulb temperature and specific humidity to achieve notable Tw values. Progressively higher Tw thresholds occur in association with lower relative humidities, which to an extent reflects the latitudinal distribution of each threshold: Tw = 27°C occurs multiple times per year in a typical moist-tropical climate, whereas Tw = 35°C occurs only in arid climates (Figure 3.1; Figure 3.3). These numbers will likely be little affected by global-mean temperature increases, as a consequence of the fact that changes in relative humidity are expected to be small (Held and Soden, 2006).

Steep and statistically significant upward trends in extreme-Tw frequency (exceedances of 27°C, 29°C, 31°C, and 33°C) and magnitude are observed for weather stations globally (Figure 3.7). Each frequency trend represents more than a doubling of occurrences of the corresponding threshold between 1979 and 2017. Trends in ERA-Interim are strongly correlated with those of HadISD but are smaller for the highest values (Figure 3.7), consistent with ERA-Interim's underestimation of extreme Tw, which is largest for the most extreme conditions (Figure 3.8). I further find that while this bias results from ERA-Interim's inability to represent the true maxima of either temperature or specific humidity, it has a tendency to more drastically underestimate temperature (that is, it exaggerates the importance of extreme specific humidity) (Figure 3.11).

Statistical Projections

Although this analysis of weather stations indicates that Tw has already exceeded 35°C in limited areas for short periods, such a value has not yet occurred at the regional scale represented

by reanalysis data, which is also the approximate scale of model projections of future Tw extremes considered in previous studies (Im et al., 2017; Pal and Eltahir, 2016). To increase the comparability of these station findings and projections, I implement a GEV analysis to estimate the amount of global warming from the pre-industrial period until Tw will regularly exceed 35°C

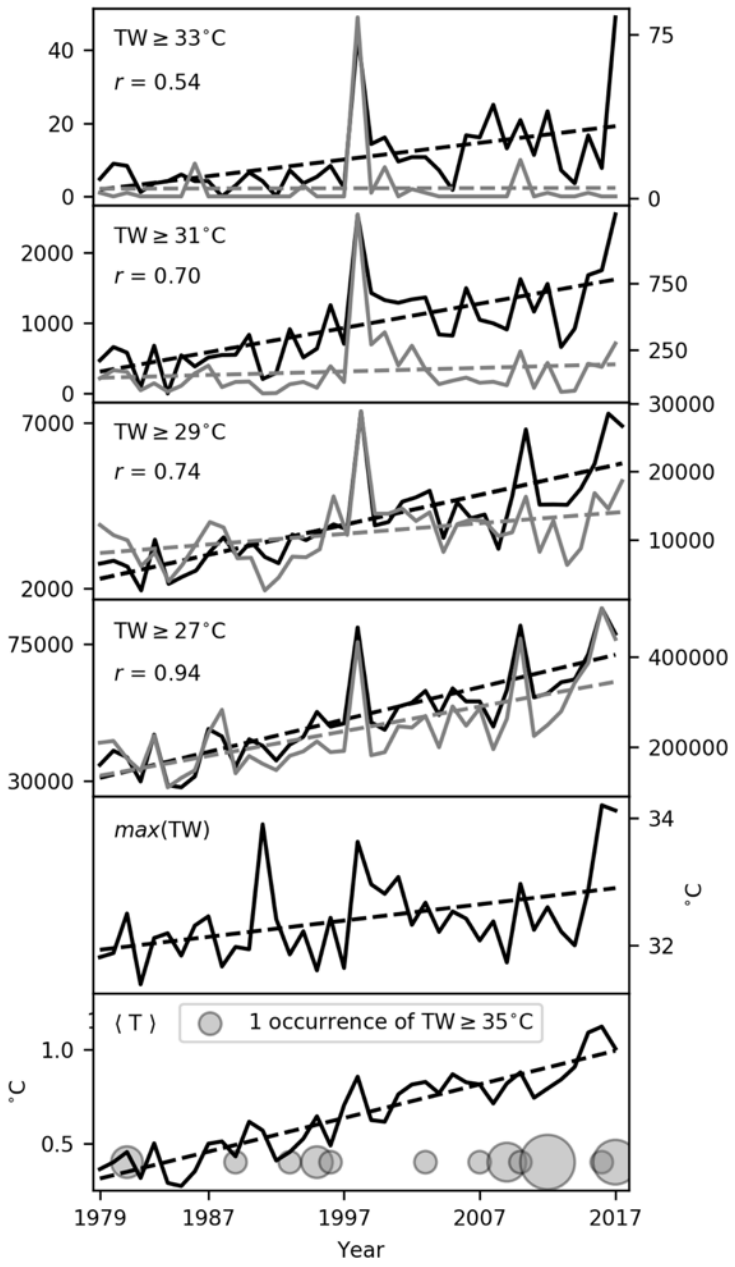

Figure 3.7: Global trends in extreme humid heat. (A-D) Annual global counts of Tw exceedances above the thresholds labeled on the respective panel, from HadISD (black, right axes, with units of station-days), and ERA-Interim grid points (gray, left axes, with units of grid-point-days). We consider only HadISD stations with at least 90% data availability over 1979-2017. Correlations between the series are annotated in the top left of each panel, and dotted lines highlight linear trends. (E) Annual global maximum Tw in ERA-Interim. (F) The line plot shows global mean annual temperature anomalies (relative to 1850-1879) according to HadCRUT4 *(33)*, which we use to approximate each year's observed warming since pre-industrial; circles indicate HadISD station occurrences of Tw exceeding 35°C, with radius linearly proportional to global annual count, measured in station-days. Steep upward trends exist in station data and in ERA-Interim, though for progressively higher thresholds, ERA-Interim's negative bias results in an inability to capture the true behavior. From Raymond, Matthews, Horton, (2019), in review.

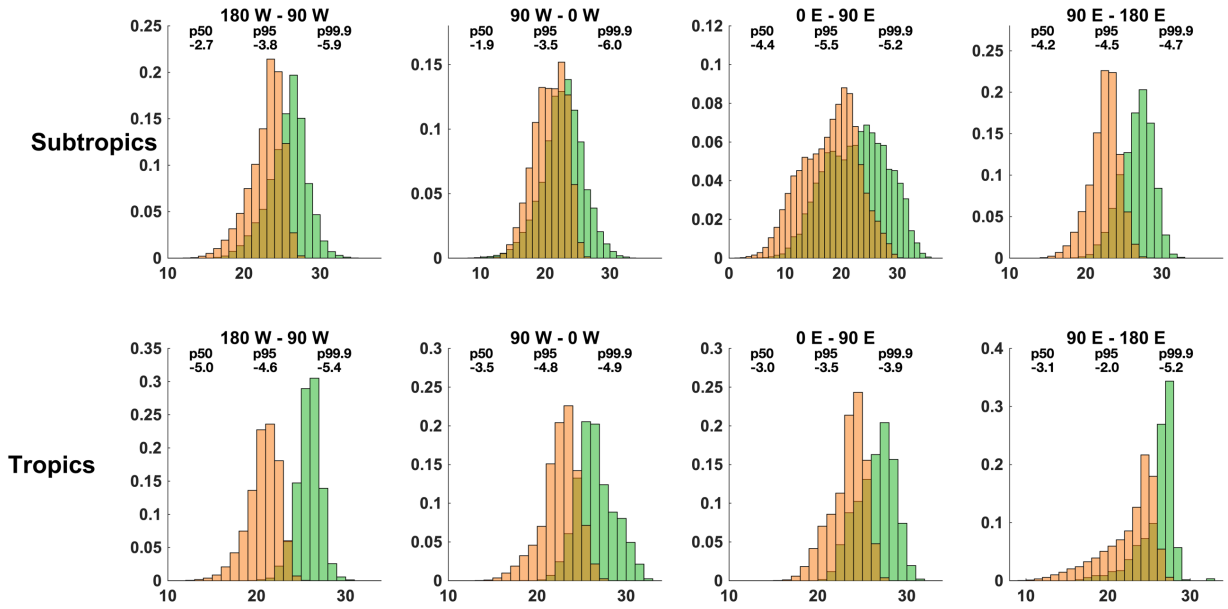

Figure 3.8: Distribution of ERA-Interim biases across regions. Normalized frequency distributions of Tw for the highest-Tw stations in HadISD (green) and hottest grid cells in ERA-Interim (orange), where stations and grid cells are defined independently between the two datasets. Small type indicates biases in °C for the 50th, 95th, and 99.9th percentiles. Tropics (subtropics) are defined as 0°-15° (15°-35°) in each hemisphere; longitudinal bounds for each region are given in the titles of the subplots. Distributions are narrowest in the subtropics and over continents, but typical ERA-Interim biases are similar across regions, generally becoming larger for higher values. From Raymond, Matthews, Horton, (2019), in review.

at the global hottest ERA-Interim grid cells. The "temperature of emergence" at the reanalysis spatiotemporal scale approximates the first occurrences of Tw = 35°C that are widespread and sustained enough to cause serious or fatal health impacts (Mora et al., 2017; Sherwood and Huber, 2010; Bynum et al., 1978). The analysis results suggest that this will first occur over the Persian Gulf at a global-mean warming of 1.3°C (median estimate of the "temperature of emergence"; 90% confidence interval: 0.81-1.73°C) (Figure 3.2a), and then over nearby land grid cells at a global-mean warming of 2.3°C (1.4-3.3°C) (Figure 3.2c). Additionally, adjusting these numbers for ERA-Interim's Persian Gulf Tw biases of -3 to -4°C (Figure 3.9) illustrates that recent warming has increased exceedances of a threshold that has been achieved on occasion throughout the

observational record (Figure 3.7). The strong marine influence on these values is also apparent in Figure 3.2.

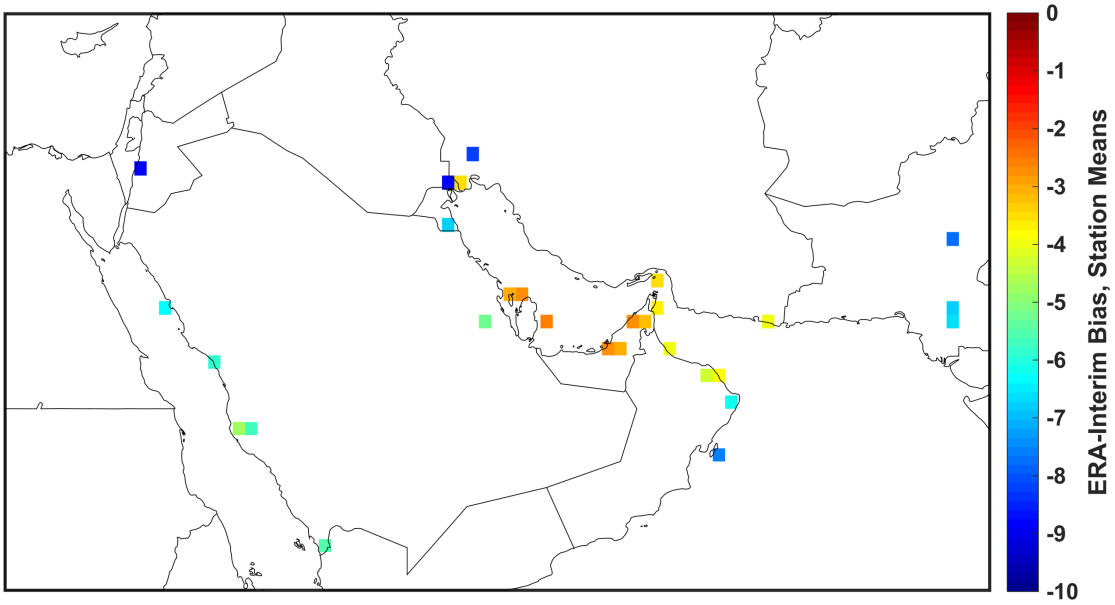

Figure 3.9: ERA-Interim biases for extreme humid heat in the Persian Gulf and Red Sea regions. Station-mean biases of ERA-Interim across all 33°C Tw observations at the shaded HadISD stations. For each station, comparisons are made with the neighboring ERA-Interim grid cell with the highest Tw value (regardless of precise distance), so as to minimize the penalty for ERA-Interim's spatial smoothing. Biases are negative everywhere, but consistently smaller along coastlines. From Raymond, Matthews, Horton, (2019), in review.

To further assess the physical realism of the GEV extrapolation, I also examine annual maximum (monthly-mean) SSTs. An atmospheric boundary layer fully equilibrated with the ocean surface would be at saturation and have the same temperature as the underlying SSTs, meaning that in principle 35°C is the lowest SST that could sustain the critical 35°C value of Tw in the air above. In reality, equilibrium will not be achieved if air-mass residence times over extreme SSTs are too short, which may be more likely if strong surface heating triggers deep convection (Sherwood and Huber, 2010). As a result, current SSTs and their trends provide some guidance as to whether these reports and projections of extreme Tw are physically plausible.

In this context, I report that for the first time monthly-mean SSTs have exceeded the 35°C threshold in the Persian Gulf, reaching 35.2°C in 2017 (Figure 3.12). However, this value is an outlier to the preceding timeseries; so, analogously to the GEV analysis, I exploit the correlation between SSTs and global-mean temperature to investigate the amount of global-mean warming required before such exceedances could be the norm at the spatial scales typical of current reanalysis products (see Methods). The results provide physically based support to the GEV analysis, predicting maximum monthly-mean SSTs will routinely reach 35°C for 1.7°C (1.3-3.4°C) of global-mean warming since the pre-industrial period, with strong agreement as to the locations at risk (Figure 3.2b,c).

Discussion

This chapter's findings indicate that occurrences of extreme Tw have increased rapidly at weather stations and in reanalysis data over the last four decades, and that parts of the subtropics are very close to the 35°C survivability limit, which has likely already been reached on the shores of the Persian Gulf. The trends described intimate with new clarity that current weather-station observations of Tw are rapidly increasing, and are more and more often reaching 35°C, as a result of the global warming to date. At the spatial scale of reanalysis, I project that Tw will regularly exceed 35°C at land grid points with less than 2.5°C of global-mean warming since the pre-industrial period — a level that will be reached in the next several decades (Van Oldenborgh et al., 2013). According to this weather-station analysis, emphasizing land grid points underplays the true risks of extreme Tw along coastlines, which tends to occur when marine air masses are advected even slightly onshore (Pal and Eltahir, 2016; Schär, 2016). The southern Persian Gulf is home to millions of people, situating them on the front lines of exposure to Tw extremes at the

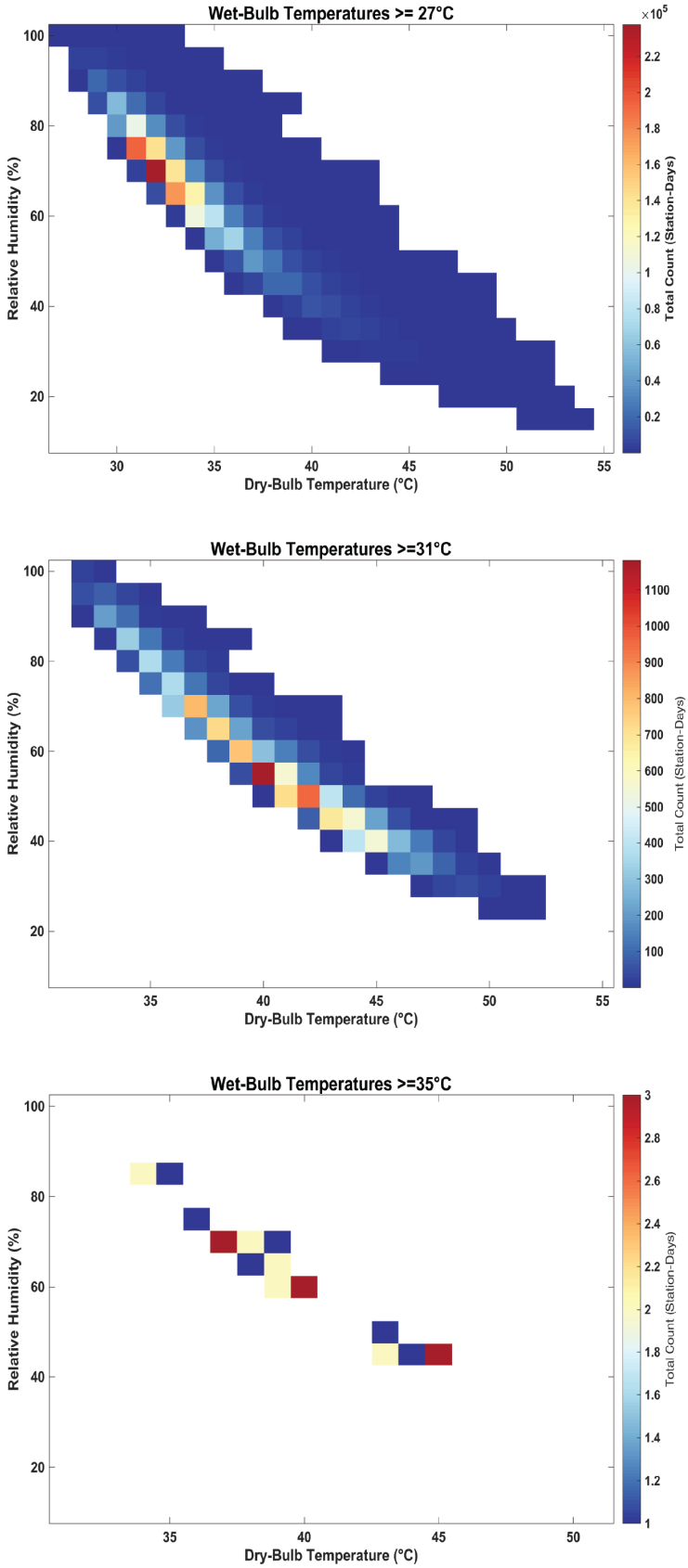

Figure 3.10: Temperature-humidity combinations leading to extreme humid heat. The frequency of dry-bulb temperature and relative humidity combinations associated with all occurrences of Tw>=27°C (top), Tw>=31°C (middle), and Tw>=35°C (bottom) in HadISD. Despite a wide spread in possible conditions, extreme Tw is associated with systematic variations in temperature and moisture. From Raymond, Matthews, Horton, (2019), in review.

edge of and outside the range of natural variability in which modern humans' physiology evolved (Marsicek et al., 2018). The deadly heat events already experienced in recent decades are indicative of the continuing trend toward increasingly extreme humid heat, and my findings underline that the diverse, consequential, and growing impacts associated with extreme humid heat represent a major societal challenge for the coming decades.

The station-oriented approach taken throughout this dissertation and the model-based approach taken in previous humid-heat studies (Coffel et al., 2018; Im et al., 2017; Pal and Eltahir, 2016) represent two different methods for obtaining valuable perspective on the genesis and characteristics of Tw extremes. The primary strength of station data is its ability to precisely capture local conditions, but even the best-available station data has limitations and uncertainties, and requires aggregation, a GEV fit, or another homogenization method for consistent comparisons. In contrast, reanalysis products and high-resolution regional models satisfy the need for spatiotemporal continuity and consistency, and allow analysis of additional variables, but often underestimate extremes for reasons that are difficult to pinpoint or disentangle (Mannshardt-Shamseldin et al., 2010). This is true of coastal air temperatures (Chapter 1), true of wet-bulb temperatures (Chapter 2), and doubly true of coastal wet-bulb temperatures (this chapter), where contingent, nonlinear, and poorly constrained processes interface with parameterized models and spotty weather-station evidence.

Efforts to better understand extreme Tw would benefit from improved integration of station data in order to alleviate reanalysis and model shortcomings, especially along coasts where Tw can vary dramatically over small distances, but this chapter, like the remainder of the dissertation, aims to demonstrate the power of leveraging the fundamental complementarity of station and physical-modeling approaches. Further research into the origins of gridded products' extreme-Tw

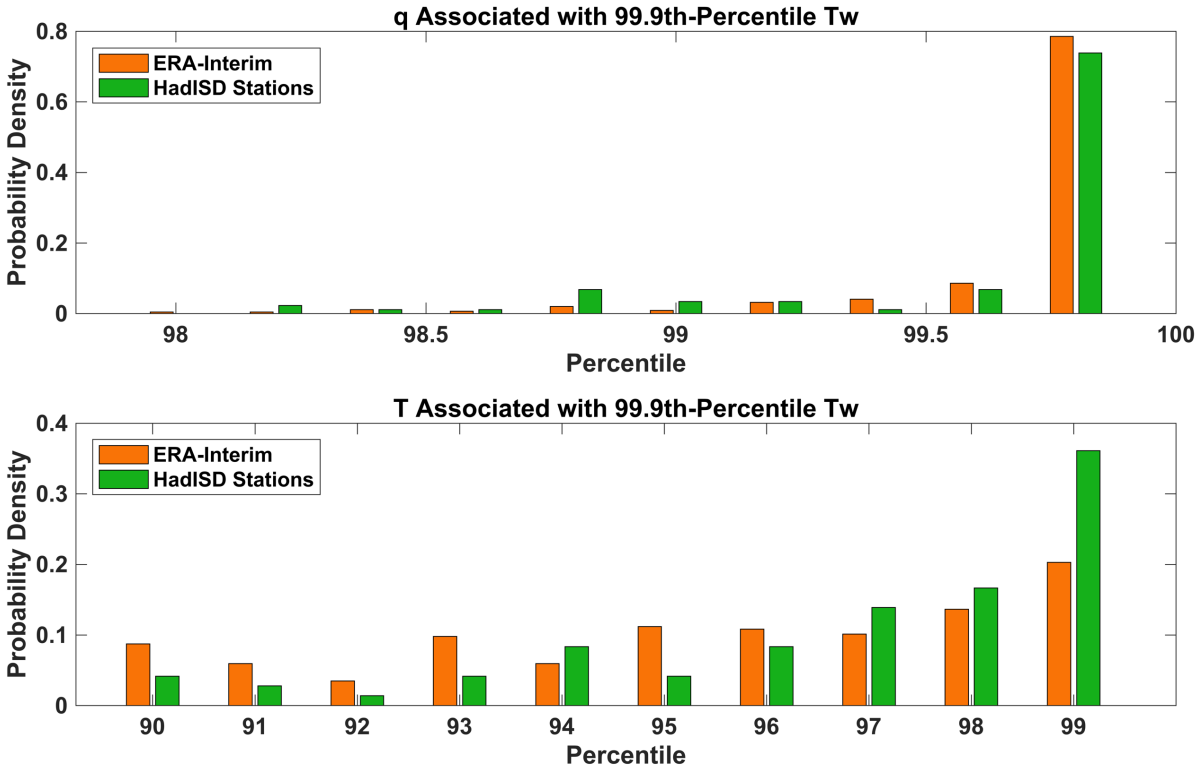

Figure 3.11: Distributions of dry-bulb temperature and specific humidity associated with 99.9th-percentile Tw occurrences for the single highest-Tw HadISD station and ERA-Interim gridpoint in eight regions: the tropics (15°S-15°N) and subtropics (15°-35° in each hemisphere), each divided into four 90° quadrants. All values are station- or gridpoint-relative. Whereas about 35% of extreme Tw occurrences at stations are associated with 99th-percentile T, this number is only about 20% at ERA-Interim gridpoints, indicating the reanalysis product's overreliance on moisture to achieve extreme Tw.

biases, and continued advances in areas such as data assimilation and high-resolution modeling, will also help enable the development of a more unified approach drawing on all available sources. This type of integrative approach is especially valuable where the scale and inherent complexity of the driving physical processes, as in heat-humidity combinations, makes the generation of clear *a priori* expectations of extreme values difficult.

As this chapter and the preceding ones have discussed, the regional and multivariate nature of extreme wet-bulb temperature requires dedicated research efforts to uncover and explain its most vital characteristics. Key multiscale Tw processes necessitating closer comparison between

observations and models include coastal upwelling, atmospheric convection, land-atmosphere interactions, and atmospheric variability linked to SSTs (Raymond et al., 2017) — particularly at the hourly, 1-10-km scale. These questions have thus far only been examined for temperature, or in a handful of case studies. More of the latter would be useful especially if targeted for coastal areas, and if giving a detailed analytical treatment to individual events. Such studies could help illuminate the unfolding interactions of processes on weather timescales, both observationally and in the sense of testing sensitivities to putative major factors such as SSTs, irrigation, and large-scale atmospheric stability. Comparisons of gridded-product biases among models and regions are sorely lacking, as are investigations of the effects of historical variability and statistical methodologies on extreme-Tw projections. Moving beyond the regional scale to the local, interactions and net effects of anthropogenic forcings like waste heat from vehicles and machinery, waste heat and moisture from air conditioners, and evapotranspiration from urban vegetation require careful assessment in the context of extreme humid heat so intense as to broadly and imminently threaten human health and economic productivity.

This level of severe humid heat also provides incentive for a broad interdisciplinary research initiative to better characterize health impacts. The collection of health data at hourly and subhourly timescales, international collaborations with public-health experts and social scientists, and dedicated high-resolution modeling projects would aid in answering questions about how vulnerable populations (such as the elderly, those with pre-existing health conditions, and those performing outdoor labor) will be adversely affected as peak Tw advances further into the extreme ranges I consider here. Of particular salience is the need to ascertain how acclimation to high-heat-stress conditions is diminished as the physiological survivability limit is approached. Such efforts

may also help resolve the reasons for the paucity of reported mortality and morbidity impacts associated with observed near-35°C conditions (Pal and Eltahir, 2016; Schär, 2016), despite the robust physiological motivation for expecting them (Hanna and Tait, 2015).

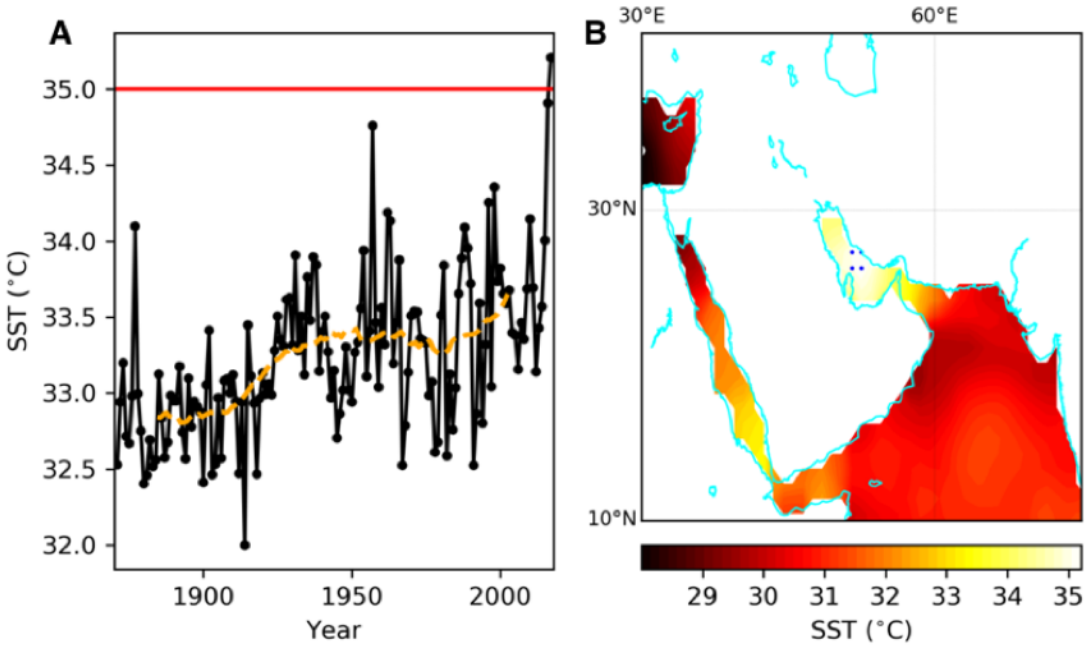

Figure 3.12: Trends and maxima of observed sea-surface temperatures. (A) Annual maximum of monthly SST across all grid cells in the HadISST dataset; orange line is a running 30-year average, and red line marks 35°C. (B) All-time maximum SST around the Persian Gulf and Arabian Sea. The blue points mark locations where monthly-mean SST rose above 35°C in 2017. This first reported crossing by SSTs of the 35°C threshold further supports the occurrence of 35°C Tw along the coastlines at the same time. From Raymond, Matthews, Horton, (2019), in review.

Conclusions and Future Work

This dissertation examines the regional patterns of extreme heat, with particular focus on taking a comprehensive approach to topics previously addressed only with case studies. This impetus largely manifests through taking a climatological view in considering the essential research questions around the interaction between water and extreme heat. Key analyses include characterizing the role of water vapor, through quantifying its facilitation of extreme humid heat and its spatiotemporal variations due to large-scale atmospheric phenomena such as monsoons and semipermanent high-pressure systems, and studying the effects of sea-surface temperature patterns on extreme heat both locally and remotely via teleconnections. In so doing, this dissertation touches on — and aims to provide the knowledge basis for improving — meteorological predictability, subseasonal forecasts, impacts assessments, and detailed regional projections of extreme heat. In addition, definitional and statistical issues, such as the most-meaningful mathematical separation of the effects of water vapor and dry-bulb temperature on wet-bulb temperature, or the most-characteristic definition of coastal cooling of extreme heat, are carefully treated, with new standards proposed and their efficacy demonstrated.

As climate-model capabilities grow more extensive, they clear the way for rapid advances in understanding of regional processes, the interactions of which may be poorly understood even if the larger-scale behavior is well-characterized. Within this context, this dissertation showcases how observationally grounded analysis retains the ability to reveal novel insights about how geographic and meteorological factors combine to shape the ultimate conditions. Such frameworks can lead to novel conclusions about what is known, and what needs to be studied, about regional-scale extreme heat in order to most effectively allocate intellectual and financial resources and to most judiciously design policies (Seneviratne et al., 2018). The fairness and efficiency of these

societal responses to extreme heat become more important as the events continue to grow in severity decade by decade.

This dissertation highlights that coastal areas remain loci of deep climate uncertainty, as a result of factors which include the small spatiotemporal scale of the atmospheric processes, their contingency on favorable large-scale conditions, their sensitivity to poorly resolved ocean currents and upwelling, and incomplete representations of the litany of complex land-cover types. Manifestations of this uncertainty include large biases, even for state-of-the-art gridded products, and an inability to capture regional and seasonal variations. Given the concentration of extreme heat stress along coastlines (Chapter 1), as well as the disproportionate fraction of the global population that inhabits them (Small and Cohen, 1998), targeted observational campaigns and greater rescue or digitization of existing but obscure data (Brunet and Jones, 2011) would greatly aid in improving climatologies and future climate projections for these ~50-km-wide swaths.

Another overarching theme in this dissertation concerns the necessity of carefully evaluating projections, using the best observational basis that can be constructed. In particular, Chapter 1 showed that even high-resolution projections produced in the last few years carry with them severe biases, and that this is true regardless of whether statistical or dynamical downscaling is employed. Furthermore, these biases cannot be explained by resolution inadequacies alone, meaning that additional factors must be at work, likely including the propagation of physical-process errors. Although such errors may be understandable, in the sense that they pertain to complex region-specific interactions that are sensitive to a range of anthropogenic and internal-to-the-climate-system parameters, their repercussions are evident in the consequent inability of gridded products to sometimes represent even the most basic observed spatial or temporal regional

patterns. And these regional-to-local patterns and processes are key contributors in shaping the ultimate manifestations of decadal climate change (Diffenbaugh et al., 2005).

Chapter 2 revealed certain similarities of extreme humid heat with extreme dry-bulb heat, most prominently in regions such as the eastern U.S. where the correlation of dry-bulb temperature and atmospheric moisture is high. There, a hot day is typically a humid one, and both variables reach their maximum values in mid-summer. In many other parts of the world, however, including locations where both temperature and moisture reach levels that far exceed those in the mid-latitudes, this correlation is much weaker. Correspondingly, the patterns of extreme humid heat are more complex, exhibiting major variations across regions and seasons. The contributions of moisture are in most cases the dominant force in determining where extreme humid heat occurs, and consequently, identifying its sources and transport mechanisms is crucial for predicting extreme humid heat on meteorological as well as climatological timescales. The relevant existing work in this field is highly localized or otherwise of narrow applicability, and broader conclusions rely, as I do here, on a certain amount of conjecture (Schär, 2016; Sherwood and Huber, 2010). In addition to further examining the role of the ocean, as mentioned above, evaporation (from natural water bodies or saturated soils), transpiration (from natural vegetation or crops), and moisture advection all must be thoroughly considered and partitioned to develop a more-complete picture of the key controlling mechanisms in a given region. The problem's complexity lies in how these mechanisms may be contingent, co-dependent, time-varying, or interactive in many other ways.

Chapter 3 expanded on Chapter 2 to consider the patterns and trends of extreme humid heat having the potential to cause the coastal Middle East, and subsequently northern South Asia, to become uninhabitable (in the absence of artificial cooling) on the hottest days within the next several decades. Indeed, Chapter 3 reported for the first time reliable exceedances of the human

physiological survivability threshold, in several cases by more than 1°C. That major health effects were not reported in conjunction with these events is likely due to their brevity, to the local population's acclimation to intense heat more generally, and perhaps to incomplete reporting or record-keeping. Nonetheless, extreme humid heat is a serious health threat via well-established mechanisms (Mora et al., 2017), making significant future increases a major public-health concern throughout the tropical and temperate regions of the world. Additional work to understand the relationship of the most-intense humid heat to global-mean warming (via energy-balance constraints) or to regional factors (such as via moisture advection or atmospheric blocking) is essential for preparing for these alarming projections.

Developing a better understanding of the regional and global mechanisms that lead to the most intense heat-humidity extremes is essential to improve present-day forecasts and impacts assessments, as well as future projections. Heat-humidity extremes are highly variable in space and time, and the statistics of this variability, as well as the dynamics that drive it, remain poorly constrained. An emerging technique for organizing inquiries into this problem, and a variety of other climate extremes besides, is that of 'correlated extremes'. By designing analyses to address head-on the inherent multivariate nature of many types of climate risk, whether purely physical or the result of some anthropogenic-physical interaction, researchers can more efficiently get to the core of the factors driving variability of and changes in the impacts of climate extremes. For example, some combinations of extreme climate events are impactful because they comprise multiple co-occurring variables; others, because they comprise multiple events occurring simultaneously in different places; and still others, because they occur in rapid sequence or persist for an exceptionally long time. In each case, all the major levers of human society — governmental policies, trade networks, agricultural practices, socioeconomic power — act to fundamentally

shape the impact and the response, and, characteristically, poor communication between actors separated in space or time is especially deleterious. The feedback of air-conditioning-related emissions on extreme humid heat, with the urban poor of developing countries suffering most, is one such correlated extreme (Salamanca et al., 2014; O'Neill et al., 2005); another is the sequence of extensive wildfires, intense rainfall, and damaging mudslides in California that has occurred multiple times just in the past decade (Crockett and Westerling, 2018). I have played the leading role in organizing a May 2019 workshop directly aimed at resolving some of these ambiguities and delineating productive multidisciplinary future research agendas for the broader climate-extremes community, but years will surely pass before this approach is utilized to its maximal effectiveness.

Remaining scientific challenges around extreme temperatures are many-fold, but can be divided into several top-level categories, elaborated in the following paragraphs.

One such area concerns the sensitivity of extreme heat to forcings at multiple scales and locations. The effects of a driving factor tend to decay with distance, but often propagate along preferred geographic pathways, resulting in causal relationships that are also functions of angular direction. Persistent factors, such as those associated with modes of large-scale climate variability, tend to exert an overwhelming influence when 'active', shaping the magnitude as well as the severity of extreme heat in many places. Local effects on extreme heat are often second-order and contingent, but can become first-order under certain locally determined conditions, resulting in, e.g., intense urban heat islands or coasts that are cool relative to inland. The relative importance of such diverse driving factors of extreme heat is difficult to assess. To improve forecasts and projections, combinations of machine-learning and dynamical-modeling approaches are necessary to identify specific places where dominant causality exists, which driving factors it consists of,

and under which sets of circumstances. Such a paradigm is analogous to, and could draw from, canonical studies of feedbacks and energy flows in the climate system (Cai et al., 2019; Plumb, 1985). Climate science is already tending in this direction to some extent, as evidenced by the recent initiation of continuous weather-to-climate research programs, but has yet to use these tools to consider extreme heat with significant depth or rigor (Mariotti et al., 2019).

Another important area where this dissertation suggests future work should concentrate is the spatiotemporal variability and complex meteorology of heat-humidity extremes. The evidence presented here indicates that detailed study is necessary of the processes that produce them on synoptic timescales and that modulate them on interannual timescales. For example, it would greatly aid long-term climate projections as well as better inform short- and medium-term adaptation efforts to have a greater ability to quantify the sources of moisture that fuel extreme humid heat, as in Chapter 2. Northern South Asia experiences near-global-maximum humid heat despite being situated distant from marine moisture sources, making it an ideal place to test the hypothesis that heat-humidity extremes can result primarily from strong moisture advection (i.e., in conjunction with the summer monsoon) (Im et al., 2017), and also to comprehensively compare for the first time the relative contributions of this with the effects of other moisture sources — most pertinently local evaporation (from local water bodies or saturated soil) and transpiration (from crops or natural vegetation) (Schär, 2016; Gershunov et al., 2009). The net effect of variations in each factor, due to internal variability combined with anthropogenic forcing, could then be isolated.

Thirdly, this dissertation points to the long-known need for coordinated interdisciplinary research and practice around extreme heat, aimed in particular at understanding and addressing demographic variations in vulnerability to combined heat-humidity events as global maximum Tw

increases overall, and exceeds the physiological survivability limit more often and for longer periods. Most of the studies establishing the theoretical basis for the 35°C Tw limit are decades old, and cannot be replicated for ethical reasons, while empirical studies are impaired by the rarity of near-35°C events and the political and data-availability limitations present in many of the countries affected. Broad research programs, comprising fieldwork, detailed observational analysis of instruments and practices, and modeling, could produce the kind of targeted results necessary for statistical confidence on the climate-science side and lay the groundwork for further progress, while initiatives to embed health, energy, urban-planning, and other experts in research teams would facilitate identification of cross-sector vulnerabilities to extreme humid heat and development of effective counter-measures.

Aiding in achieving these objectives would be continued refinements to gridded products, aimed at reducing their biases relative to weather-station data, and especially in ways that are geographically-aware; for example, developing interpolation methods that allow spatial autocorrelation functions to vary according to time of day, season, or large-scale meteorological forcing. Thorough scrutiny of observational datasets can reveal unreported or under-reported regional phenomena, and intercomparison among such datasets can aid in constraining the spread in a given statistic, useful in assessing the realism of highly extreme observations.

Most prominently, this dissertation uncovers a drastic increase in extreme heat due to the observed ~1°C increase in global-mean temperature since the pre-industrial period, and describes further rapid increases over the coming century, to levels that will pose major and diverse difficulties even with the aid of technological advancements. In many places, regional-scale influences such as monsoons and marine-air incursions dominate the spatiotemporal patterns of extreme heat, and accurately capturing the characteristics of these systems is essential for

projections. Long-term changes in these systems may scramble the relationships on which coarse-resolution projections are predicated, further underscoring the need for additional integrative research on how the factors combine to shape extreme heat at regional scales.

References

Adams, D. K., and Comrie, A. C. (1997). The North American Monsoon. *Bull. Amer. Meteorol. Soc., 78* (10), 2197-2213. doi:10.1175/1520-0477(1997)078<2197:TNAM>2.0.CO;2.

AghaKouchak, A., Cheng, L., Mazdiyasni, O., and Farahmand, A. (2014). Global warming and changes in risk of concurrent climate extremes: insights from the 2014 California drought. *Geophys. Res. Lett., 41,* 8847-8852. doi:10.1002/2014gl062308.

Alter, R. E., Douglas, H. C., Winter, J. M., and Eltahir, E. A. B. (2018). Twentieth century regional climate change during the summer in the central United States attributed to agricultural intensification. *Geophys. Res. Lett., 45.* doi:10.1002/2017gl075604.

Alvarez-Castro, M. C., Faranda, D., and Yiou, P. (2018). Atmospheric dynamics leading to West European summer hot temperatures since 1851. *Complexity*, *2494509,* 1–10. doi:10.1155/2018/2494509.

Anderson, B. G., and Bell, M. L. (2009). Weather-related mortality: how heat, cold, and heat waves affect mortality in the United States. *Epidem., 20,* 205-213. doi:10.1097/EDE.0b013e318190ee08.

Anderson, B. G., and Bell, M. L. (2011). Heat waves in the United States: Mortality risk during heat waves and effect modification by heat wave characteristics in 43 U.S. communities. *Env. Health Persp., 119,* 210-218. doi:10.1289/ehp.1002313.

Andreadis, K. M., Clark, E. A., Wood, A. W., Hamlet, A. F., and Lettenmaier, D. P. (2005). Twentieth-century drought in the conterminous United States. *J. Hydrometeorol., 6,* 985-1001. doi:10.1175/jhm450.1.

Argüeso, D., Di Luca, A., Perkins-Kirkpatrick, S. E., and Evans, J. P. (2016). Seasonal mean temperature changes control future heat waves. *Geophys. Res. Lett., 43,* 7653-7660. doi:10.1002/2016gl069408.

Argüeso, D., Evans, J. P., Fita, L., and Bormann, K. J. (2014). Temperature response to future urbanization and climate change. *Clim. Dyn., 42,* 2183-2199. doi:10.1007/s00382-013-1789-6.

Argüeso, D., Evans, J. P., Pitman, A. J., and Di Luca, A. (2015). Effects of city expansion on heat stress under climate change conditions. *PLoS One, 10 (2),* e0117066. doi:10.1371/journal.pone.0117066.

Arritt, R. W. (1993). Effects of the large-scale flow on characteristic features of the sea breeze. *J. Appl. Meteorol., 32,* 116-125. doi:10.1175/1520-0450(1993)032<0116:EOTLSF>2.0.CO;2.

Ashfaq, M., Rastogi, D., Mei, R., Kao, S.-C., Gangrade, S., Naz, B. S., and Touma, D. (2016). High-resolution ensemble projections of near-term regional climate over the continental United States. *J. Geophys. Res. Atmos., 121,* 9943-9963. doi:10.1002/2016jd025285.

Barriopedro, D., Fischer, E. M., Luterbacher, J., Trigo, R. M., and Garcia-Herrera, R. (2011). The hot summer of 2010: redrawing the temperature record map of Europe. *Science, 332* (6026)*,* 220-224. doi:10.1126/science.1201224.

Bartos, M. D., and Chester, M. V. (2015). Impacts of climate change on electric power supply in the Western United States. *Nat. Clim. Change, 5,* 748-752. doi:10.1038/nclimate2648.

Battisti, D. S., and Naylor, R. L. (2009). Historical warnings of future food insecurity with unprecedented seasonal heat. *Science, 323* (5911)*,* 240-244. doi:10.1126/science.1164363.

Bobb, J. F., Obermeyer, Z., Wang, Y., and Dominici, F. (2014). Cause-specific risk of hospital admission related to extreme heat in older adults. *J. Amer. Med. Assoc., 312,* 2659-2667. doi:10.1001/jama.2014.15715.

Brunet, M., and Jones, P. (2011). Data rescue initiatives: Bringing historical climate data into the 21st century. *Clim. Res., 47,* 29-40. doi:10.3354/cr00960.

Burkart, K., Meier, F., Schneider, A., Breitner, S., Canario, P., Alcoforado, M. J., Scherer, D., and Endlicher, W. (2016). Modification of heat-related mortality in an elderly urban population by vegetation (urban green) and proximity to water (urban blue): Evidence from Lisbon, Portugal. *Env. Health Persp., 124* (7), 927-934. doi:10.1289/ehp.1409529.

Burke, M., Hsiang, S. M., and Miguel, E. (2015). Global non-linear effect of temperature on economic production. *Nature, 527,* 235-250. doi:10.1038/nature15725.

Byers, E., Gidden, M., Leclere, D., Balkovic, J., Burek, P., Ebi, K., Greve, P., Grey, D., Havlik, P., Hillers, A., Johnson, N., Kahil, T., Krey, V., Langan, S., Nakicenovic, N., Novak, R., Obersteiner, M., Pachauri, S., Palazzo, A., Parkinson, S., Rao, N. D., Rogelj, J., Satoh, Y., Wada, Y., Willaarts, B., and Riahi, K. (2018). Global exposure and vulnerability to multi-sector development and climate change hotspots. *Env. Res. Lett., 13,* 055012. doi:10.1088/1748-9326/aabf45.

Bynum, G. D., Pandolf, K. B., Schuette, W. H., Goldman, R. F., Lees, D. E., Whang-Peng, J., Atkinson, E.R., and Bull, J. M. (1978). Induced hyperthermia in sedated

humans and the concept of critical thermal maximum. *Amer. J. Physiol., 235,* R228-R236. doi:10.1152/ajpregu.1978.235.5.R228.

Cai, W., et al. (2019). Pantropical climate interactions. *Science, 363,* eaav4236. doi:10.1126/science.aav4236.

Center for International Earth Science Information Network - CIESIN - Columbia University. 2016. Gridded Population of the World, Version 4 (GPWv4): Population Count Adjusted to Match 2015 Revision of UN WPP Country Totals. Palisades, NY: NASA Socioeconomic Data and Applications Center (SEDAC). doi:10.7927/H4SF2T42. Accessed 05 May 2018.

Chapman, L., Azevedo, J. A., and Prieto-Lopez, T. (2013). Urban heat and critical infrastructure networks: a viewpoint. *Urban Clim., 3,* 7-12. doi:10.1016/j.uclim.2013.04.001.

Cheng, L., and AghaKouchak, A. (2014). Nonstationary precipitation intensity-duration-frequency curves for infrastructure design in a changing climate. *Sci. Rep., 4,* 7093. doi:10.1038/srep07093.

Christidis, N., Stott, P. A., Hegerl, G. C., and Betts, R. A. (2013). The role of land use change in the recent warming of daily extreme temperatures. *Geophys. Res. Lett., 40,* 1-6. doi:10.1002/grl.50159.

Clemesha, R. E. S., Guirguis, K., Gershunov, A., Small, I. J., and Tardy, A. (2018). California heat waves: their spatial evolution, variation, and coastal modulation by low clouds. *Clim. Dyn., 50,* 4285-4301. doi:10.1007/s00382-017-3875-7.

Coffel, E., Horton, R. M., and de Sherbinin, A. (2018). Temperature and humidity based projections of a rapid rise in global heat stress exposure during the 21st century. *Env. Res. Lett., 13,* 014001. doi:10.1088/1748-9326/aaa00e.

Coffel, E., Thompson, T., and Horton, R. M. (2017). The impacts of rising temperatures on aircraft takeoff performance. *Clim. Change 144 (2),* 381-388. doi:10.1007/s10584-017-2018-9.

Cohen, J. E., and Small, C. (1998). Hypsographic demography: The distribution of human population by altitude. *Proc. Nat. Acad. Sci., 95,* 14009-14014. doi:10.1073/pnas.95.24.14009.

Coumou, D., Petoukhov, V., Rahmstorf, S., Petri, S., and Schellnhuber, H. J. (2014). Quasi-resonant circulation regimes and hemispheric synchronization of extreme weather in boreal summer. *Proc. Nat. Acad. Sci., 111 (34),* 12331-12336. doi:10.1073/pnas.1412797111.

Craig, A. B. Jr., and Dvorak, M. (1966). Thermal regulation during water immersion. *J. Appl. Physiol., 21* (5), 1577-1585. doi:10.1152/jappl.1966.21.5.1577.

Crockett, J. L., and Westerling, A. L. (2018). Greater temperature and precipitation extremes intensify Western U.S. droughts, wildfire severity, and Sierra Nevada tree mortality. *J. Clim., 31,* 341-354. doi:10.1175/jcli-d-17-0254.1.

Daly, C., Helmer, E. H., and Quiñones, M. (2003). Mapping the climate of Puerto Rico, Vieques, and Culebra. *Int. J. Clim., 23,* 1359-1381. doi:10.1002/joc.937.

Daly, C., Halbleib, M., Smith, J. I., Gibson, W. P., Doggett, M. K., Taylor, G. H., Curtis, J., and Pasteris, Phillip P. (2008). Physiographically sensitive mapping of climatological temperature and precipitation across the conterminous United States. *Int. J. Climatol., 28,* 2031-2064. doi:10.1002/joc.1688.

Davies-Jones, R. (2008). An efficient and accurate method for computing the wet-bulb temperature along pseudoadiabats. *Mon. Wea. Rev., 136,* 2764-2785. doi:10.1175/2007mwr2224.1.

Davis, R. E., McGregor, G. R., and Enfield, K. B. (2016). Humidity: a review and primer on atmospheric moisture and human health. *Env. Res., 144,* 106-116. doi:10.1016/j.envres.2015.10.014.

Davis, L. W., and Gertler, P. J. (2015). Contribution of air conditioning adoption to future energy use under global warming. *Proc. Nat. Acad. Sci., 112*(19), 5962-5967. doi:10.1073/pnas.1423558112.

Dee, D. P., and Coauthors (2011). The ERA-Interim reanalysis: configuration and performance of the data assimilation system. *Q. J. R. Meteorol. Soc., 137,* 553-597. doi:10.1002/qj.828.

Dell, M., Jones, B. F., and Olken, B. A. (2012). Temperature shocks and economic growth: evidence from the last half century. *Amer. Econ. J. Macroecon., 4*(3), 66-95. doi:10.1257/mac.4.3.66

Diffenbaugh, N. S. (2009). Influence of modern land cover on the climate of the United States. *Clim. Dyn., 33,* 945-958. doi:10.1007/s00382-009-0566-z.

Diffenbaugh, N. S., Pal, J. S., Giorgi, F., and Gao, X. (2007). Heat stress intensification in the Mediterranean climate change hotspot. *Geophys. Res. Lett., 34,* L11706. doi:10.1029/2007gl030000.

Diffenbaugh, N. S., Pal, J. S., Trapp, R. J., and Giorgi, F. (2005). Fine-scale processes regulate the response of extreme events to global climate change. *Proc. Nat. Acad. Sci. 102 (44),* 15774-15778. doi:10.1073/pnas.0506042102.

Donat, M. G., Pitman, A. J., and Seneviratne, S. I. (2017). Regional warming of hot extremes accelerated by surface energy fluxes. *Geophys. Res. Lett., 44,* 7011-7019. doi:10.1002/2017gl073733.

Dong, B., Gregory, J. M., and Sutton, R. T. (2009). Understanding land-sea warming contrast in response to increasing greenhouse gases. Part I: Transient Adjustment. *J. Clim., 22,* 3079-3097. doi:10.1175/2009jcli2652.1.

Dunn, R. J. H., Willet, K. M., Thorne, P. W., Woolley, E. V., Durre, I., Dai, A., Parker, D. E., and Vose. R. S. (2012). HadISD: a quality-controlled global synoptic report database for selected variables at long-term stations from 1973-2011. *Clim. Past, 8,* 1649-1679. doi:10.5194/cp-8-1649-2012.

Dunn, R. J. H., Willett, K. M., Parker, D. E., and Mitchell, L. (2016). Expanding HadISD: quality-controlled, sub-daily station data from 1931. *Geosci. Instrum. Method. Data Syst., 5,* 473-491. doi:10.5194/gi-5-473-2016.

Dunne, J. P., Stouffer, R. J., and John, J. G. (2013). Reductions in labour capacity from heat stress under climate warming. *Nat. Clim. Change, 3,* 563-566. doi:10.1038/nclimate1827.

Dvorak, M. J., Corcoran, B. A., Ten Hoeve, J. E., McIntyre, N. G., and Jacobson, M. Z. (2013). US East Coast offshore wind energy resources and their relationship to peak-time electricity demand. *Wind Energ., 16,* 977-997. doi:10.1002/we.1524.

Eager, R. E., Raman, S., Wootten, A., Westphal, D. L., Reid, J. S., and Al Mandoos, A. (2008). A climatological study of the sea and land breezes in the Arabian Gulf region. *J. Geophys. Res., 113,* D15106. doi:10.1029/2007jd009710.

Feudale, L., and Shukla, J. (2011). Influence of sea surface temperature on the European heat wave of 2003 summer. Part II: a modeling study. *Clim. Dyn.*, 36, 1705-1715. doi:10.1007/s00382-010-0789-z.

Finkele, K. (1998). Inland and offshore propagation speeds of a sea breeze from simulations and measurements. *Boundary-Layer Meteorol., 87,* 307-329. doi:10.1023/a:1001083913327.

Fiore, A. M., et al. (2012). Global air quality and climate. *Chem. Soc. Rev., 41,* 6663-6683. doi:10.1039/c2cs35095e.

Fischer, E. M., and Knutti, R. (2013). Robust projections of combined humidity and temperature extremes. *Nat. Clim. Change, 3,* 126-130. doi:10.1038/nclimate1682.

Freychet, N., Tett, S. F. B., Hegerl, G. C., and Wang, J. (2018). Central-Eastern China persistent heat waves: Evaluation of the AMIP models. *J. Clim., 31,* 3609-3624. doi:10.1175/jcli-d-17-0480.1.

Gao, Y., Fu, J. S., Drake, J. B., Liu, Y., and Lamarque, J.-F. (2012). Projected changes of extreme weather events in the eastern United States based on a high resolution climate modeling system. *Env. Res. Lett., 7.* doi:10.1088/1748-9326/7/4/044025.

Gasparrini, A., et al. (2015). Mortality risk attributable to high and low ambient temperature: a multicountry observational study. *Lancet, 386,* 369-375. doi:10.1016/S0140-6736(14)62114-0.

Gershunov, A., Cayan, D. R., and Iacobellis, S. F. (2009). The great 2006 heat wave over California and Nevada: signal of an increasing trend. *J. Clim., 22,* 6181-6203. doi:10.1175/2009jcli2465.1.

Gilliam, R. C., Raman, S., and Niyogi, D. D. S. (2004). Observational and numerical study on the influence of large-scale flow direction and coastline shape on sea-breeze evolution. *Boundary-Layer Meteorol., 111* (2)*,* 275-300. doi:10.1023/B:BOUN.0000016494.99539.5a.

Gosling, S. N., McGregor, G. R., and Páldy, A. (2007). Climate change and heat-related mortality in six cities. Part I: Model construction and validation. *Int. J. Biometeorol., 51,* 525-540. doi:10.1007/s00484-007-0092-9.

Grotjahn, R., et al. (2016). North American extreme temperature events and related large-scale meteorological patterns: a review of statistical methods, dynamics, modeling, and trends. *Clim. Dyn., 46,* 1151-1184. doi:10.1007/s00382-015-2638-6.

Hall, A. (2014). Projecting regional change. *Science, 346* (6216), 1461-1462. doi:10.1126/science.aaa0629.

Hall, A., Qu, X., and Neelin, J. D. (2008). Improving predictions of summer climate change in the United States. *Geophys. Res. Lett., 35,* L01702. doi:10.1029/2007gl032012.

Hanna, E. G., and Tait, P. W. (2015). Limitations to thermoregulation and acclimatization challenge human adaptation to global warming. *Int. J. Env. Res. Public Health, 12,* 8034-8074. doi:10.3390/ijerph120708034.

Hartmann, D. L. (2015). Pacific sea surface temperature and the winter of 2014. *Geophys. Res. Lett., 42*, 1894-1902. doi:10.1002/2015gl063083.

Hass, A. L., Ellis, K. N., Mason, L. R., Hathaway, J. M., and Howe, D. A. (2016). Heat and humidity in the city: neighborhood heat index variability in a mid-sized city

in the southeastern United States. *Int. J. Env. Res. Public Health, 13,* 117. doi:10.3390/ijerph13010117.

Held, I. M., and Soden, B. J. (2006). Robust responses of the hydrological cycle to global warming. *J. Clim., 19,* 5686-5699. doi:10.1175/jcli3990.1.

Herold, N., Kala, J., and Alexander, L. V. (2016). The influence of soil moisture deficits on Australian heatwaves. *Env. Res. Lett.*, *11*(6). doi:10.1088/1748-9326/11/6/064003.

Higgins, R. W., and Shi, W. (2000). Dominant factors responsible for interannual variability of the summer monsoon in the southwestern United States. *J. Clim., 13* (4)*,* 759-776. doi:10.1175/1520-0442(2000)013<0759:DFRFIV>2.0.CO;2.

Horton, R. M., Mankin, J. S., Lesk, C., Coffel, E., and **Raymond, C.** (2016). A review of recent advances in research on extreme heat events. *Curr. Clim. Change Rep., 2,* 242-259. doi:10.1007/s40641-016-0042-x.

Hsiang, S. M., Kopp, R., Jina, A., Delgado, M., Rising, J., Mohan, S., Muir-Wood, R., Rasmussen, D. J., Mastrandrea, M., Wilson, P., Larsen, K., and Houser, T. (2014). *American Climate Prospectus: Economic Risks in the United States.* New York: Rhodium Group.

Hu, X.-M., and Xue, M. (2016). Influence of synoptic sea-breeze fronts on the urban heat island intensity in Dallas-Fort Worth, Texas. *Mon. Wea. Rev., 144,* 1487-1507. doi:10.1175/mwr-d-15-0201.1.

Im, E.-S., Pal, J. S., and Eltahir, E. A. B. (2017). Deadly heat waves projected in the densely populated agricultural regions of South Asia. *Sci. Adv., 3,* e1603322. doi:10.1126/sciadv.1603322.

Im, E.-S., Kang, S., and Eltahir, E. A. B. (2018). Projections of rising heat stress over the western Maritime Continent from dynamically downscaled climate simulations. *Glob. Planet. Change, 165,* 160-172. doi:10.1016/j.gloplacha.2018.02.014.

Jones, B., O'Neill, B. C., McDaniel, L., McGinnis, S., Mearns, L. O., and Tebaldi, C. (2015). Future population exposure to US heat extremes. *Nat. Clim. Change.* doi:10.1038/nclimate2631.

Jones, B., Tebaldi, C., O'Neill, B. C., Oleson, K., and Gao, J. (2018). Avoiding population exposure to heat-related extremes: demographic change vs climate change. *Clim. Change, 146,* 423-437. doi:10.1007/s10584-017-2133-7.

Jones, R. H., Westra, S., and Sharma, A. (2010). Observed relationships between extreme sub-daily precipitation, surface temperature, and relative humidity. *Geophys. Res. Lett., 37, L22805.* doi:10.1029/2010gl045081.

Joshi, M. M., Gregory, J. M., Webb, M. J., Sexton, D. M. H., and Johns, T. C. (2008). Mechanisms for the land/sea warming contrast exhibited by simulations of climate change. *Clim. Dyn., 30,* 455-465. doi:10.1007/s00382-007-0306-1.

Kalkstein, L. S., and Davis, R. E. (1989). Weather and human mortality: an evaluation of demographic and interregional responses in the United States. *Ann. Assoc. Amer. Geog., 79 (1),* 44-64.

Kalkstein, L. S., and Valimont, K. M. (1986). An evaluation of summer discomfort in the United States using a relative climatological index. *Bull. Amer. Meteorol. Soc., 67 (7)*, 842-848.

Kamae, Y., Watanabe, M., Kimoto, M., and Shiogama, H. (2014). Summertime land-sea thermal contrast and atmospheric circulation over East Asia in a warming climate—Part II: Importance of CO2-induced continental warming. *Clim. Dyn., 43,* 2569-2583. doi:10.1007/s00382-014-2146-0.

Kanda, M. (2007). Progress in urban meteorology: a review. *J. Meteorol. Soc. Japan, 85B,* 363-383. doi:10.2151/jmsj.85b.363.

Kenyon, J., and Hegerl, G. C. (2008). Influence of modes of climate variability on global temperature extremes. *J. Clim., 21,* 3872-3889. doi:10.1175/2008jcli2125.1.

Kharin, V. V., Zwiers, F. W., Zhang, X., and Wehner, M. (2013). Changes in temperature and precipitation extremes in the CMIP5 ensemble. *Clim. Change, 119,* 345-357. doi:10.1007/s10584-013-0705-8.

Kjellstrom, T., Briggs, D., Freyberg, C., Lemke, B., Otto, M., and Hyatt, O. (2016). Heat, human performance, and occupational health: A key issue for the assessment of global climate change impacts. *Annu. Rev. Public Health, 37,* 97-112. doi:10.1146/annurev-publhealth-032315-021740.

Knutson, T. R., and Ploshay, J. J. (2016). Detection of anthropogenic influence on a summertime heat stress index. *Clim. Change.* doi:10.1007/s10584-016-1708-z.

Kolokotroni, M., Ren, X., Davies, M., and Mavrogianni, A. (2012). London's urban heat island: impact on current and future energy consumption in office buildings. *Energy and Buildings, 47,* 302-311. doi:10.1016/j.enbuild.2011.12.019.

Kunkel, K. E., Changnon, S. A., Reinke, B. C., and Aritt, R. W. (1996). The July 1995 heat wave in the Midwest: a climatic perspective and critical weather factors. *Bull. Amer. Meteorol. Soc. 77 (7),* 1507-1518. doi:10.1175/1520-0477(1996)077<1507:TJHWIT>2.0.CO;2.

Kunreuther, H., Heal, G., Allen, M., Edenhofer, O., Field, C. B., and Yohe, G. (2013). Risk management and climate change. *Nat. Clim. Change, 3,* 447-451. doi:10.1038/nclimate1740.

Lebassi, B., Gonzalez, J., Fabris, D., Maurer, E., Miller, N., Milesi, C., Switzer, P., and Bornstein, R. (2009). Observed 1970-2005 cooling of summer daytime temperatures in coastal California. *J. Clim., 22,* 3558-3573. doi:10.1175/2008jcli2111.1.

Lebassi-Habtezion, B., Gonzalez, J., and Bornstein, R. (2011). Modeled large-scale warming impacts on summer California coastal-cooling trends. *J. Geophys. Res., 116,* (D20114). doi:10.1029/2011jd015759.

Lee, Y.-Y., and Grotjahn, R. (2016). California Central Valley summer heat waves form two ways. *J. Clim., 29,* 1201-1217. doi:10.1175/jcli-d-15-0270.1.

Lee, Y.-Y., and Grotjahn, R. (2019). Evidence of specific MJO phase occurrence with summertime California Central Valley extreme hot weather. *Adv. Atmos. Sci., 36,* 589-602. doi:10.1007/s00376-019-8167-1.

Li, L., Li, W., and Jin, J. (2015). Contribution of the North Atlantic subtropical high to regional climate model (RCM) skill in simulating southeastern United States summer precipitation. *Clim. Dyn, 45,* 477-491. doi:10.1008/s00382-014-2352-9.

Li, L., Li, W., and Kushnir, Y. (2012). Variation of the North Atlantic subtropical high western ridge and its implication to Southeastern US summer precipitation. *Clim. Dyn., 39,* 1401-1412. doi:10.1007/s00382-011-1214-y.

Liang, X.-Z., Pan, J., Zhu, J., Kunkel, K. E., Wang, J. X. L., and Dai, A. (2006). Regional climate model downscaling of the U.S. summer climate and future change. *J. Geophys. Res., 111,* D10108. doi:10.1029/2005jd006685.

Lhotka, O., Kysely, J., and Plavcová, E. (2018). Evaluation of major heat waves' mechanisms in EURO-CORDEX RCMs over Central Europe. *Clim. Dyn., 50,* 4249-4262. doi:10.1007/s00382-017-3873-9.

Loikith, P. C., and Broccoli, A. J. (2012). Characteristics of observed atmospheric circulation patterns associated with temperature extremes over North America. *J. Clim., 25,* 7266-7281. doi:10.1175/JCLI-D-11-00709.1.

Lowe, D., Ebi, K. L., and Forsberg, B. (2011). Heatwave early warning systems and adaptation advice to reduce human health consequences of heatwaves. *Int. J. Environ. Res. Public Health, 8,* 4623-4648. doi:10.3390/ijerph8124623.

Lynch, C., Seth, A., and Thibeault, J. (2016). Recent and projected annual cycles of temperature and precipitation in the Northeast United States from CMIP5. *J. Clim., 29,* 347-365. doi:10.1175/jcli-d-14-00781.1.

Lyon, B. (2004). The strength of El Niño and the spatial extent of tropical drought. *Geophys. Res. Lett., 31,* L21204. doi:10.1029/2004gl020901.

Maddox, R. A., McCollum, D. M., and Howard, K. W. (1995). Large-scale patterns associated with severe summertime thunderstorms over central Arizona. *Wea. Forecasting, 10,* 763-778. doi:10.1175/1520-0434(1995)010<0763:LSPAWS>2.0.CO;2.

Mankin, J. S., Viviroli, D., Mekonnen, M. M., Hoekstra, A. Y., Horton, R. M., Smerdon, J. E., and Diffenbaugh, N. S. (2017). Influence of internal variability on population exposure to hydroclimatic changes. *Env. Res. Lett., 12,* 044007. doi:10.1088/1748-9326/aa5efc.

Mannshardt-Shamseldin, E. C., Smith, R. L., Sain, S. R., Mearns, L. O., and Cooley, D. (2010). Downscaling extremes: A comparison of extreme value distributions in point-source and gridded precipitation data. *Ann. Appl. Stat., 4* (1), 484-502. doi:10.1214/09-aoas287.

Mantua, N. J., and Hare, S. R. (2002). The Pacific Decadal Oscillation. *J. Ocean., 58,* 35-44. doi:10.1023/a:1015820616384.

Maraun, D., Shepherd, T. G., Widmann, M., Zappa, G., Walton, D., Gutierrez, J. M., Hagemann, S., Richter, I., Soares, P. M. M., Hall, A. and Mearns, L. O. (2017). Towards process-informed bias correction of climate change simulations. *Nat. Clim. Change,* 764-773. doi:10.1038/nclimate3418.

Mariotti, A., Barnes, E. A., Chang, E. K.-M., Lang, A., Dirmeyer, P. A., Pegion, K., Barrie, D., and Baggett, C. (2019). Bridging the weather-to-climate prediction gap. *Eos, 100.* doi:10.1029/2019eo115819.

Marsicek, J., Shuman, B. N., Bartlein, P. J., Shafer, S. L., and Brewer, S. (2018). Reconciling divergent trends and millennial variations in Holocene temperatures. *Nature, 554,* 92-110. doi:10.1038/nature25464.

Matthews, T. K. R., Wilby, R. L., and Murphy, C. (2017). Communicating the deadly consequences of global warming for human heat stress. *Proc. Nat. Acad. Sci., 114* (15), 3861-3866. doi:10.1073/pnas.1617526114.

Matthews, T. (2018). Humid heat and climate change. *Prog. Phys. Geog., 42* (3), 391-405. doi:10.1177/0309133318776490.

McCabe, G. J., Palecki, M. A., and Betancourt, J. L. (2004). Pacific and Atlantic Ocean influences on multidecadal drought frequency in the United States. *Proc. Nat. Acad. Sci., 101,* 4136-4141. doi:10.1073/pnas.0306738101.

McCarthy, M. P., Best, M. J., and Betts, R. A. (2010). Climate change in cities due to global warming and urban effects. *Geophys. Res. Lett., 37,* L09705. doi:10.1029/2010gl042845.

McKinnon, K. A., Rhines, A., Tingley, M. P., and Huybers, P. (2016). Long-lead predictions of eastern United States hot days from Pacific sea surface temperatures. *Nat. Geosci., 9,* 389-396. doi:10.1038/ngeo2687.

Meehl, G. A., Tebaldi, C., Walton, G., Easterling, D., and McDaniel, L. (2009). Relative increase of record high maximum temperatures compared to record low minimum temperatures in the U.S. *Geophys. Res. Lett., 36,* L23701. doi:10.1029/2009gl040736.

Meinshausen, M., Smith, S. J., Calvin, K., Daniel, J. S., Kainuma, M. L. T., Lamarque, J.-F., Matsumoto, K., Montzka, S. A., Raper, S. C. B., Riahi, K., Thomson, A., Velders, G. J. M., and van Vuuren, D. P. P. (2011). The RCP greenhouse gas concentrations and their extensions from 1765 to 2300. *Clim. Change, 109,* 213-241. doi:10.1007/s10584-011-0156-z.

Meir, T., Orton, P. M., Pullen, J., Holt, T., Thompson, W. T., and Arend, M. F. (2013). Forecasting the New York City urban heat island and sea breeze during extreme heat events. *Wea. Forecasting, 28,* 1460-1477. doi:10.1175/WAF-D-13-00012.1.

Melecio-Vázquez, D., Ramamurthy, P., Arend, M., and González-Cruz, J. E. (2018). Thermal structure of a coastal-urban boundary layer. *Boundary-Layer Meteorol.* doi:10.1007/s10546-018-0361-7.

Melillo, J. M., Richmond, T. C., and Yohe, G. W. (Eds.). (2014). Climate change impacts in the United States: The third National Climate Assessment. *U.S. Global Change Research Program, 841 pp.* Washington, DC: U.S. Government Printing Office. doi:10.7930/j0z31wj2.

Menne, M. J., Durre, I., Vose, R. S., Gleason, B. E., and Houston, T. G. (2012). An overview of the Global Historical Climatology Network-Daily Database. *J. Atmos. Ocean. Tech., 29,* 897-910. doi:10.1175/jtech-d-11-00103.1.

Mesinger, F., et al. (2006). North American Regional Reanalysis. *Bull. Amer. Meteorol. Soc., 87,* 343–360. doi:10.1175/BAMS-87-3-343.

Miller, N. L., Hayhoe, K., Jin, J., and Auffhammer, M. (2008). Climate, extreme heat, and electricity demand in California. *J. Appl. Meteorol. Clim., 47,* 1834-1844. doi:10.1175/2007jamc1480.1.

Miller, S. T. K., and Keim, B. D. (2003). Synoptic-scale controls on the sea breeze of the central New England coast. *Wea. Forecasting, 18,* 236-248. doi:10.1175/1520-0434(2003)018<0236:SCOTSB>2.0.CO;2.

Miralles, D. G., Teuling, A. J., van Heerwaarden, C. C., and de Arellano, J. V.-G. (2014). Mega-heatwave temperatures due to combined soil desiccation and atmospheric heat accumulation. *Nat. Geosci. 7,* 345-349. doi:10.1038/ngeo2141.

Mishra, V., Ganguly, A. R., Nijssen, B., and Lettenmaier, D. P. (2015). Changes in observed climate extremes in global urban areas. *Env. Res. Lett., 10,* 024005. doi:10.1088/1748-9326/10/2/024005.

Misra, V., Moeller, L., Stefanova, L., Chan, S., O'Brien, J. J., Smith, T. J. III, and Plant, N. (2011). The influence of the Atlantic Warm Pool on the Florida panhandle sea breeze. *J. Geophys. Res., 116,* D00Q06. doi:10.1029/2010jd015367.

Mitchell, D., Heaviside, C., Vardoulakis, S., Huntingford, C., Masato, G., Guillod, B. P., Frumhoff, P., Bowery, A., Wallom, D., and Allen, M. (2016). Attributing human mortality during extreme heat waves to anthropogenic climate change. *Env. Res. Lett., 11,* 074006. doi:10.1088/1748-9326/11/7/074006.

Mora, C., Dousset, B., Caldwell, I. R., Powell, F. E., Geronimo, R. C., Bielecki, C. R., Counsell, C. W. W., Dietrich, B. S., Johnston, E. T., Louis, L. V., Lucas, M. P., McKenzie, M. M., Shea, A. G., Tseng, H., Giambelluca, T. W., Leon, L. R., Hawkins, E., and Trauernicht, C. (2017). Global risk of deadly heat. *Nat. Clim. Change, 7.* doi:10.1038/nclimate3322. Nakamura, N., and Oort, A. H. (1988). Atmospheric heat budgets of the polar regions. *J. Geophys. Res., 93 (D8),* 9510-9524. doi:10.1029/jd093id08p09510.

Morignat, E., Perrin, J. B., Gay, E., Vinard, J. L., Calavas, D., and Hénaux, V. (2014). Assessment of the impact of the 2003 and 2006 heat waves on cattle mortality in France. *PLoS ONE*, *9*(3). doi:10.1371/journal.pone.0093176.

Mueller, N. D., Butler, E. E., McKinnon, K. A., Rhines, A., Tingley, M., Holbrook, N. M., and Huybers, P. (2016). Cooling of US Midwest summer temperature extremes from cropland intensification. *Nat. Clim. Change, 6.* doi:10.1038/nclimate2825.

Mueller, V., Gray, C., and Kosec, K. (2014). Heat stress increases long-term human migration in rural Pakistan. *Nat. Clim. Change, 4*, 182-185. doi:10.1038/nclimate2103.

Ning, L., Riddle, E. E., and Bradley, R. S. (2015). Projected changes in climate extremes over the northeastern United States. *J. Clim., 28,* 3289-3310. doi:10.1175/JCLI-D-14-00150.1.

Novak, D. R., and Colle, B. A. (2006). Observations of multiple sea breeze boundaries during an unseasonably warm day in metropolitan New York City. *Bull. Amer. Meteorol. Soc., 87,* 169-174. doi:10.1175/bams-87-2.169.

Oleson, K. W., Anderson, G. B., Jones, B., McGinnis, S. A., and Sanderson, B. (2015). Avoided climate impacts of urban and rural heat and cold waves over the U.S. using large climate model ensembles for RCP8.5 and RCP4.5. *Clim. Change.* doi:10.1007/s10584-015-1504-1.

O'Neill, M. S., Zanobetti, A., and Schwartz, J. (2005). Disparities by race in heat-related mortality in four US cities: The role of air conditioning prevalence. *J. Urban Health, 82* (2), 191-197. doi:10.1093/jurban/jti043.

Pal, J. S., and Eltahir, E. A. B. (2016). Future temperature in southwest Asia projected to exceed a threshold for human adaptability. *Nat. Clim. Change, 6.* doi:10.1038/nclimate2833.

Papalexiou, S. M., AghaKouchak, A., Trenberth, K. E., and Foufoula-Georgiou, E. (2018). Global, regional, and megacity trends in the highest temperature of the year: diagnostics and evidence for accelerating trends. *Earth's Future.* doi:10.1002/2017ef000709.

Parsons, K. (2006). Heat stress standard ISO 7243 and its global application. *Indust. Health, 44,* 368-379. doi:10.2486/indhealth.44.368.

Perkins, S. E. (2015). A review on the scientific understanding of heatwaves — their measurement, driving mechanisms, and changes at the global scale. *Atm. Res. 164-165,* 242-267. doi:10.1016/j.atmos.res.2015.05.0140169.

Petkova, E. P., Gasparrini, A., and Kinney, P. L. (2014). Heat and mortality in New York City since the beginning of the 20th century. *Epidem., 25,* 554-560. doi:10.1097/ede.00000000000000123.

Pielke, R. A., Davey, C., and Morgan, J. (2004). Assessing "global warming" with surface heat content. *Eos, 85 (21),* 210-211. doi:10.1029/2004eo210004.

Pierce, D. W., Cayan, D. R., and Thrasher, B. L. (2014). Statistical downscaling using localized constructed analogs (LOCA). *J. Hydrometeorol., 15,* 2558-2585. doi:10.1175/jhm-d-14-0082.1.

Pierce, D. W., Cayan, D. R., Maurer, E. P., Abatzoglou, J. T., and Hegewisch, K. C. (2015). Improved bias correction techniques for hydrological simulations of climate change. *J. HydroMeteorol., 16,* 2421-2442. doi:10.1175/jhm-d-14-0236.1.

Plumb, R. A. (1985). On the three-dimensional propagation of stationary waves. *J. Atmos. Sci., 42* (3), 217-229. doi:10.1175/1520-0469(1985)042<0217:OTTDPO>2.0.CO;2.

Porter, J. R., and Coauthors (2014). Food security and food production systems. In Christopher B. Field, Vicente R. Barros, David Jon Dokken, Katharine J. Mach, Michael D. Mastrandrea, T. Eren Bilir, Monalisa Chatterjee, Kristie L. Ebi, Yuka Otsuki Estrada, Robert C. Genova, Betelhem Girma, Eric S. Kissel, Andrew N. Levy, Sandy MacCracken and Patricia R. Mastrandrea (eds.), Climate change 2014: impacts, adaptation, and vulnerability. Part A: Global and sectoral aspects (pp. 485-533) New York, United States: Cambridge University Press.

Pullen, J., Allard, R., Seo, H., Miller, A. J., Chen, S., Ponzi Pezzi, L., Smith, T., Chu, P., Alves, J., and Caldeira, R. (2017). Coupled ocean-atmosphere forecasting at short and medium time scales. *J. Marine Res., 75* (6), 877-921. doi:10.1357/002224017823523991.

Quinn, A., Tamerius, J. D., Perzanowski, M., Jacobson, J. S., Goldstein, I., Acosta, L., and Shaman, J. (2014). Predicting indoor heat exposure risk during extreme heat events. *Sci. Total Environ., 490,* 686-693. doi:10.1016/j.scitotenv.2014.05.039.

Radakovic, S. S., Maric, J., Surbatovic, M., Radjen, S., Stefanova, E., Stankovic, N., and Filipovic, N. (2007). Effects of acclimation on cognitive performance in soldiers during exertional heat stress. *Milit. Med., 172* (2), 133-136. doi:10.7205/milmed.172.2.133.

Raymond, C., Coumou, D., Foreman, T., King, A., Kornhuber, K., Lesk, C., Mora, C., Perkins-Kirkpatrick, S., Russo, S., and Vijverberg, S. (in press). Projections and hazards of future extreme heat. In *Planning for Climate Change Hazards* [Pfeffer, T., and Smith, J., Eds.]. Oxford University Press.

Raymond, C., and Mankin, J. S. Coastal moderation of extreme heat in the eastern United States. In second-stage review at *Geophys. Res. Lett.*

Raymond, C., Matthews, T. K., and Horton, R. M. The emergence of heat and humidity too severe for human tolerance. In revision at *Sci. Adv.*

Raymond, C., Singh, D., and Horton, R. M. (2017). Spatiotemporal patterns and synoptics of extreme wet-bulb temperature in the contiguous United States. *J. Geophys. Res. Atmos., 122*. doi:10.1002/2017jd027140.

Robine, J.-M., Cheung, S. L. K., Le Roy, S., Van Oyen, H., Griffiths, C., Michel, J.-P., and Herrmann, F. R. (2008). Death toll exceeded 70,000 in Europe during the summer of 2003. *C. R. Biologies, 331,* 171-178. doi:10.1016/j.crvi.2007.12.001.

Rosenthal, J. K., Kinney, P. L., and Metzger, K. B. (2014). Intra-urban vulnerability to heat-related mortality in New York City, 1997-2006. *Health & Place, 30,* 45-60. doi:10.1016/j.healthplace.2014.07.014.

Russo, S., Sillmann, J., and Sterl, A. (2017). Humid heat waves at different warming levels. *Nat. Sci. Rep., 7,* 7477. doi:10.1038/s41598-017-07536-7.

Salamanca, F., Georgescu, M., Mahalov, A., Moustaoui, M., and Wang, M. (2014). Anthropogenic heating of the urban environment due to air conditioning. *J. Geophys. Res. Atmos., 119,* 5949-5965. doi:10.1002/2013jd021225.

Sawka, M. N., Wenger, C. B., Mountain, S. J., Kolka, M. A., Bettencourt, B., Flinn, S., Gardner, J., Matthew, W. T., Lovell, M., and Scott, C. (2003). Heat stress control and heat casualty management. *US Army Research Institute of Environmental Medicine Technical Bulletin 507*.

Schär, C. (2016). The worst heat waves to come. *Nat. Clim. Change, 6,* 128-129. doi:10.1038/nclimate2864.

Schinasi, L. H., Benmarhnia, T., and De Roos, A. J. (2018). Modification of the association between high ambient temperature and health by urban microclimate indicators: A systematic review and meta-analysis. *Env. Res., 161,* 168-180. doi:10.1016/j.envres.2017.11.004.

Schnell, J. L., and Prather, M. P. (2017). Co-occurrence of extremes in surface ozone, particulate matter, and temperature over eastern North America. *Proc. Nat. Acad. Sci., 114* (11), 2854-2859. doi:10.1073/pnas.1614453114.

Schwartz, J. D., Lee, M., Kinney, P. L., Yang, S., Mills, D., Sarofim, M. C., Jones, R., Streeter, R., St. Juliana, A., Peers, J., and Horton, R. M. (2015). Projections of temperature-attributable premature deaths in 209 U.S. cities using a cluster-based Poisson approach. *Env. Health,* 14:85. doi:10.1186/s12940-015-0071-2.

Seneviratne, S. I., Lüthi, D., Litschi, M., and Schär, C. (2006). Land-atmosphere coupling and climate change in Europe. *Nature, 443* (14), 205-209. doi:10.1038/nature05095.

Seneviratne, S. I., Rogelj, J., Séférian, R., Wartenburger, R., Allen, M. R., Cain, M., Millar, R. J., Ebi, K. L., Ellis, N., Hoegh-Guldberg, O., Payne, A. J., Schleussner, C.-F., Tschakert, P., and Warren, R. F. (2018). The many possible climates from the Paris Agreement's aim of 1.5°C warming. *Nature, 558,* 41-49. doi:10.1038/s41586-018-0181-4.

Sequera, P., Gonzalez, J. E., McDonald, K., Bornstein, R., and Comarazamy, D. (2015). Combined impacts of land cover changes and large-scale forcing on Southern

California summer daily maximum temperatures. *J. Geophys. Res. Atmos., 120,* 9208-9219. doi:10.1002/2015jd023536.

Sherwood, S. C., and Huber, M. (2010). An adaptability limit to climate change due to heat stress. *Proc. Nat. Acad. Sci., 107,* 9552-9555. doi:10.1073/pnas.0913352107.

Sillmann, J., Kharin, V. V., Zhang, X., Zwiers, F. W., and Bronaugh, D. (2013). Climate extremes indices in the CMIP5 multimodel ensemble: Part 2. Future climate projections. *J. Geophys. Res. Atmos., 118,* 2473-2493. doi:10.1002/jgrd.50188.

Smith, A., Lott, N., and Vose, R. (2011). The Integrated Surface Database: Recent developments and partnerships. *Bull. Amer. Meteorol., Soc.,* 704-708. doi:10.1175/2011bams3015.1.

Smith, T. T., Zaitchik, B. F., and Gohlke, J. M. (2013). Heat waves in the United States: definitions, patterns, and trends. *Clim. Change, 118,* 811-825. doi:10.1007/s10584-012-0659-2.

Sobel, A. H., Held, I. M., and Bretherton, C. S. (2002). The ENSO signal in tropical tropospheric temperature. *J. Clim., 15,* 2702-2706. doi:10.1175/1520-0442(2002)015<2702:TESITT>2.0.CO;2.

Sobel, A. H., Nilsson, J., and Polvani, L. M. (2001). The weak temperature gradient approximation and balanced tropical moisture waves. *J. Atmos. Sci., 58,* 3650-3665. doi:10.1175/1520-0469(2001)058<3650:TWTGAA>2.0.CO;2.

Stull, R. (2011). Wet-bulb temperature from relative humidity and air temperature. *J. Appl. Meteorol. Clim., 50,* 2267-2269. doi:10.1175/JAMC-D-11-0143.1.

Takane, Y., and Kusaka, H. (2011). Formation mechanisms of the extreme high surface air temperature of 40.9°C observed in the Tokyo Metropolitan Area: Considerations of dynamic foehn and foehnlike wind. *J. Appl. Meteorol. Clim., 50* (9), 1827-1841. doi:10.1175/jamc-d-10-05032.1.

Teng, H., and Branstator, G. (2017). Causes of extreme ridges that induce California droughts. *J. Clim., 30,* 1477-1492. doi:10.1175/jcli-d-16-0524.1.

Teng, H., Branstator, G., Wang, H., Meehl, G. A., and Washington, W. M. (2013). Probability of US heat waves affected by a subseasonal planetary wave pattern. *Nat. Geosci. 6,* 1056-1061. doi:10.1038/ngeo1988.

Thibeault, J. M., and Seth, A. (2014). Changing climate extremes in the Northeast United States: observations and projections from CMIP5. *Clim. Change, 127,* 273-287. doi:10.1007/s10584-014-1257-2.

Trenberth, K. E., Fasullo, J. T., and Mackaro, J. (2011). Atmospheric moisture transports from ocean to land and global energy flows in reanalyses. *J. Clim., 24,* 4907-4924. doi:10.1175/2011jcli4171.1.

Van Oldenborgh, G. J., Collins, M., Arblaster, J., Christensen, J. H., Marotzke, J., Power, S. B., Rummukainen, M., and Zhou, T. (2013). In *Climate Change 2013: The Physical Science Basis. Contribution of Working Group I to the Fifth Assessment Report of the Intergovernmental Panel on Climate Change* [eds Stocker, T. F., et al.]. Annex 1.

Vogel, M. M., Orth, R., Cheruy, F., Hagemann, S., Lorenz, R., van den Hurk, B. J. J. M., and Seneviratne, S. I. (2017). Regional amplification of projected changes in extreme temperatures strongly controlled by soil moisture-temperature feedbacks. *J. Geophys. Res. Atmos., 44,* 1511-1519. doi:10.1002/2016gl071235.

Vose, R. S., Easterling, D. R., Kunkel, K. E., LeGrande, A. N., and Wehner, M. F. (2017). Temperature changes in the United States. In: *Climate Science Special Report: Fourth National Climate Assessment, Volume I* [Wuebbles, D.J., D.W. Fahey, K.A. Hibbard, D.J. Dokken, B.C. Stewart, and T.K. Maycock (eds.)]. U.S. Global Change Research Program, Washington, DC, USA, pp. 185-206. doi:10.7930/J0N29V45.

Wang, H., and Schubert, S. (2014). Causes of the extreme dry conditions over California during early 2013. In "Explaining Extreme Events of 2013 from a Climate Perspective". *Bull. Amer. Meteorol. Soc., 95* (9).

Wang, J., and Kotamarthi, V. R. (2014). Downscaling with a nested regional climate model in near-surface fields over the contiguous United States. *J. Geophys. Res. Atmos., 119,* 8778-8797. doi:10.1002/2014jd021696.

Wehner, M., Stone, D., Krishnan, H., AchutaRao, K., and Castillo, F. (2016). The deadly combination of heat and humidity in India and Pakistan in summer 2015. In "Explaining Extreme Events of 2015 from a Climate Perspective" [Herring, S. C., Hoell, A., Hoerling, M. P., Kossin, J. P., Schreck III, C. J., and Stott, P. A., Eds.]. *Bull. Amer. Meteorol. Soc., 97* (12), Suppl. doi:10.1175/bams-d-16-0145.1.

Willett, K. M., and Sherwood, S. (2012). Exceedance of heat index thresholds for 15 regions under a warming climate using the wet-bulb globe temperature. *Int. J. Clim., 32,* 161-177. doi:10.1002/joc.2257.

Wilson, S. G., and Fischetti, T. R. (2010). Coastline population trends in the United States: 1960 to 2008. *U.S. Census Bureau, Population Division,* Report P25-1139.

Wouters, H., De Ridder, K., Poelmans, L., Willemsn, P., Brouwers, J., Hosseinzadehtalaei, P., Tabari, H., Vanden Broucke, S., van Lipzig, N. P. M., and Demuzere, M. (2017). Heat stress increase under climate change twice as large in cities as in rural areas: A study for a densely populated midlatitude maritime region. *Geophys. Res. Lett., 44,* 8997-9007. doi:10.1002/2017gl074889.

Wu, J., Zhou, Y., Gao, Y., Fu, J. S., Johnson, B. A., Huang, C., Kim, Y.-M., and Liu, Y. (2014). Estimation and uncertainty analysis of impacts of future heat waves on mortality in the eastern United States. *Env. Health Persp., 122 (1),* 10-16. doi:10.1289/ehp.1306670.

Wuebbles, D., Meehl, G., Hayhoe, K., Karl, T. R., Kunkel, K. E., Santer, B., Wehner, M., Colle, B., Fischer, E. M., Fu, R., Goodman, A., Janssen, E., Kharin, V., Lee, H., Li, W., Long, L. N., Olsen, S. C., Pan, Z., Seth, A., Sheffield, J., and Sun, L. (2015). CMIP5 climate model analyses: climate extremes in the United States. *Bull. Amer. Meteorol. Soc.,* 571-583. doi:10.1175/bams-d-12-00172.1.

Xie, S.-P., Deser, C., Vecchi, G. A., Collins, M., Delworth, T. L., Hall, A., Hawkins, E., Johnson, N. C., Cassou, C., Giannini, A., and Watanabe, M. (2015). Towards predictive understanding of regional climate change. *Nat. Clim. Change, 5,* 921-930. doi:10.1038/nclimate2689.

Zander, K. K., Wouter, J. W., Opperman, E., Kjellstrom, T., and Garnett, S. T. (2015). Heat stress causes substantial labour productivity loss in Australia. *Nat. Clim. Change, 5,* 647-651. doi:10.1038/nclimate2623.

Zhao, L., Oppenheimer, M., Zhu, Q., Baldwin, J. W., Ebi, K. L., Bou-Zeid, E., Guan, K., and Liu, X. (2018). Interactions between urban heat islands and heat waves. *Env. Res. Lett., 13,* 034003. doi:10.1088/1748-9326/aa9f73.

Zhao, Z., Chen, S.-H., Kleeman, M. J., and Mahmud, A. (2011). The impact of climate change on air quality-related meteorological conditions in California. Part II: present versus future time simulation analysis. *J. Clim., 24,* 3362-3376. doi:10.1175/2010jcli3850.1.

Zivin, J. G., and Neidell, M. (2014). Temperature and the allocation of time: implications for climate change. *J. Labor Econ., 32*(1), 1-26. doi:10.1086/671766.

Zobel, Z., Wang, J., Wuebbles, D. J., and Kotamarthi, V. R. (2018). Evaluations of high-resolution dynamically downscaled ensembles over the contiguous United States. *Clim. Dyn., 50,* 863-884. doi:10.1007/s00382-017-3645-6.

Zobel, Z., Wang, J., Wuebbles, D. J., and Kotamarthi, V. R. (2017). High-resolution dynamical downscaling ensemble projections of future extreme temperature distributions for the United States. *Earth's Future, 5,* 1234-1251. doi:10.1002/2017ef000642.